MODELLING FLUID FLOW IN AN OPEN HORSESHOE CHANNEL WITH LATERAL INFLOW CHANNELS

JOMBA JASON

A Thesis Submitted to the Graduate school in Partial Fulfilment of the Award of the Degree of Doctor of Philosophy in Applied Mathematics of Chuka University

CHUKA UNIVERSITY

OCTOBER, 2024

DECLARATION AND RECOMMENDATION

Declaration

This Thesis is my original work and has not been presented for an award of diploma or conferment of degree in any other University.

Signature:..... Date: 15/10/2024

JOMBA JASON
SD12/40017/19

Recommendation

This Thesis has been examined, passed and submitted with our approval as university supervisors.

Signature:..... Date: 15/10/2024

Dr. Mark Okongo , PhD.
Chuka University.

CHUKA UNIVERSITY
DIRECTOR BOARD OF POSTGRADUATE STUDIES AND RESEARCH
P.O. Box 109-60400, CHUKA

Signature:..... Date: 15/10/2024

Dr. Jacob Kirimi., Ph.D.
Chuka University.

DEDICATION

To my spouse Rhoda Munene, my children Angel kanana and Peace Mutuma. Thank you for your total support.

To Tharaka University, thank you for creating a conducive environment for my studies and research.

ACKNOWLEDGMENTS

I am deeply grateful to my supervisors, Dr. Mark Onyango Okong'o and Dr. Jacob Kirimi, for their constant guidance, encouragement and valuable corrections and suggestions. It was essential in making sure my thesis was finished on schedule. May the All-Powerful God reward them for their kindness and encouragement during this research. My deep appreciation for the support comes from my colleagues in Chuka University's Department of physical Sciences and Tharaka University's Department of Basic Sciences. Prof. Paul Kamweru, Prof. Sammy Musundi, Prof Joel Gichumbi, Dr. Fidelis Ngugi, Dr. Daniel Murithi, Mr. Alex Rwanda, and Mr. Erick Osoro provided invaluable counsel. I also extend my gratitude to Dr. Ochwach Jimrise, who, despite his busy schedule, dedicated time to assist me with computer programming. His expertise in this area was immensely beneficial to my work. I learned the value of persistence during difficult times and realized that persistence indeed overcomes resistance when we achieved the desired results. I am deeply grateful to my wife, Rhoda Kainyu Munene, my daughter, Angel Kanana, and my son, Peace Mutuma, for their patience, understanding, and tremendous support throughout this study. May God bless them and open doors for them as well. Finally, I want to express my sincere thankfulness to the All powerful God for providing me with the power necessary to finish this work. This achievement demonstrates his grace. Blessed be His name.

ABSTRACT

Flooding has been an issue for many years, particularly during periods of heavy rainfall. Channels have been constructed to reduce flooding by directing water to rivers, lakes and oceans. Engineers have faced a challenge of designing a hydraulically efficient channel for conveying maximum amount of water for generating electric power, drainage ditches, floodways, navigation channels and irrigation canals. Horseshoe-shaped channels with lateral inputs have received less attention in open channel flow studies than rectangular, parabolic, trapezoidal, and circular channels. This study aims at modeling a uniform flow with horseshoe cross-section with lateral inflows. The choice of a lateral horseshoe shape is due to its distinctive combination of geometric and functional advantages. In fluid dynamics, this shape is particularly valuable for promoting streamlined flow. Its curved form allows fluids to move around it with reduced turbulence and drag, making it ideal for minimizing flow resistance. This study investigates the effects of increasing lateral inflows, varying lateral inflow channel angles, increasing lateral inflows' cross-sectional areas, and increasing lateral inflows' lengths on the velocity of the primary channel's flow. To obtain particular governing equations, the physical conditions of the flow problem were applied to conservation equations. The finite difference technique is utilized to resolve the differential equations governing the flow due to its accuracy, consistency and convergence. The equations are first represented in dimensionless form. Numerical values are simulated using the Python program, and the results obtained from this study are represented graphically. The findings showed that when lateral inflows increased, the main channel's velocity reduced. Furthermore, it was noted that the velocity decreased as the lateral inflows' angles increased. Similarly, the velocity in the primary channel decreased as the cross-sectional area of the lateral inflows increases. Conversely, the results showed that when the length of the lateral inflows increased, it also increased the main channel's velocity. This research will help engineers construct open horseshoe channels with lateral inflows that are hydraulically efficient and can transfer the most water possible for a variety of uses. One of the main applications is irrigation, because efficient water flow is necessary for productive farming. The findings of the study will also be helpful in the production of hydroelectric power since they offer information on how to optimize water flow to improve energy output. The research also intends to improve channel designs that can manage high water volumes in an effort to aid in flood reduction efforts.

TABLE OF CONTENTS

DECLARATION AND RECOMMENDATION . . . . . **ii**

COPYRIGHT ©2024 . . . . . **iii**

DEDICATION . . . . . **iv**

ACKNOWLEDGMENTS . . . . . **v**

ABSTRACT . . . . . **vi**

TABLE OF CONTENTS . . . . . **vii**

LIST OF FIGURES . . . . . **xi**

SYMBOLS AND INDEX OF NOTATION . . . . . **xii**

ABBREVIATIONS AND ACRONYMS . . . . . **xiv**

CHAPTER ONE: INTRODUCTION **1**

1.1 Background Information 1

1.2 Statement of the Problem 4

1.3 Objectives of the Study 4

1.3.1 Main Objective 4

1.3.2 Specific Objectives 5

1.4 Significance of the Study 5

1.5 Basic Assumptions 5

1.6 Operational Definition of Terms 6

1.6.1 Fluid 6

1.6.2 Incompressible flow 7

1.6.3 Laminar Flow 7

1.6.4 Viscosity 8

1.6.5 Unsteady Flow 8

1.6.6 Prismatic Channel 9

1.6.7 Boundary Layer 10

1.6.8 Dimensional Analysis 10

CHAPTER TWO: LITERATURE REVIEW **12**

2.1 Overview 12

2.2 Lateral Inflows 12

2.3 Variation of the Angle of Lateral Inflow 15

2.4 Cross-Sectional Area of Lateral Inflow 16

2.5 Length of the Channel 25
CHAPTER THREE: METHODOLOGY 29
3.1 Model Formulation 29
3.2 Mathematical Model Development 29
3.3 Model Assumptions 30
3.4 Mathematical Model Formulation 30
3.4.1 Equation of Continuity 30
3.4.2 Equation of Conservation of Momentum 32
3.5 Non-dimensional Numbers 33
3.5.1 Reynold Number, Re 33
3.5.2 Froude Number, Fr 34
3.5.3 Manning's Roughness Coefficient 35
3.5.4 Chezy Coefficient,(C) 36
3.5.5 Flow Aspect Ratio (W/h) in Open Channels 37
3.6 Geometrical Properties 38
3.7 Non-Dimensionalising the Governing Equations 40
3.7.1 Equation of Continuity 40
3.7.2 Equation of Conservation of Momentum 42
3.8 Boundary Conditions 44
3.8.1 Equation of continuity and momentum 44
3.9 Equations Governing the Fluid flow in Nondimensional Form 45
3.9.1 Equation of Continuity 45
3.9.2 Momentum Equation 45
3.10 Specific Equations Governing the Fluid Flow in nondimensional Form . 45
3.10.1 Continuity Equations 45
3.10.1.1 Continuity Equation for zone 1 45
3.10.1.2 Continuity Equation for zone 2 46
3.10.1.3 Continuity Equation for zone 3 47
3.10.2 Momentum Equation 48
3.10.2.1 Momentum Equation for Zone 1 48
3.10.2.2 Momentum Equation for Zone 2 48
3.10.2.3 Momentum Equation for Zone 3 49

CHAPTER FOUR: ANALYSIS OF RESULTS AND DISCUSSION **50**
4.1 Model Simulation 50
4.2 Model Equations in the Form of Finite Difference 51
4.2.1 Continuity Equation 51
4.2.2 Momentum Equation 51
4.3 Specific Model Equations in Finite Difference Form 52
4.3.1 Continuity Equation 52
4.3.1.1 Continuity Equation for Zone 1 52
4.3.1.2 Continuity Equation for Zone 2 53
4.3.1.3 Continuity Equation for Zone 3 53
4.3.2 Momentum Equation 53
4.3.2.1 Momentum Equation for Zone 1 54
4.3.2.2 Momentum Equation for Zone 2 54
4.3.2.3 Momentum Equation for Zone 3 54
4.4 Results and Discussion 54
4.4.1 Velocity profiles for zone 1 55
4.4.1.1 Effects of Increasing Lateral Inflows (K) on Velocity of the Main Channel in Zone 1 55
4.4.1.2 Effects of the Varying Angle 58
4.4.1.3 Effects of Cross-Sectional Variation on Velocity in the Main Channel 59
4.4.1.4 Effects of Variation of Length of Lateral Inflows on Velocity in the Main Channel 61
4.4.2 Velocity profiles for zone 2 62
4.4.2.1 Effects of Increasing K on Velocity of the Main Channel in Zone 2 63
4.4.2.2 Effects of Angle Variation on Velocity in the Main Channel 64
4.4.2.3 Effects of Cross-Sectional Variation on Velocity in the Main Channel in Zone 2 66
4.4.2.4 Effects of Variation of Length of Lateral Inflows on Velocity in the Main Channel in Zone 2 68

4.4.3 Velocity profiles for zone 3 70
4.4.3.1 Effects of Increasing K on Velocity of the Main Channel 71
4.4.3.2 Effects of Angle Variation on Velocity in the Main Channel 72
4.4.3.3 Effects of Cross-Sectional Area Variation on Velocity in the Main Channel 73
4.4.3.4 Effects of Variation of Length of Lateral Inflows on rate of the primary Channel 75
CHAPTER FIVE: SUMMARY, CONCLUSION AND RECOMMENDATION 77
5.1 Summary and Conclusion 77
5.2 Recommendation 79

REFERENCES 80

APPENDICES 85
Appendix A: Python Codes for Simulating Profiles 85
Appendix B: Research Permit 88
Appendix C: Research Authorization (NACOSTI) 89

LIST OF FIGURES

Figure 3.1: Mathematical Model Channel 29
Figure 3.2: Horseshoe cross section..... 38
Figure 4.1: Finite Difference Mesh..... 50
Figure 4.2: Effects of Increasing K on Velocity at $\vartheta = 40^0$ 56
Figure 4.3: Effects of Varying Angle on Main Channel Velocity for Different Co-efficient of K..... 58
Figure 4.4: Effects of Variation of Cross-Sectional Area on Velocity 60
Figure 4.5: Effects of Variation of Length of Lateral Inflow 61
Figure 4.6: Effects of Increasing K on Velocity of the Main Channel 63
Figure 4.7: Effects of Angle Variation on Velocity..... 65
Figure 4.8: Effects of Cross-Sectional Area Variation on Velocity in the Main Channel 67
Figure 4.9: Effects of Variation of Length of Lateral Inflows on Velocity in the Main Channel..... 69
Figure 4.10:Effects of Increasing K on Velocity of the Main Channel 71
Figure 4.11:Effects of Angle Variation on Velocity in the Main Channel..... 72
Figure 4.12:Effects of Cross-Sectional Area..... 74
Figure 4.13:Effects of Variation of Length of Lateral Inflows on Velocity in the Main Channel..... 75

SYMBOLS AND INDEX OF NOTATIONS

A	Cross-section area of the main channel flow (m^2)
A_1	Cross-section area of zone 1 (m^2)
A_2	Cross-section area of zone 2 (m^2)
A_3	Cross-section area of zone 3 (m^2)
Q	Discharge of the main channel ($m^3 s^{-1}$)
q_1	Discharge per unit width of the channel of the first lateral inflow
q_2	Discharge per unit width of the channel of the second lateral inflow
q_k	Discharge per unit width of the channel of the k^{th} lateral inflow
ϑ_1	Inclined angle of the first lateral inflow
ϑ_2	Inclined angle of the second lateral inflow
ϑ_k	Inclined angle of the k^{th} lateral inflow
L	Length of the main channel (m)
L_1	Length of the first lateral inflow (m)
L_2	Length of the second lateral inflow (m)
L_k	Length of the k^{th} lateral inflow (m)
T_w	Top width of the main channel (m)
T_1	Top width of the first lateral inflow (m)
T_2	Top width of the second lateral inflow (m)
T_k	Top width of the k^{th} lateral inflow (m)

H	Radius (m)
h	Depth (m)
h_1	Depth of the flow in zone 1 (m)
h_2	Depth of the flow in zone 2 (m)
h_3	Depth of the flow in zone 3 (m)
v	Mean velocity of the main channel (m/s)
g	Acceleration due to gravity (ms^{-2})
n	Manning coefficient of roughness
s_0	Slope of the channel bottom
s_f	Friction slope
p	Wetted perimeter of the channel cross-section (m)
t	Time (s)
u	Uniform inflow (m^2s^{-1})
x	Displacement in the main flow direction (m)
β	Momentum coefficient
D_h	Hydraulic depth (m)
C	Chezy Coefficient
Fr	Froude Number
Re	Reynold Number

ABBREVIATION AND ACRONYMS

MATLAB	Matrix Laboratory
HELB	Higher Education Loans Board
CFD	Computational Fluid Dynamics
RNG	Re Normalization Group
3D	Three Dimensional
HEC-RAS	Hydrologic Engineering Center - River Analysis System
VZ-MC	Near Bank Vegetated Zone - Main Channel
CRC	Cyclic Redundancy Check
W/H	Flow Aspect Ratio
RMM	Rough Model Method
CUIRF	Chuka University Internal Research Fund
NACOSTI	National Commission for Science Technology and Innovation

CHAPTER ONE

INTRODUCTION

1.1 Background Information

A structure that allows liquids to pass through and can enable liquid flow through pipes is called a conduit or open channels, (Chow, 1959).The free surface of pipe flow doesn't exist in open channel flow. The term "free surface" refers to the interface between a liquid and the gaseous fluid above it (Chow, 1959). Open channels typically refer to natural or constructed water conveyance systems that have open tops, allowing for unrestricted water flow (Henderson, 1957). These channels are essential for many hydraulic and environmental uses, including irrigation, drainage, and stormwater management (Chow, 1959). In many cases, open channel designers encounter challenges in managing unforeseen volumes of water, particularly in regions like Kenya and other countries. To address these challenges, canals with diverse cross-sections, including circular, triangular, rectangular, trapezoidal, elliptical, parabolic, and horseshoe shapes, has been constructed (Linsley *et al*.,1991).

Ojiambo *et al*., (2014) developed a mathematical model of fluid flow with a circular cross-section. The study found that the rate increases from the conduit's lowest point to the uninterrupted flow, with the highest rate in a static flow sector situated directly under the free surface. The findings also indicated that lowering the flow depth and cross-sectional area of the conduit increases the velocity. The study did not consider the effects of lateral inflows. Jomba *et al*., (2015) developed a mathematical model with a horseshoe-shaped cross-section for fluid flow in an open conduit. The research found out that when flow velocity increases and approaches the free stream in a constant flow area, the depth increases. Furthermore, the study found that greater shear stresses cause a decrease in velocity in response to increases in the roughness coefficient and hydraulic radius. This study focused on a horseshoe cross-section without accounting for lateral inflows.

Omari *et al*., (2018) developed circular conduits for wastewater pipes. As sewage flow cross-sectional area grows, the results indicate that sewer depth decreases. It was also noted that sewage flow velocity is increased by decreasing the friction slope and by increasing the tunnel's degree of inclination.

Floods remain a persistent issue in Kenya, necessitating the design of an efficient system to divert water from flood-prone areas to regions where it can be used for agricultural irrigation and hydroelectric power production. The flow in open channels is driven by differential potential energy. Discharge from a lateral inflow channel occurs when water or fluid is introduced in the direction of flow (Henderson, 1966). Lateral inflow channels replenish water in streams, rivers, or lakes, whereas lateral outflow channels remove water from these bodies. Additional lateral influx can come from overland and groundwater flow. Open channel flow is a well-studied area, with research conducted on both man-made and natural channels, including irrigation canals and rivers.

The main forces affecting open-channel flows include gravity, viscosity, and inertia, each playing a significant role. Open-channel research has been of interest, and the Chézy formula stands out as one of the earliest formulas used to determine the average velocity of uniform flow. Developed by the French engineer Antoine Chézy, the Chézy formula is widely applied in hydraulic engineering to estimate flow velocities in open channels. However, it has been criticized for providing unsatisfactory results in certain situations. One of the primary limitations lies in its simplicity and generalization. The formula assumes a constant roughness coefficient, which may not accurately represent the varying roughness conditions in real-world open channels (Linsley *et al*.,1992).

Additionally, Chézy's formula may struggle to capture the complexities of flow patterns in channels with irregular geometry or significant changes in slope. Advances in hydraulic modeling and understanding of fluid dynamics have led to the development of more sophisticated methods, such as the Manning's equation, which allows for a more nuanced consideration of channel characteristics. The limitations of the Chézy formula highlight the need for improved models that can better accommodate the diverse conditions encountered in open channels, ensuring more accurate and reliable results for designers and engineers in hydraulic applications (Henderson *et al*.,1966).

The Manning formula, devised by Manning in 1895, is the most frequently employed equation in the study of open channels. It incorporates the Manning constant, a roughness coefficient, to calculate flow characteristics in open channel scenarios. This equation's reliability and suitability have made it a preferred choice in the design of open channels. According to Chadwick Morfeit *et al*., (1993), the Manning coefficient con-

siders factors such as the channel's irregularity, size, bed material, shape variability, and the impacts of obstructions, meandering, and vegetation growth. The continuity equation is a differential formula that controls the motion of a retained variable, often mass (Batchelor, 1967). It is a fundamental idea in fluid dynamics. According to this equation, each region's total conserved quantity can only vary by the amount that enters or leaves across its boundary (Chow, 1959). It embodies the principle that while a conserved quantity can move from one place to another, it cannot be created or destroyed, integrating the transport theorem and the law of mass conservation (Chow, 1959).Equation 1.1: represents St. Venant's continuity equation, which governs flows in open channels of various shapes.

$$\frac{\partial A}{\partial t} + \frac{\partial Q}{\partial x} = q \tag{1.1}$$

Equation 1.1 can be modified to obtain the specific continuity equation governing fluid flow with a horseshoe cross-section with lateral inflows.

The second law of motion of Newton, which forms the basis of the conservation of momentum equation, states that the alteration in momentum of an object equates to the cumulative external force exerted upon it. External forces are classified into two categories: surface forces and body forces. Body forces encompass gravitational, magnetic, centrifugal, or electric fields, while surface forces include static pressure and viscous stresses. Surface forces arise from the interaction between the body and its surroundings, acting on the bounding surfaces. They are quantified as stress, representing force per unit area. Body forces, on the other hand, act within the body itself. A system of partial differential equations known as Saint-Venant's equations characterizes the one-dimensional flow of shallow water in open channels (Chow (1959).

The Navier-Stokes equations serve as the foundation for these equations, which have been simplified to accommodate the shallow water assumption, wherein the characteristic length scale is significantly smaller than the flow depth (White, 1999). The Navier-Stokes equations are simplified into Saint-Venant's equations, which are essential for understanding the dynamics of shallow water flow. The key components of Saint-Venant's formula is the momentum formula, which is crucial to understanding the complex physics of fluid flow in such situations.The Navier-Stokes equations are vertically integrated to get the simplified equation, which takes the pressure gradient, bed

slope, and frictional effects into account (Chow, 1959). Utilizing the momentum equation in Saint-Venant's form, engineers and scientists can forecast water levels, velocities, and other relevant parameters, enabling the prediction and analysis of open channel flow behavior. Equation 1.2 represents St. Venant's momentum equation, which governs flows in open channels of various shapes.

$$\frac{\partial v}{\partial t} + \beta\frac{\partial v}{\partial x} + g\frac{\partial y}{\partial x} = g(s_f - s_0) \tag{1.2}$$

The general momentum equation 1.2 can be modified to get the specific momentum equation controlling fluid flow in a horseshoe cross-section with lateral inflows.This research aims to explore the design of a channel capable of efficiently transporting maximum discharge from flood-prone areas to land designated for irrigation. Flooding remains a persistent problem. While there has been extensive research on open channels with diverse cross-sectional shapes, there is a notable lack of studies focusing on horseshoe-shaped channels with lateral inflows.

1.2 Statement of the Problem

Horseshoe-shaped channels have not gotten much attention in open channel flow studies, which have largely concentrated on trapezoidal, circular, parabolic, and rectangular channels. Since horseshoe channels have larger bottoms than circular channels, they have a higher space utilization rate. Numerous investigations on various channel cross-sections have been conducted, but none in horseshoe. Rapid development and inadequate planning lead to excessive runoff that exceeds the capacity of the current storm water drains, which is one of the primary causes of flooding. This research aims to investigate the effects of changing lateral inflow cross-sectional area, lateral inflow conduit length, lateral inflow rate increases, and lateral inflow conduit angle variations on the flow rate in an open horseshoe-shaped conduit.

1.3 Objectives of the Study

1.3.1 Main Objective

The main objective of the research is to model fluid flow in an open horseshoe conduit with lateral inflows

1.3.2 Specific Objectives

The specific objectives of this study is to:

i Determine the effects of increase of lateral inflows on the main channel velocity.

ii Evaluate how increase of lateral inflow channels angles affect the main channel velocity.

iii Establish how increasing the lateral inflow channels' cross-sectional area affects the rate of primary channel .

iv Compare how increasing the lateral inflow canal length affects the main channel velocity.

1.4 Significance of the Study

Flooding has long been an issue, particularly after a lot of rain. In an effort to lessen flooding, people have built canals and channels that channel water into rivers, lakes, and the ocean. Even engineers have encountered difficulties while creating drainage ditches, floodways, navigation channels, irrigation canals, and other hydraulically efficient channels for transporting the most water possible for the purpose of producing electricity. Among the difficulties are seasonal variations, such as runoff- and rainfall-induced sedimentation and flooding according to Chow (1988).

Previous research on open channel flow has primarily concentrated on rectangular, parabolic, trapezoidal, and circular shapes, while horseshoe channels with lateral inflows have received limited attention. The rapid urban development and insufficient planning often result in excessive runoff that exceeds the capacity of existing stormwater drains, contributing significantly to flooding issues.The goal of this suggested study is to shed light on flood control structure design. Additionally, this research will assist engineers in creating open horseshoe channels that are hydraulically effective for transferring the most water possible for agriculture, producing hydroelectric power, and minimizing flooding.

1.5 Basic Assumptions

The model equations governing fluid flow in this study will be developed based on the following assumptions and approximations.

i The fluid is considered to be incompressible.

ii It is assumed that the flow is laminar.

iii The fluid flow is unsteady (time dependent).

iv The fluid is a newtonian flow.

v The channel is prismatic.

vi The principal velocity component of the one-dimensional flow is dependent only on x and is along the x-axis.

vii The flow is driven solely by gravitational forces.

viii The region between the lateral inflow conduit and the primary open conduit has minimal accumulation of sediment.

ix The lateral inflow conduit and the primary open conduit have minimal turbulence.

1.6 Operational Definition of Terms

In this study some terms used often are defined in subsection 1.7.1.

1.6.1 Fluid

Fluids are substances that flow and change constantly when they are subjected to outside forces. They consist of both liquids and gases and are neither characterized by a fixed shape nor by the ability to take on the shape of their container. A classic definition places emphasis on a fluid's capacity to flow; liquids like water and gasses like air are examples of this property. An fundamental component of fluid mechanics, the scientific and technical field that analyzes fluid movement, is viscosity, a measurement of a fluid's resistance to deformation. Truesdell *et al*.,(1949), defined fluids as substances that even under even minimal shear stress will undergo continuous deformation. Moreover, the continuum assumption is frequently used in fluid science, regarding fluids as continuous materials as opposed to discrete particles. This assumption allows differential equations to be used to macroscopically describe fluid behavior and motion. As defined by Cengel and Cimbala (2014), a fluid is a substance that constantly deforms upon the application of shear (tangential) stress, regardless of how little the stress may

be. This method included the significant element of shear stress, which highlighted the fluids' adaptability to forces applied parallel to their surfaces. Both definitions retain the crucial aspect of flow and deformation caused by applied forces, which is necessary to comprehend fluids in the context of fluid mechanics.

1.6.2 Incompressible flow

The kind of fluid flow known as incompressible flow is one in which pressure variations have no effect on the fluid's density. This assumption simplifies the mathematical analysis of fluid dynamics because it eliminates the need to account for density variations within the flow field. Incompressible flow is often applicable to liquids, such as water, and to gases moving at low velocities where changes in pressure do not significantly affect density. The assumption of incompressibility is a cornerstone in the study of fluid mechanics, particularly in areas like hydrodynamics and aerodynamics, where it allows for more straightforward modeling and prediction of fluid behavior.

The concept of incompressible flow is crucial in engineering applications such as pipeline design, pump systems, and open channel flow. Equations like the Navier-Stokes equations and the continuity equation are used to characterize the conservation of mass and momentum when analyzing incompressible flow. The incompressible flow assumption simplifies these equations, making it easier for engineers to design and optimize fluid systems. The incompressible flow assumption is a crucial tool in both theoretical and applied fluid dynamics since it offers a sufficiently accurate approximation for many practical applications, even though real fluids may occasionally show modest compressibility.

1.6.3 Laminar Flow

There are two different forms of fluid motion: laminar flow and turbulent flow. Each has its own patterns and characteristics. Laminar flow is the term used to describe the smooth and organized passage of fluid particles as the fluid's layers slide past one another. According to Icha *et al.*, (2012), Laminar flow happens when fluid elements travel in adjacent layers, experiencing minimal intermixing between them." Because it usually happens at lower speeds and has clearly defined streamlines, this kind of flow is simpler to forecast and study in fluid dynamics. In turbulent flow, however, the movement of

the fluid particles is more unpredictable and chaotic. Swirls, eddies, and mixing are produced throughout the flow field by the random changes in fluid velocity components that occur in turbulent flow. According to Munson *et al.*, (2012), turbulent flow is described as ”an irregular condition of fluid motion characterized by fluctuations in velocity and pressure.” Higher velocities are typically associated with turbulent flow, which is controlled by variables like the Reynolds number, which measures the fluid’s ratio of viscous to inertial forces. The transition from laminar to turbulent flow is determined by the Reynolds number, a dimensionless metric characterizing the flow regime. Flow is typically laminar at lower Reynolds numbers and more turbulence-prone at higher Reynolds numbers. This transition’s critical Reynolds number varies according to the fluid’s properties and flow shape, among other things. Reynolds number thresholds are used by engineers and researchers to assess and forecast the kind of flow that a given system might display.

1.6.4 Viscosity

A key characteristic of fluids that describes their resistance to flow and deformation is called viscosity. It measures how easily a fluid’s particles can pass one another or how much internal friction it is. Icha *et al.*, (2012) described Viscosity as ”the property of a fluid that opposes the relative motion between its adjacent layers or particles”.” This definition highlighted the role of viscosity in impeding the flow of one layer of fluid past another, contributing to the fluid’s overall resistance to deformation. Shear resistance, often known as frictional drag, is the equal and opposite force that a boundary, in reaction to a fluid’s shear stress, applies to the fluid. The Reynolds number and the channel’s form both affect the drag coefficient. At low Reynolds numbers, where viscosity dominates, the fluid experiences significant deformation drag. As the Reynolds number increases, indicating lower viscosity effects, such as in air and water, the influence of viscosity becomes confined to the boundary layer. In such cases, deformation drag is primarily frictional drag, where shear forces on the channel surface due to the boundary layer formation contribute to the overall friction drag.

1.6.5 Unsteady Flow

Steady flow and unsteady flow are two distinct states of fluid motion, each exhibiting specific differences in how they vary over time and space.The characteristics of the fluid

at any one point in the system do not change over time when there is steady flow. Icha *et al*., (2012) defined steady flow as ”a condition in which the fluid characteristics at a point in the fluid do not vary with time.” At any fixed point in the fluid across time, the velocity, pressure, density, and other fluid parameters stay the same while there is steady flow. This allows for a simplified analysis of fluid behavior since there is no need to consider the effects of time-varying conditions. Conversely, Unsteady flow, also referred to as transient flow, occurs when fluid characteristics at a specific location change continuously over time. According to Munson *et al*., (2012), unsteady flow is described as ”fluid properties that can change with time and location.” In unsteady flow, variations in velocity, pressure, and density occur, introducing time-dependent considerations into the analysis. This type of flow often occurs during the initiation or cessation of flow, as well as in scenarios with rapidly changing conditions.The transition between steady and unsteady flow depends on the specific circumstances of the fluid system. For instance, the sudden opening or closing of a valve in a pipeline may induce unsteady flow until the system reaches a new equilibrium. In engineering applications, knowing the difference between steady and unsteady flow is important, especially in fields like fluid dynamics where the design and optimization of diverse systems depend on the ability to predict and manage fluid behavior.

1.6.6 Prismatic Channel

Prismatic channels and non-prismatic channels represent two distinct types of water-course geometries, each with its own implications for hydraulic and hydrodynamic characteristics. A prismatic channel maintains a uniform cross-sectional shape throughout its entire length, ensuring consistent geometry from the beginning to the end of the channel. Chow (1981) defined prismatic channel as a channel ”whose cross-section is the same at all sections along its length.” The uniformity of the channel geometry simplifies the analysis of flow properties, making it easier to predict water depths, velocities, and other hydraulic parameters. Conversely, non-prismatic channels exhibit varying cross-sectional shapes along their length. These variations can result from changes in channel width, depth, or slope. The irregularity in cross-sectional geometry introduces additional complexities into the analysis of flow characteristics. According to Chaudhry (2008), non-prismatic channels are characterized by ”cross-sections that change grad-

ually or abruptly along the channel length." The variability in channel geometry may lead to changes in flow velocity, turbulence, and sediment transport, requiring more sophisticated modeling techniques to accurately predict and manage the flow dynamics.

1.6.7 Boundary Layer

The no-slip condition, which is defined as having zero fluid velocity at the solid surface, and the boundary layer, which is the fluid layer separating the surface from the free stream fluid, are key concepts in fluid dynamics (White, 1999). Thin layers of fluid particles near a surface where viscous forces predominate are known as boundary layers. The free stream area, where viscous forces have very little effect, is located beyond this layer. An understanding of boundary layer thickness is essential when examining convective transport flow problems. The quantity that relates the relative thicknesses of hydrodynamic and thermal boundary layers is called the Prandtl number, after Ludwig Prandtl, a well-known German aerodynamicist who was instrumental in the development of boundary layer theory (Schlichting, 1979). This dimensionless number is essential in linking the velocity and temperature distributions. When the fluid temperature at the plate surface differs from the free stream temperature, a thermal boundary layer is created. Surface temperature of the plate is reached equilibrium by fluid particles in contact with it. Temperature gradients form as a result of these particles exchanging heat with surrounding fluid layers. The thermal boundary layer refers to this area of the fluid where these temperature variations happen. The surface of the plate and the fluid particles in contact with it both attain the same temperature. They transfer heat to adjacent fluid layers, creating temperature gradients. This area within the fluid is known as the thermal boundary layer. As real fluid particles contact a surface, their velocities gradually decrease, slowing down the adjacent fluid layers' motion (Incropera DeWitt, 2002).

1.6.8 Dimensional Analysis

Dimensional analysis is a technique used to describe natural phenomena through equations that correctly balance dimensions among key variables influencing the phenomenon (Barenblatt, 2003). It enables the derivation of equations that interrelate all physical aspects of a problem. By employing dimensionless groups like Reynolds number, Froude number, and Prandtl number, dimensional analysis simplifies equations into a

non-dimensional form. The method relies on the principle of dimensional homogeneity, ensuring that equations expressing physical relationships between quantities are dimensionally consistent.

Dimensional analysis yields quantitative insights through experimental data and is crucial for studying fluid flow problems. It efficiently condenses experimental findings into a concise format. This approach involves using dimensional properties of relevant variables from a prototype to analyze the behavior of actual objects. The primary techniques in dimensional analysis include the Rayleigh method and the Buckingham theorem (Fink, 2009).

CHAPTER TWO

LITERATURE REVIEW

2.1 Overview

Open channels were first investigated in 1768 by the French engineer Chezy, who carried out pioneering studies. He introduced Chezy's formula and the concept of Chezy's constant. However, Chezy's formula did not meet engineers' expectations as it oversimplified the intricate dynamics of open-channel flows and lacked broad applicability under various conditions. Additionally, Chezy's coefficient can vary widely for different channels, making it challenging to predict accurate velocities in situations where the formula's assumptions are not met or where channel characteristics deviate significantly from the conditions under which it was developed (Chezy 1768). Manning discovered the manning formula (Chow, 1958). A roughness coefficient called the Manning Coefficient was found during the investigation. The channel's size and shape fluctuations, the degree of irregularity in the conduit, the vegetation growing in the conduit, meandering, and the relative influence of impediments in the path are all taken into account by this coefficient.

Jebeli *et al*., (2022) used computational fluid dynamics (CFD) to study numerical simulations of the impact of lateral input in an open conduit in order to minimize disturbances in the mainline conduit. According to the study, branch placement becomes more difficult the longer and more curved the channel is. When the circulation was reduced, the water flow after the curve was determined and replicated. Computational fluid dynamics was used to calculate the flow simulation inside the conduit, assuming incompressible, unstable, two-phase channel flow. Furthermore, the Naiver-Stokes formula and the Re Normalization Group (RNG) model were used to simulate the flow. The findings showed that a higher number of system inlets and appropriate placement of each inlet significantly minimize the strength of turbulence in the flow at the inlet, all while keeping a consistent inflow and fluid velocity.

2.2 Lateral Inflows

Neary *et al*., (1999) focused on lateral-intake inflows with a numerical model in three dimensions. A three-dimensional (3D) computational model was developed to predict turbulent, stable flows via lateral intakes with mean-oriented rough walls.In the Reynolds-

averaged Navier-Stokes formula, the method used Wilcox's isotropic k-ω turbulence model to compute the near-wall flow and easily takes roughness effects into account. The flows via rectangular T-junctions with closed ducts and open channels were calculated. It is evident that the model quite properly describes most experimental patterns when comparing the expected mean velocity field with laboratory results.A variety of aspect ratios, flow rate ratios and major conduit-bed-roughness distributions are considered for estimating flows for the parametric study. An study of the numerical solutions shows complex three-dimensional flow patterns of lateral-intake flows, including singular points, vortices, and zones of flow division, separation, and reversal within the bed-shear stress vector field. The model offers fresh insights into the intricate hydraulics and sediment dynamics while replicating well-known 3D flow patterns.

Kadia *et al*., (2024) investigated the impact of cross-sectional geometry on high-speed narrow open conduit flows. Investigating the impact of conduit cross-sectional geometries (horseshoe, circular, and archway) on bed shear stress distributions, secondary currents, turbulence features, and mean velocity fields in supercritical narrow open channel flows was the goal of the study. Furthermore, it limits the lateral growth of the bottom vortex and the vertical expansion of the emerging intermediate vortex, both of which are linked to the reduced turbulence anisotropy gradient in the corner zone. Moreover, since sidewall curvature alters the near sidewall longitudinal velocity gradient, it reduced the convergence of the main contour lines that reflect Reynolds shear stress.

Marjang & Merkley, (2009) studied into the velocity profiles in cross sections with rectangular and compound open channels. The study found out that rectangular channels, the velocity profile are relatively uniform in the central region of the channel but decreased near the channel boundaries due to friction. This boundary layer effect is caused by the interaction between the flowing water and the channel walls and bed, which slows the flow near these surfaces. The study constructed a 3-D hydraulic model to compute discharge, surface rate coefficients and rate profiles for rectangular and compound open-conduit cross sections under continuous, uniform flow conditions. The Reynolds-averaged Navier-Stokes formulas, Reynolds stress formulas, and kinetic energy and dissipation formulas were applied to the model using the k–ε turbulence model and the finite-volume technique.

Liu *et al*., (2010) developed the equations for determining the critical depth and shape of typical horseshoe tunnels. General equations for the geometric components of all varieties of horseshoe cross-sections, which are utilized in water transportation projects including irrigation, drainage, and water supply projects, were given by the study. Iterative formulas for determining the critical depth of a horseshoe cross-section were obtained through research. These formulas can be used to precisely handle significant depth concerns in computer programming.Moreover, general estimation formulas were developed for the direct computation of critical depth for any typical horseshoe cross-section types, based on the idea of gradual optimization fitting. Hydraulic designers can employ the estimation equations because, when compared to the exact critical depth determined by means of the iterative formulae, they exhibit a high degree of accuracy.

Macharia *et al.,* (2014) studied a fluid flow in an open rectangular conduit with lateral input conduits. The research revealed that increasing the angle of lateral inflow did not lead to higher fluid velocities in the primary conduit. In fact, as the cross-sectional area of the lateral inflow expanded, the flow rate in the primary conduit diminished. Furthermore, while the flow rate in both conduits decreased with a longer lateral inflow conduit, it did increase in the open rectangular conduit when the velocity of the lateral inflow increased. The study found that the primary flow was unaffected by changes in the lateral inflows.

Karimi *et al*., (2018) investigated a flow in a rectangular open channel with a lateral input conduit. The findings showed that the rate in the primary conduit increases with both the area and length of the lateral inflow conduit. Conversely, as the rate within the lateral inflows increases, the velocity in the primary conduit itself tends to decrease. Additionally, contrary to what was anticipated, there is not always a direct positive correlation between the angle of the lateral inflow conduit and the velocity of the primary conduit.

Omari *et al*., (2018) conducted a research on circular closed conduits of effluent lines. According to the study's conclusions, a sewer's depth can be decreased by increasing its cross-sectional flow area. It was shown that sewage flow velocity increases when the friction slope decreases. Furthermore, increasing the incline of the tunnel also results in higher sewer velocities. This study focused on circular closed channels for sewer lines

without lateral inputs, highlighting the need for similar investigations into sewer lines with lateral inflows.

2.3 Variation of the Angle of Lateral Inflow

Chaudhry *et al*., (1983) modelled unsteady-flow water temperatures. Simulating one-dimensional unsteady flows in a river-lake system with time-varying lateral inflows and different cross-sectional fluctuations throughout its length was the key objective of the study. Initial steady state conditions for the hydraulic section were determined by applying an implicit finite difference method to the numerical integration of the one-dimensional Saint Venant equations, which yielded the unsteady flow conditions, and a fourth-order Runge-Kutta method to the flow equation that varied gradually. By using an upwind implicit finite difference method to solve the partial differential equation, the water temperature of unsteady flows was determined.

Kwanza *et al*., (2007) investigated the Impacts of channel flow rate, breadth, and gradient of the conduits that are trapezoidal in shape and rectangular in shape.The study demonstrated that trapezoidal open channels have greater hydraulic efficiency than rectangular ones. An increase in these parameters was found to enhance the flow volume. However, this study did not look at how changing the lateral input angle affected the velocity of the main flow.

Marangu *et al*., (2016) developed a fluid flow model with a segmented base and a trapezoidal shape.The study found that a decrease in flow rate is the outcome of increasing the flow's cross-sectional area. Similarly, decreased flow velocities are also caused by an increase in the flow conduit's radius and cross-sectional area as well as a higher roughness index. Furthermore, the research revealed that a decrease in flow velocity occurs when the circular segment's radius increases.The findings showed that when cross-sectional area, conduit radius and flow depth increase, fluid velocity drops correspondingly. The findings also showed that higher flow velocities are a direct consequence of increasing the waterway's bed slope. The impact of lateral inflow on channel velocity.

Natasha & Noviantri (2019) used the finite difference method to study the Saint-venant model analysis of trapezoidal open conduit water flow. The study focused on simulating unsteady flow in such conduits, demonstrating that the method effectively captures

changes in flow depth and velocity over time. The results showed that the trapezoidal channel shape significantly influences flow behavior, especially in terms of water surface elevation and velocity distribution. The study concluded that the finite difference approach is a reliable tool for predicting flow characteristics in trapezoidal channels, aiding in the design and management of water conveyance systems.

Al Omari *et al*., (2012) conducted a laboratory research examining the impact of branching angle and branching channel slope on flow. According to the study, the branching conduit's bed slope increases as the discharge ratio does as well. Additionally, it was discovered that the angle 60° yields the maximum discharge ratio, followed by 90° and 30°. The results of the study also demonstrated a negative link between the discharge ratio and the Froude number in the downstream primary conduit and a linear, direct proportionality to the Froude number in the upstream primary conduit and the branching conduit. The discharge ratio has an inverse and linear relationship with the ratio of the water depth in the branching conduit to the water depth in the primary conduit downstream.

2.4 Cross-Sectional Area of Lateral Inflow

Tuitoek and Hicks (2001) constructed a model to manage floods by simulating unsteady flow in compound channels. The model demonstrated that the interaction between the faster flows in the main channel and the slower flows on the floodplains plays a critical role in predicting flood dynamics. The findings emphasized that accurate flood forecasting in compound channels requires accounting for the complexity of these flow interactions to better manage flood risks. To address momentum transfer problems the work established the St. Venant equations of flow and improved them with extra elements. The full dynamic equations were applied to the main channel, while a diffusive model was employed for the floodplains. The study introduced terminology to describe both momentum and mass transfer processes within the system.

Litrico and Fromion (2004) investigated open-channel flow frequency modeling. The study introduced an alternative computational technique for producing a frequency domain model of the Saint-Venant equations linearized around any stationary state, including backwater curves. The technique allowed for more efficient and flexible modeling

of flow dynamics, particularly for systems where flow conditions change slowly over time. This approach provided a more accurate and computationally efficient way to analyze flow control in open channels, enhancing the understanding of flow behaviors under various conditions.

Qiu *et al*.,(2023) studied the effect of cross-sectional form on the flow capacity of open channels. The study developed an extensive formula for flow capacity and determined a parameter that describes how cross-sectional geometries impact flow capacity using ideas from viscous fluid theory. The method's formula simplifies the process of figuring out the parameter, which varies depending on the overall flow field parameters. To establish cross-sectional forms in the investigation, the width to wetted perimeter ratio was specifically utilized. As a summary, the following describes the relationship between this parameter and several cross-sectional shapes. The variable was related to the ratio of width to wetted perimeter as well as the Reynolds number in turbulent flow at medium or low Reynolds numbers. However in turbulent flow, at high Reynolds numbers, the parameter no longer depended on these characteristics.

Thiong'o *et al*., (2013) conducted a research on examining fluid flows in open rectangular and triangular channels, yielding important insights into fluid behavior in these particular geometries. The study revealed distinct differences in flow characteristics between rectangular and triangular channels. In rectangular channels, the researchers found that flow velocities were relatively uniform across the width of the channel, with higher velocities occurring near the center. However, in triangular channels, flow velocities varied significantly between the channel's apex and base, with the highest velocities concentrated near the apex. Additionally, the study highlighted the impact of channel geometry on flow resistance, with triangular channels experiencing higher friction losses compared to rectangular ones. These findings underscored the importance of understanding how channel geometry influences flow behavior for effective design and management of open channel systems. Furthermore, the research provided valuable insights into the hydraulic performance of different channel shapes, which can inform engineering decisions in various applications, such as urban drainage systems and irrigation networks.

Merkley (2005) modelled a standard horseshoe cross section geometry. According to the study, many open-conduits and pressurized conduit water conveyance tunnels embrace the standard horseshoe-cross design. The exact geometric connections for this cross section are necessary for mathematical modeling and hydraulic research, since look-up tables with numerically estimated values are typically just as weak, if not slower, when implemented in computer systems. The implicit solutions of the unstable hydraulic equations require precise, analytical partial derivatives of certain of the relationships for numerical stability and accuracy. Standard horseshoe sections include partial derivatives of the two parameters, depth to area centroid and wetted perimeter with regard to water depth, as well as equations for cross-sectional area, wetted perimeter, top width, and depth to area centroid as functions of water depth.

Shashkin *et al*., (2017) investigated a multi-channel complex fluid flow mathematical model. The study concentrated on a numerical hydraulic model that permits the automatic visualization of the structure while simulating fluid flow in a complex, arbitrarily designed multi-conduit system. A system's primary components are its conduits, which were joined together by a specific combination of coupling elements (knots, local resistance). The continuity equation and momentum conservation served as the foundation for the conduit process models. Using the devised approach, matrices of internal and regional boundary conditions were formed to create the system structure. The model was used to generate the algorithm, which was then used to develop the application program. The application program makes it possible to ascertain the properties of a fluid flow steady state in the complex multichannel structures. Harmizi*et al*., (2023) investigated the flow depth behavior in a splitting open-conduit for a trapezoidal and rectangular shapes. To calculate the upstream flow depth in rectangular and trapezoidal cross-sectional conduit, the study adapted the general equations of splitting open-conduit flow for both forms into non-linear polynomial equations. Using the Newton-Raphson method in Maple software, the water flow depth as affected by the discharge ratio and Froude number was calculated. The research demonstrated that there is a resemblance in the flow depth between trapezoidal and rectangular conduit when the discharge ratio is low. On the other hand, the rectangular conduit's flow depth exceeded the trapezoidal conduit's when the discharge ratio rises. Moreover, the rectangular conduit has a deeper flow than the trapezoidal conduit when the Froude number grows.

Kinyanjui *et al*., (2011) conducted a study to examine fluid movement through unobstructed channels with a circular shape. According to the work, fluid velocity decreases as flow depth increases. Moreover, it was shown that flow velocity increased with higher channel slopes and reduced with increasing channel radius. The study also discovered that lowering the channel slope lowers flow velocity since these variables are directly proportionate. Moreover, it was found that the flow rate increased with depth from the conduit bottom to the free stream for a constant flow area, peaking just below the free surface. The flow equations were solved by the researchers using the finite difference method, however they pointed out that the finite element method could potentially yield better accuracy.

Thiong'o *et al*., (2011) modelled a fluid flow in open conduit with cross-sections that were both triangular and rectangular. The findings demonstrated that hydraulic efficiency is higher in conduits with rectangular cross-sections than in conduits with triangular cross-sections. They also found that larger flow velocities in both types of conduits are caused by increasing the conduit's energy coefficient, top width, and slope. It was also observed that the flow velocity increased with depth, peaking a little below the free surface. Velocity profiles showed that a rectangular conduit flows water more efficiently than an open triangular conduit of the same depth and width. Nevertheless, the impact of lateral inflow on primary flow velocity was not investigated in this study.

Simons *et al*., (2019) studied physical hydrology. The study noted that water on the surface of the world has always been transported by flow through open channels by nature. The study arrived at the conclusion that fluid properties affect sediment transport, fluid motion, and channel shape. Among these are surface tension, temperature, elasticity, viscosity, shear, mass, density, weight, and specific weight. Flow in open channels can take many distinct forms. Among them are the following: steady and erratic flow; uniform and non-uniform flow; silent, fast, and ultra-rapid flow. Turbulence randomly produces small velocity fluctuations with an average duration value of zero in all directions.

Thiong'o *et al*., (2013) focused on the flow characteristics of open rectangular and triangular channels to evaluate their hydraulic efficiency.The investigation required the solution of partial differential equations that were nonlinear and based on the conserva-

tion of momentum and mass. Due to the complexity of these equations, the researchers employed the finite difference method, as analytical solutions were not feasible. Key variables such as flow depth and velocity played crucial roles in determining discharge, with extensive research conducted on how varying parameters affect velocity and how flow velocity changes with depth. The study acknowledged that employing the finite element method could potentially yield more precise results compared to the finite difference method used in their analysis.

The evaluation of velocity and discharge in D-shape and horseshoe cross sections was the main emphasis of Samani *et al.*, (2013). The investigation looked into the physical equations governing the cross sections. The discharge depth and maximum velocity were discovered concurrently by differentiating the Manning equation. Furthermore, dimensionless graphs were provided, making it simple to calculate area, perimeter, and water surface width. Eventually, dimensionless graphs were discovered for the purpose of determining the discharge, velocity, and profiles.

Jomba *et al*., (2015) developed a mathematical model to describe fluid flow in an open conduit with a Horseshoe cross-section. The results showed that, under constant flow area conditions, flow depth increases towards the free stream as flow velocity increases. Additionally, the study observed that higher roughness coefficients and hydraulic radii lead to increased shear stresses, which in turn decrease velocity.Additionally, a direct correlation between flow velocity and channel slope was observed by the researchers, indicating that a drop in channel slope leads to a comparable fall in velocity flow. Furthermore, when the flow's cross-sectional area increases, flow velocity falls. The study did not take lateral inflow effects into account and instead concentrated on the horseshoe cross-section.

Khosravinia & Hosseinzadeh Dalir (2019) studied the effect of the side slope of the channel on the flow in an open conduit junction by numerical analysis. According to the study, an increase in the Froude number and intake discharge ratio would cause turbulence to rise and reduce the analytical model's precision. Additionally, the main channel's side slope increased, which reduced turbulence and improved the analytical model's correctness. Chirchir *et al.*, (2021) investigated on how two lateral inflow channels affected the main river's discharge. The study found that an increase in the

cross-sectional area of the lateral inflow canals increases the flow velocity in the main conduit and a decrease in the length of the lateral inflow conduits increases the flow rate in the main conduit as well. Furthermore, lateral inflow conduits that are inclined at an angle of 45^0 enhance the flow velocity in the main channel more than those that are inclined at 60^0 and 72^0. Conversely, channels that are inclined at an angle of 90^0 keep the flow velocity in the primary conduit constant.

Ojiambo *et al*., (2016) conducted a comprehensive study on Finite Difference to investigate a fluid movement in a Circular Cross-Section Open Channel. The research yielded valuable insights into the behavior of fluid flow within such channels. One key finding was the confirmation of the accuracy and effectiveness of finite difference methods in modeling fluid flow dynamics. The study demonstrated that by discretizing the governing equations and solving them numerically, it was possible to accurately predict flow velocities and pressure distributions in circular open channels. Additionally, the researchers noticed that the flow velocity distribution changed along the channel's radial direction, with higher velocities happening nearer the center. This finding underscored the importance of considering radial variations in flow velocity for precise analysis and design of open channel systems. Overall, the study contributed significantly to the understanding of fluid flow in circular open channels and provided valuable insights for engineering applications.

Zhao *et al*., (2017) modeled an open conduit flow with a suspended canopy. Aquatic settings are frequently found with suspended canopies. Numerical simulations and lab tests were used to examine the mean flow velocity and Reynolds stress in the open channels with the suspended canopies. Numerical modeling was conducted using a modified Delft 3D-Flow model with a k–ε turbulence closure technique. To simulate the resistance effects of the hanging canopy, production and dissipation terms were added to the k and ε equations, respectively, and a resistance term was added to the fluid flow momentum equations.eynolds stress and mean flow velocity computed results agreed well with both the experimental data from this work and Plew (2010) published data.There are three broad zones that characterize the mixing layer's geographic progression toward the bottom of the suspended canopy: the fully established, developing, and diverging

flow zones. The investigation revealed a substantial relationship between the flow parameters and the density and thickness of the hanging canopy.

Gerrard *et al*., (1977) investigated Mathematical model representing blood flow in arteries. The model accounted for factors like pulsatile flow, arterial elasticity, and the non-Newtonian behavior of blood, which differs from standard fluid dynamics due to the complex nature of blood as a mixture of cells and plasma. The findings highlighted that understanding arterial flow requires considering both the mechanical properties of the arteries and the unique characteristics of blood flow, which can help in predicting circulatory issues.

Hasheminejad Wan (2022) used the finite volume method to model the Saint-Venant equations. A mathematical model for many different natural phenomena, including flood movement, was made possible by the Saint-Venant equations. The traditional horseshoe-cross design is used in many open-conduit and pressurized conduit water conveyance tunnels, according to the study. For mathematical modeling and hydraulic research, the precise geometric connections for this cross section are required because look-up tables with numerically approximated values are usually just as weak, if not slower, when implemented in computer systems. For numerical stability and accuracy, the implicit solutions of the unstable hydraulic equations require exact, analytical partial derivatives of some of the relationships. Equations for cross-sectional area, wetted perimeter, top width, and depth to area centroid as functions of water depth are included in standard horseshoe sections, as are partial derivatives of the two parameters, depth to area centroid and wetted perimeter, with respect to water depth. A solution flowchart was then used to solve the collection of discretized equations. In the end, the findings of the HEC-RAS computer program and the finite difference approach were used to compare the introduced model. The findings of the comparison showed that the solution flowchart was well-established and the suggested numerical model was accurate.

Maghrebi & Moghaddam (2022) modeled flow in both closed and open rectangular channels using moving walls. During the experiment, velocity contours and depth-averaged velocities were obtained and plotted in a rectangular channel with moving barriers. The walls moved in the opposite directions at the same speed. The study indi-

cated that the depth-averaged velocities and velocity contours will closely resemble the Couette flow between the two plates.

Mohammadiun *et al*., (2015) investigated the effects of flow pattern in a 90^0 junction caused by open-conduit geometry. The study noted that in order to lessen the possibility of sedimentation and erosion at a 90^0 open-channel junction, the study explored four new geometrical modifications using the streamlinization concept as a foundation. The numerical model was initially validated by means of earlier experimental study. Next, in order to improve their functionality, various efficiency metrics were developed after the effects of the aforementioned adjustments were assessed. Applying the recommended geometrical modifications significantly improves the flow pattern, as demonstrated by the results, by removing the recirculation zone and lowering the maximum flow velocity after the junction. As a result, the stagnation zone shrinks and the possibility for sedimentation and erosion is completely reduced.

Rezaei & Derakhshandeh (2023) carried out an experimental study on flow in a prismatic compound conduit with sloping floodplains. According to their research, the flow velocity is at its maximum immediately below the free surface. Relative depth increases in prismatic compound conduits lessen the velocity differential between the main channel and floodplains. The shear layer that forms between the primary conduit and floodplains has less of an impact at high relative depths (Knight *et al*., 2018). At relative depths between 0.1 and 0.3, the primary conduit and floodplains interacted at their maximum (Shiono and Knight, 1991; Rezaei, 2006).

Weber *et al*., (2011)developed a simulation of an investigation on flow at a 90^0 open-conduit junction. The study calculated the average velocity and turbulence intensity using a time series of measured velocities at each site. The basic flow characteristics observed and the specifics of the experimental approach are presented in this study. You can obtain the entire data set created during this experimental study from the Internet. An assessment of several previously offered theories of combining flow at open-channel junctions is presented using a subset of the collected data. According to the study, the experimental results can be reasonably predicted by the reduced mathematical model. The whole collection of data depicting combining flows at an open-channel 90^0 junction

is provided as a tool for 3D computational fluid dynamics codes that use a free-surface model to be validated.

Shi *et al*., (2023) studied the impact of submerged riparian vegetation on coherent structures, secondary currents, and velocity distributions in open channel flow was carried out by Shi *et al* in 2023. The study brought to light the important impact that riparian vegetation—which is typically seen in open channels and natural rivers—has on flow patterns. The lab experiment examined velocity distributions, secondary currents, and coherence structures in narrow open-conduit flow in the presence of submerged riparian vegetation. The Prandtl mixing length model was utilized in the investigation to examine the horizontal Reynolds stress's lateral distribution.The study revealed new information about the secondary current patterns in narrow open channels caused by riparian vegetation. These current patterns are responsible for the S-shaped vertical profile of longitudinal velocity at the interface between the vegetated zone (VZ) and the primary conduit (MC). This S-shaped velocity profile was ascribed to the creation of coherent structures, which resulted from vertical shear inside two vertical mixing layers. Correlations between longitudinal and vertical velocity fluctuations are facilitated by these features. Additionally, the investigation found that secondary transverse velocities, which show different degrees and orientations of inclination (clockwise or counterclockwise), have an impact on horizontal coherent structures along the VZ-MC interface.

Khosronejad *et al*., (2014) examined a computer model of sand waves in an open channel flow that was turbulent. The study demonstrated that the instability of the originally flat sand bed is caused by near-bed sweeps. The stratification effects that develop later in the bed evolution as a result of an increase in the concentration of suspended material in the flow must be taken into consideration in realistic simulations. When the amplitude and wavelength of bedforms develop and horseshoe-shaped vortices, which are dynamic, coherent structures that move near-bed fluid with low momentum and suspended particles away from the bed, form, boil events take place at the water's surface. It is demonstrated that sediment is trapped in the lee side of the crestlines by flow separation off the bedform crestlines. besides the sediment erosion caused by the faster flow over the stoss side.

2.5 Length of the Channel

Moramarco *et al*., (1999) established an analytical solution for channel routing with uniform lateral input. An analytical solution for the linearized Saint-Venant formula with uniformly distributed lateral inflow along the conduit was developed as a result of the research. The product of two functions was provided as the response. The response to the upstream input is represented by the first function, which has been determined by a number of earlier authors. The contribution from lateral or hillslope influx is represented by the second function, which has been determined in this study. The latter was also assessed in the study on a straightforward channel, and the outcomes showed strong agreement with a thorough numerical model for channels with bed slopes ranging from quite soft to high. The effects of the reference velocity and the channel-bed slope are investigated, and the linearization errors were demonstrated. A comparison of their execution times shows that analytical solutions are computationally more efficient than numerical answers. They are therefore the ideal option to incorporate into a dispersed rainfall-runoff model.

Rahman *et al*., (2012) studied a mathematical model of blood flow. The study noted that the study of fluid dynamics was crucial to understanding fluid movement within the human body, and cardiovascular physics places a lot of emphasis on blood flow models. Nevertheless, the models with three-dimensional analysis that have been constructed thus far are extremely complex. A brand-new, straightforward mathematical model was presented to explain blood pressure and flow.Blood is the primary fluid component of the cardiovascular system and flows via the arteries in the body. Although blood is a non-Newtonian fluid, the Navier-Stokes formula allow it to behave Newtonian-like most of the time. Simple differential equations that, under specific assumptions, characterized the circulatory system were created using the continuity formula and the Navier-Stokes formula. A general mathematical model of normal blood flow was developed using these assumptions. The typical blood pressure factors were then incorporated into this model by integrating Poiseuille's equation. After the investigation was finished, an analysis was done to confirm the suggested model. The investigation proved that the model accurately represents a number of blood pressure and blood flow properties.

Labadin *et al*., (2006) modelled a Mathematical model on arterial blood flow. The study of blood flow involves determining blood vessel flow and blood pressure. Understanding the factors that contribute to high blood pressure has motivated centuries of research on the blood flow problem. When a blood artery narrows from its typical size, this happens. This study provides a mathematical modeling of arterial blood flow that was created with the Navier-Stokes formula and a few presumptions. To determine blood flow and the cross-sectional area of arteries, a system of nonlinear partial differential equations was developed. Numerical solutions for the equations were obtained using the finite difference method. This contributes to the explanation of the hypertensive state since the result is highly sensitive to the beginning condition values.

Chepkonga *et al*., (2024) did a thorough investigation on the topic of mathematical modeling of fluid flow in sewerage systems' open circular channels.. The study revealed several crucial insights into the behavior of fluid flow in such systems. One significant discovery was the confirmation of the complex interplay between various parameters such as flow velocity, channel diameter, and slope, and how they affect the flow characteristics. The researchers observed that as the flow velocity increased, the flow became more turbulent, leading to higher friction losses along the channel. Additionally, they found that changes in channel diameter significantly influenced flow velocity distribution, with narrower channels experiencing higher velocities. Moreover, the research highlighted the importance of accurately predicting flow behavior to optimize sewerage system design and operation, emphasizing the necessity of robust mathematical models for such analyses.

Liu *et al*., (2010) modelled iterative formulas and estimating formulas for determining the normal depth of a horseshoe-shaped cross-section tunnel. The normal depth for various horseshoe cross sections can be determined using the iterative methods employed in the study. General estimation formulas were developed for the direct computation of the normal depth for all types of typical horseshoe cross sections, based on the progressive optimization fitting approach. The estimating formulas have a high degree of precision that hydraulic designers may use, and the largest relative error is less than 0.5% when compared to the exact normal depths calculated using iterative formulae.

Ojiambo *et al*., (2014) developed a mathematical model for fluid flow in an open conduit Using a circular cross-section. According to the research, flow velocity climbs from the conduit bottom to the free stream under conditions of constant flow area, reaching its maximum velocity somewhat beneath the free surface. The findings also demonstrated that increasing flow velocity is possible by decreasing the channel's cross-sectional area and flow depth. Furthermore, a decrease in the lateral input rate per unit length of the conduit results in higher flow velocity.

Agrawal *et al*., (2021) studied a mathematical modeling of blood flow. The interface between biology and mathematics has provided rise to and embraced new fields of mathematics where concepts from biology and mathematics are utilized in a complementary way. The study demonstrated that blood flow mathematical modeling using the study of fluid dynamics. Blood flow modeling is a major focus of cardiovascular physics, and fluid dynamics is important for understanding fluid flow in the human body. This research introduced a novel and simple mathematical representation of the blood flow and blood pressure through an artery. Blood is the primary fluid component of the cardiovascular system and flows through the body's many blood vessels. Although blood is not a Newtonian fluid, it behaves as such in many situations.The cardiovascular system equation, a simple differential equation, was developed with the assistance of the continuity equation and the Navier-Stokes equations under certain assumptions. Through the use of nonlinear partial differential equations, the artery's cross-sectional area and blood flow were determined. The finite modification method was applied to give the equations a numerical interpretation. The result found is very sensitive to the values of the initial conditions, which provides insight into the hypertensive state. A basic mathematical model of normal blood flow was established by applying this equation to the cardiovascular system and reasonable conventions.

Mose *et al*., (2019) modelled a fluid flow in an elliptical cross-section. A higher hydraulic radius led to an increased hydraulic depth, according to the study's findings. However, the fluid velocity falls along the channel as eroded particles accumulate up and the fluid flow depth drops. Variations in the friction slope also have an impact on flow velocity, with higher friction resulting in lower velocity. This study did not examine how the velocity of the channel is affected by lateral inflow. Loukam *et al*., (2020)

modelled a fluid flow in an open conduit. Chezy's resistance coefficient in a tunnel with a horseshoe form. The work led to the establishment of the resistance coefficient's mathematical formulation. Using various geometric profiles of conduits and channels particularly the horseshoe-shaped tunnel a general explicit relation of the resistance coefficient in turbulent flow was developed using the rough model method (RMM). The filling rate, discharge, longitudinal slope, kinematic viscosity of the liquid, and absolute roughness of the internal walls of the conduit are some of the variables that influence CRC. Additionally, the study's computation of CRC was based on a narrow range of variables, such as the discharge, the conduit's slope, the kinematic viscosity, and the absolute roughness. An additional explicit equation to efficiently compute this coefficient after its maximum value is attained is supplied. This is based on an analysis of the variation of CRC as a function of filling rate. The computation of Chezy's resistance coefficient in a tunnel with a horseshoe form is demonstrated using a few example calculations.

Rotich *et al*., (2021) examined open channel flows including a parabolic shape. The findings indicated that increased flow velocities are a function of channel slope and energy coefficient. On the other hand, velocity increases with decreasing top breadth. This study did not look at how lateral input affects the velocity of the channel. The finite element approach needs to be applied in order to solve the governing equations with greater accuracy. In order to address the persistent problem of flooding, current research focuses on building a canal that can transport maximum flow from flooded areas to irrigational land. A great deal of research has been conducted on open channels with various cross-sectional forms during the last 20 years, but not many of these studies have particularly addressed horseshoe channels with lateral inflows.The aforementioned research findings indicate that there hasn't been much focus on how lateral inflows. Consequently, the body of literature now in existence is insufficient to address the intricate dynamics relevant to the interaction between lateral inflows and the horseshoe channel, underscoring the necessity of conducting more in-depth research in this specific area.

CHAPTER THREE

METHODOLOGY

3.1 Model Formulation

The flow's mathematical model was developed in this chapter. The assumptions and approximations made in order to modify the Saint Venant equations, which regulate incompressible, laminar fluid flow. The universal rules of conservation of mass and momentum serve as the base for the equations controlling the fluid flow.

3.2 Mathematical Model Development

Let Q, q_1, $q_2 \ldots q_k$ represent the volume flow into the horseshoe open channel and the respective k^{th} lateral inflow channels. Let L_1, $L_2 \ldots L_K$ represents the length of the k^{th} and ϑ_1, $\vartheta_2 \ldots \vartheta_K$ denote the inclination angle of the k^{th} lateral inflow conduits. Let T_1, $T_2 \ldots T_k$ represent top width of k lateral inflow conduits over time duration dt, the net amount of fluid flow reaching the cell dx is considered as shown in Figure3.1 below.

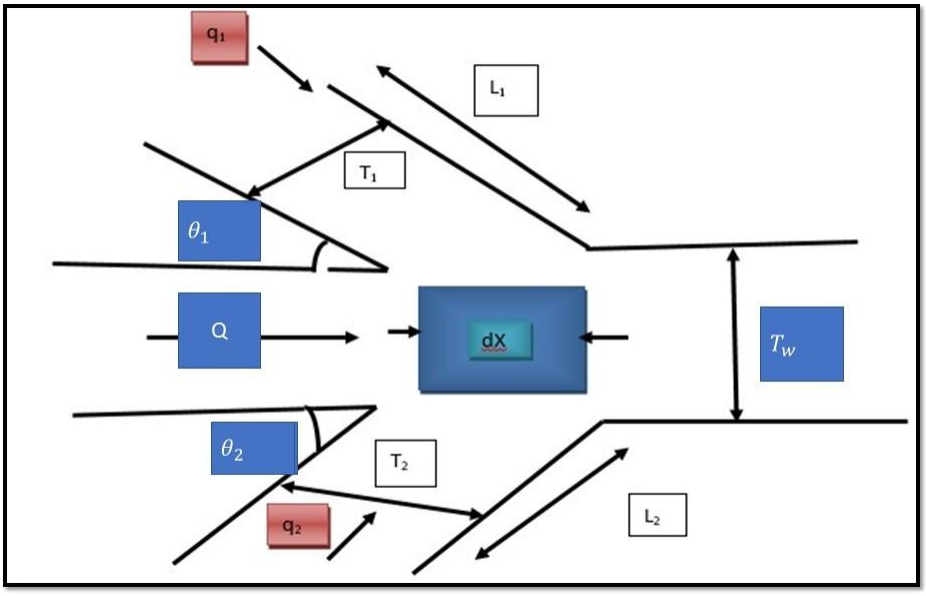

Figure 3.1: Mathematical Model Channel

3.3 Model Assumptions

1. The lateral inflow velocities, length, angles and depth of the k lateral inflows are directly proportional to each other.Namely $q_1 = q_2 = \cdots = q_k, L_1 = L_2 = \ldots L_k, \vartheta_1 = \vartheta_2 = \ldots = \vartheta_k$

2. A negligible amount of solid particle accumulation occurred between the k lateral inflow channels and the main open channel.

3. Lateral inflows and the main channel had horseshoe crosssections.

3.4 Mathematical Model Formulation

3.4.1 Equation of Continuity

A differential equation referred to as the continuity equation defines the movement of a conserved variable, in this case mass. All continuity equations serve as demonstrations of the concept that the total conserved quantity within any region changes just by the amount entering or leaving across its boundary. A conserved quantity can relocate but not increase or decrease. Hence, this equation combines the transport theorem with the principle of mass conservation, reflecting the fundamental principle that matter cannot be created or destroyed. Equation 3.1 represents the St. Venant's continuity equation governing open channel flows of arbitrary shapes (Karimi 2018).

$$\frac{\partial A}{\partial t} + \frac{\partial Q}{\partial x} = q \tag{3.1}$$

According to the model of the cell with lateral influx above ∂x and time duration ∂t is supposed to have total volume of $\frac{\partial Q}{\partial x} dxdt$. Discharge from k lateral inflow channels will be k times $\frac{q}{L} \sin\vartheta dxdt$ while increment of fluid is $\frac{\partial A}{\partial t} dxdt$. Equation 3.1 will be modified to equation 3.2:

$$\frac{\partial Q}{\partial x} dxdt + \frac{\partial A}{\partial t} dxdt = \frac{q_1}{L_1} \sin\vartheta_1 dxdt + \frac{q_2}{L_2} \sin\vartheta_2 dxdt + \cdots + \frac{q_k}{L_k} \sin\vartheta_k dxdt \tag{3.2}$$

Using the assumptions stated earlier;

$q_1 = q_2 = \ldots = q_k$ i.e $q_1 + q_2 + \cdots + q_k = kq, L_1 = L_2 = \ldots = L_k$,i.e$L_1 + L_2 + \ldots + L_k = kL$ and $\vartheta_1 = \vartheta_2 = \ldots = \vartheta_kie\vartheta_1 + \vartheta_2 + \ldots + \vartheta_k = k\vartheta$

Applying on the equation 3.2, equation 3.3 is obtained:

$$\frac{\partial Q}{\partial x}dxdt + \frac{\partial A}{\partial t}dxdt = k\frac{q}{L}\sin\vartheta dxdt \tag{3.3}$$

Dividing equation 3.3 by *dxdt* both sides equation 3.4 is obtained:

$$\frac{\partial Q}{\partial x} + \frac{\partial A}{\partial t} = k\frac{q}{L}\sin\vartheta \tag{3.4}$$

However, the flow rate is determined by

$$Q = Av \tag{3.5}$$

By partially differentiating 3.5 with respect to x and substituting in 3.4, it becomes equation3.6:

$$v\frac{\partial A}{\partial x} + A\frac{\partial v}{\partial x} + \frac{\partial A}{\partial t} = k\frac{q}{L}sin\vartheta \tag{3.6}$$

Since it is assumed that flow area depends on depth, the derivatives of A in equation 3.6 can be stated as

$$\frac{\partial A}{\partial x} = \frac{\partial A}{\partial y}\frac{\partial y}{\partial x} = T\frac{\partial y}{\partial x} \tag{3.7}$$

$$\frac{\partial A}{\partial t} = \frac{\partial A}{\partial y}\frac{\partial y}{\partial t} = T\frac{\partial y}{\partial t} \tag{3.8}$$

T is given by $T = \frac{\partial A}{\partial y}$ in this modification as described by Franz (1982). When equations 3.7 and 3.8 are inserted into in equation 3.6, it yields equation 3.9:

$$vT\frac{\partial y}{\partial x} + A\frac{\partial v}{\partial x} + T\frac{\partial y}{\partial t} = k\frac{q}{L}\sin\vartheta \tag{3.9}$$

Dividing 3.9 through by T, equation 3.10 is obtained.

$$v\frac{\partial y}{\partial x} + \frac{A}{T}\frac{\partial v}{\partial x} + \frac{\partial y}{\partial t} = k\frac{q}{TL}\sin\vartheta \tag{3.10}$$

Equation 3.10 represents the generalized continuity equation for open channel flow with k lateral inflows.

3.4.2 Equation of Conservation of Momentum

The basic principle of the equation of momentum conservation is found in Newton's second law of motion, which states that the total external forces acting on an object equal its rate of change of momentum. There are two kind of forces that make up this external force: body forces and surface forces. Body forces include centrifugal, magnetic, electric, and static forces; surface forces include static pressure and viscous strains.The interaction between the body and its immediate surroundings causes surface forces, which act on the bounding surfaces. Force per unit area is used to describe their intensities, which are quantified in terms of stress. The term "body forces" denotes forces exerted on a body from a distance, usually expressed as force per unit mass. Referring to Figure 3.1, the total momentum within the cell dx over time interval dt is expressed as $\frac{\partial Qv}{\partial x}dxdt$, while the momentum change within the same cell is $\frac{\partial Q}{\partial t}dxdt$. The lateral input momentum within the cell dx over time period dt is determined by $u\cos\vartheta$, which also provides the lateral inflow rate in the flow direction. considering k lateral inflows the lateral input momentum is given by $k\frac{q}{L}\sin\vartheta u\cos\vartheta dxdt$. Using the law of conservation of momentum according to karimi (2018), equation 3.11 is obtained.

$$\frac{\partial Q}{\partial t}dxdt+\frac{\partial Qv}{\partial x}dxdt+g\frac{\partial yA}{\partial x}dxdt+gA\left(s_f-s_0\right)dxdt=k\frac{q}{L}sin\vartheta u\cos\vartheta dxdt \quad (3.11)$$

Dividing equation 3.11 by $dxdt$ both sides to obtain equation 3.12:

$$\frac{\partial Q}{\partial t}+\frac{\partial Qv}{\partial x}+g\frac{\partial yA}{\partial x}+gA\left(s_f-s_0\right)=k\frac{q}{L}\sin\vartheta u\cos\vartheta \quad (3.12)$$

However, the discharge is represented by $Q=Av$,and substituting this into equation 3.12 yields equation 3.13.

$$\frac{\partial Av}{\partial t}+\frac{\partial Avv}{\partial x}+g\frac{\partial yA}{\partial x}+gA\left(s_f-s_0\right)=k\frac{q}{L}\sin\vartheta u\cos\vartheta \quad (3.13)$$

By taking a partial derivative of equation 3.13 with respect to x and reorganizing the terms, we derive equation 3.14:

$$\frac{\partial v}{\partial t}+v\frac{\partial v}{\partial x}+g\frac{\partial y}{\partial x}+g\left(s_f-s_0\right)=k\frac{q}{AL}\sin\vartheta(u\cos\vartheta-v) \quad (3.14)$$

The Manning or Chezy resistance equations are typically used to compute the friction slope s_f in computations involving unsteady flow (Chow, 1973). Equation 3.15 presents the Manning resistance equation:

$$s_f = \frac{n^2 v^2}{R^{\frac{4}{3}}} \tag{3.15}$$

Substituting equation 3.15 in equation 3.14 yields equation 3.16:

$$\frac{\partial v}{\partial t} + v\frac{\partial v}{\partial x} + g\frac{\partial y}{\partial x} + g\left(\frac{n^2 v^2}{R^{\frac{4}{3}}} - s_0\right) = k\frac{q}{AL}\sin\vartheta(u\cos\vartheta - v) \tag{3.16}$$

Equation 3.16 shows the general momentum equation for an open conduit with k lateral inflows.

3.5 Non-dimensional Numbers

Non-dimensional numbers, also known as dimensionless numbers, are fundamental in fluid mechanics and engineering as they provide insights into the relative importance of different physical quantities and parameters. They are mathematical ratios that express the relationship between various forces, velocities, and dimensions in a system, helping to simplify and generalize the analysis of complex phenomena. Non-dimensional numbers, according to Icha (2012), are especially helpful for comparing and classifying flows, such as describing how much of a role inertial forces and viscous forces have in a fluid. The Reynolds number (Re), which determines whether a flow is laminar or turbulent, is one of the most well-known dimensionless numbers. Understanding the flow behavior in various settings requires an understanding of the Reynolds number, which can be defined as the ratio of viscous forces to inertial forces.

3.5.1 Reynold Number, Re

In fluid dynamics, the dimensionless Reynolds number (Re) is used to characterize the flow of liquids or gases around objects. Osborne Reynolds, a British engineer who promoted its use in the late 19th century, inspired the name. grasp the change from laminar to turbulent flow requires a grasp of the Reynolds number. Within a fluid flow, the ratio of inertial forces to viscous forces is known as the Reynolds number (Re). Insight into flow dynamics and assistance in predicting the flow regime (laminar or

turbulent) are provided. Reynolds number is given by equation 3.17:

$$Re = \frac{Inertiaforce}{Viscousforce} = \frac{\rho uL}{\mu} \tag{3.17}$$

where:

ρ is the fluid density.

u is the characteristic velocity of the fluid.

L is a characteristic length .

μ is the dynamic viscosity of the fluid. Low Reynolds Number ($Re < 2000$) : shows laminar flow, which is the situation where inertial forces are subordinated to viscous ones. Parallel fluid layers are moving with little to no mixing, creating a smooth and well-organized flow. Transitional Reynolds Number ($2000 < Re < 4000$) : Flow regime is in transition between laminar and turbulent. The behavior of the flow is not well-predicted and can be highly variable. High Reynolds Number ($Re > 4000$) : Indicates turbulent flow, where inertial forces dominate over viscous forces. The flow is characterized by chaotic, swirling motion, and there is significant mixing of fluid.

Reynolds number is crucial in designing and analyzing fluid flow systems, such as pipes, channels, and aerodynamic surfaces. It helps determine if the flow will be stable or turbulent, which affects factors like pressure drop, heat transfer, and drag. It finds application in many different fields, including as chemical engineering, biofluidics, civil engineering, automotive, and aerospace. Disadvantages: The Reynolds number makes the assumption that fluids behave steadily, incompressibly, and Newtonianly. In situations with non-Newtonian fluids, compressible flows, or unstable conditions, it might not be able to forecast flow behavior with enough accuracy.

3.5.2 Froude Number, Fr

The Froude number (Fr) is a dimensionless quantity used in fluid dynamics to characterize the flow of fluids in open channels, such as rivers, canals, and streams. It was named after the Scottish engineer William Froude, who introduced the concept in the 19th century. In open channel hydraulics, the Froude number is essential for determining

the type of flow; subcritical, critical or supercritical. Defined as the ratio of a characteristic velocity to a gravitational wave velocity, the Froude number is a dimensionless quantity.The Froude number is given by equation 3.18:

$$Fr = \frac{v}{\sqrt{gL}} \tag{3.18}$$

where:

v is the flow velocity in the channel.

g is the acceleration due to gravity.

L is a characteristic length .

$Fr < 1$ (Subcritical flow): Indicates that the flow is slower than the waves it generates. The flow is controlled by bottom friction, and changes in water surface elevation are gradual. $Fr = 1$ (Critical flow): Indicates that the flow rate is equal to the speed of gravity waves. This is a special condition where the flow is on the verge of transitioning between subcritical and supercritical. It corresponds to the highest flow rate for a given channel geometry.

$Fr > 1$ (Supercritical flow): Indicates that the flow is faster than the waves it generates. The water surface is characterized by standing waves and roller-type features. In supercritical flow, the control is more related to the slope and geometry of the channel rather than bottom friction.

In the design and study of open channel flow systems, the Froude number is essential. It assists in determining whether the flow conditions will be subcritical, critical, or supercritical, which has significant effects on hydraulic structures, sediment transport, and flood control. The Froude number is used by engineers in many different domains, such as hydrology, hydraulic engineering, environmental engineering, and civil engineering.

3.5.3 Manning's Roughness Coefficient

Characterizing the resistance to flow in a channel, Manning's Roughness Coefficient (n) is an important parameter in open channel hydraulics. It is a part of Manning's Equation, which establishes a relationship between slope, flow velocity and conduit geometry.The

Manning's roughness coefficient is given by equation 3.19:

$$v = \frac{1}{n} R^{\frac{2}{3}} S^{\frac{1}{2}} \tag{3.19}$$

Where:

n is the roughness coefficient of Manning

R is the hydraulic radius

S is the slope of the channel Manning's n can change widely depending on the type and condition of the conduit. For instance, natural streams with vegetation, boulders, and irregularities tend to have higher values of n compared to well-maintained, smooth concrete channels. Higher values of Manning's n indicate greater roughness, which leads to lower flow velocities for a given slope and hydraulic radius. Conversely, lower values of n represent smoother channels with higher velocities. Manning's Roughness Coefficient is extensively used in open channel flow calculations, including water surface profile computations, floodplain modeling, river channel design, and drainage system design. The value of n is influenced by factors such as the presence of vegetation, bed material size, channel alignment, slope, and flow conditions (steady or unsteady). The construction and study of hydraulic structures, such as rivers, culverts, stormwater systems, and channels, depend heavily on Manning's Roughness Coefficient. Manning's n can range from as low as 0.01 for very smooth surfaces (e.g., well-maintained concrete channels) to 0.1 or higher for extremely rough conditions (e.g., heavily vegetated natural streams or channels with large boulders).Accurate selection of n is essential for reliable flow predictions.

3.5.4 Chezy Coefficient,(C)

The channel bed and banks' roughness properties are represented by the dimensionless Chezy Coefficient (C). It quantifies the resistance of the channel to the flow of water.The Chezy formula was introduced by the French engineer Antoine Chezy in the 18th century. It was one of the earliest attempts to mathematically describe open channel flow. The Chezy Coefficient is given by equation 3.20 (Chow, 1958)

$$c = \frac{v}{\sqrt{RS}} \tag{3.20}$$

Where: v is the velocity of the channel

S is the channel slope

R is the hydraulic radius

Higher values of the Chezy coefficient indicate smoother channels with lower resistance to flow. This results in higher flow velocities for a given slope and hydraulic radius. Conversely, lower values of C represent rougher channels with lower velocities. The Chezy-Manning equation, which includes the Chezy coefficient, is widely used in hydraulic engineering for calculations related to open channel flows, including water surface profiles, floodplain modeling, and the design of channels and drainage systems.Typical values of the Chezy coefficient (C) range from around 20 to 80 for well-maintained, smooth concrete channels, to values above 100 for natural streams with significant vegetation and irregularities.

3.5.5 Flow Aspect Ratio (W/h) in Open Channels

Flow Aspect Ratio (W/h), also known as the width-to-depth ratio, is a crucial parameter in open channel hydraulics. It characterizes the geometric shape of a channel cross-section and plays a significant role in determining flow behavior, velocity distribution, and energy losses.In the planning, evaluation, and administration of open channel systems, this parameter is crucial. Understanding the relative proportions of the channel cross-section is possible with this dimensionless measurement.. The flow aspect ration is given by equation 3.21:

$$\frac{w}{h} = \frac{channel\ width}{flow\ depth} \tag{3.21}$$

Flow aspect ratio influences the hydraulic efficiency of a channel. Channels with an optimal flow aspect ratio for a given flow rate tend to minimize energy losses due to friction and turbulence, resulting in more efficient flow conveyance.

3.6 Geometrical Properties

As illustrated in figure 3.2, the horseshoe cross section is divided into three zones of flow depth. Merkley (2005), calculated the depths h_1, h_2 and h_3 as shown in Figure 3.2.

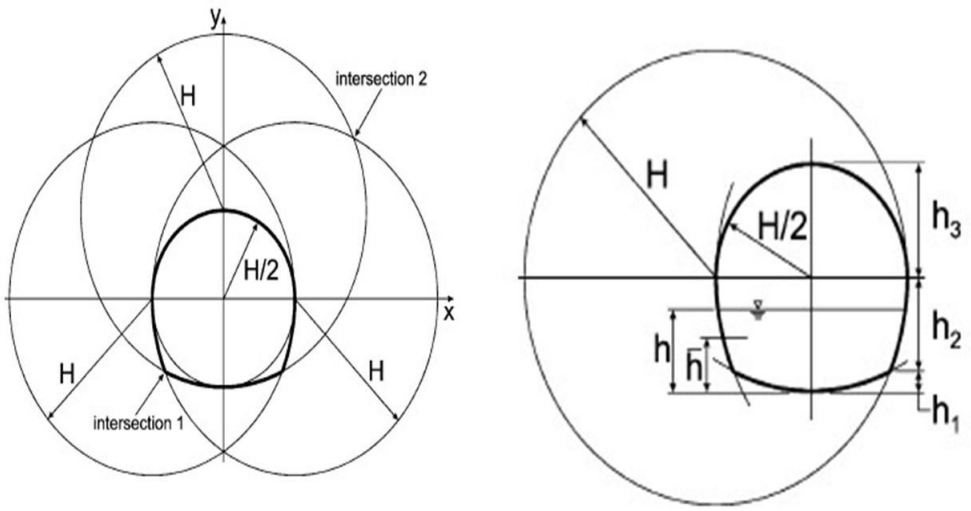

Figure 3.2: Horseshoe cross section

Equations regarding height, area, perimeter and water surface width differ based on Figure 3.2 (Merkley, 2005). These equations are shown in 3.22 to 3.35:

i Height

$$h_1 = H\left(1 - \left(\frac{1+\sqrt{7}}{4}\right)\right) \tag{3.22}$$

$$h_2 = \frac{H}{2} - h_1 \tag{3.23}$$

$$h_3 = \frac{H}{2} \tag{3.24}$$

ii Wetted Area

$0 \le h \le h_1$

$$A_1 = (h-H)\sqrt{h(2H-h)} + H^2 \sin^{-1}\left(\frac{h-H}{H}\right) + \frac{\pi}{2} \tag{3.25}$$

$0 \le h \le h_2$

$$A_2 = H^2 \left[c_2 + \sin^{-1}\left(\frac{2h-H}{2H}\right) \right] - \left(h - \frac{H}{2}\right)\left\{H - \sqrt{H^2 - \left(h - \frac{H}{2}\right)^2}\right\} \quad (3.26)$$

$\frac{H}{2} \le h \le H$

$$A_3 = \left(h - \frac{H}{2}\right)\sqrt{h(H-h)} + \frac{H^2}{4}\sin^{-1}\left(\frac{2h-H}{H}\right) + A_2 \quad (3.27)$$

iii Wetted Perimeter

$0 \le h \le h_1$

$$P_1 = 2H\cos^{-1}\left(1 - \frac{h}{H}\right) \quad (3.28)$$

$0 \le h \le h_2$

$$P_2 = 2H\left[\cos^{-1}\left(\frac{H-2h}{H}\right) - \cos^{-1}\left(-\frac{c_1}{2}\right)\right] + P_1 \quad (3.29)$$

$\frac{H}{2} \le h \le H$

$$P_3 = H\left[\cos^{-1}\left(1 - \frac{2h}{H}\right) - \frac{\pi}{2}\right] + P_2 \quad (3.30)$$

iv Top Width $0 \le h \le h_1$

$$T_1 = 2H\sqrt{1 - \left(1 - \frac{h}{H}\right)^2} \quad (3.31)$$

$0 \le h \le h_2$

$$T_2 = 2\left[\sqrt{H^2 - \left(h - \frac{H}{2}\right)^2} - H\right] \quad (3.32)$$

$\frac{H}{2} \le h \le H$

$$T_3 = H\sqrt{1 - \left(1 - \frac{2h}{H}\right)^2} \quad (3.33)$$

where c_1 and c_2 are

$$c_1 = 1 - \left(\frac{1+\sqrt{7}}{4}\right) \quad (3.34)$$

$$c_2 = \frac{c_1}{2}\left(1 - \sqrt{\frac{c_1^2}{4} - 1}\right) - \sin^{-1}\left(\frac{c_1}{2}\right) \quad (3.35)$$

The continuity and momentum equations were solved using the previously provided equations to find the hydraulic depth and hydraulic radius.

3.7 Non-Dimensionalising the Governing Equations

The process of non-dimensionalizing the equations that govern a specific fluid flow is part of the broader field of study called dimensional analysis. Dimensional analysis is a technique that describes natural phenomena using dimensionally accurate equations involving specific variables that influence the phenomena. For this particular problem, let L,V,Pand T represent the characteristic length, velocity, pressure, and temperature, respectively. To non-dimensionalize the equations governing the flow, we applied the following transformations: $x=x^{*}L,\ y = y^{*}L,\ q = q^{*}v,\ v = v^{*}v,\ p = p^{*}p,\ and t = \frac{t^{*}L}{v}$

3.7.1 Equation of Continuity

Equation 3.10 gives the continuity equation for this particular fluid flow.

$$v\frac{\partial y}{\partial x} + \frac{A}{T}\frac{\partial v}{\partial x} + \frac{\partial y}{\partial t} = k\frac{q}{TL}\sin\vartheta \tag{3.36}$$

dimensionalising equation 3.36 by substituting the scaling values and simplify each term:

$$x = x^{*}L,\ y = y^{*}L,\ q = q^{*}v,\ v = v^{*}v,\ p = p^{*}p,\ and t = \frac{t^{*}L}{v}$$

$$v\frac{\partial(y^{*}L)}{\partial(x^{*}L)} + \frac{A}{T}\frac{\partial(v^{*}v)}{\partial(x^{*}L)} + \frac{\partial(y^{*}L)}{\partial\frac{t^{*}L}{v}} = k\frac{q^{*}v}{TL}\sin\vartheta$$

Simplify each term:

For the first term $v\frac{\partial(y^{*}L)}{\partial(x^{*}L)}$:

$$v\frac{\partial(y^{*}L)}{\partial(x^{*}L)} = v\cdot\frac{L}{L}\frac{\partial y^{*}}{\partial x^{*}} = v\frac{\partial y^{*}}{\partial x^{*}}$$

For the second term$\frac{A}{T}\frac{\partial(v^{*}v)}{\partial(x^{*}L)}$:

$$\frac{A}{T}\frac{\partial(v^{*}v)}{\partial(x^{*}L)} = \frac{A}{T}\cdot\frac{v}{L}\frac{\partial v^{*}}{\partial x^{*}}$$

For the third term $\frac{\partial(y^{*}L)}{\partial\ \frac{t^{*}L}{v}}$:

$$\frac{\partial(y^{*}L)}{\partial\ \frac{t_{*}L}{v}} = \frac{\partial(y^{*}L)}{\partial t^{*}}\cdot\frac{\partial t^{*}}{\partial\ \frac{t_{*}L}{v}} = v\frac{\partial y^{*}}{\partial t^{*}}$$

For the right-hand side $k\frac{q^{*}v}{TL}\sin\vartheta$:

$$k\frac{q^{*}v}{TL}\sin\vartheta$$

Combine the simplified terms:

$$v\frac{\partial y^{*}}{\partial x^{*}} + \frac{A}{T}\cdot\frac{v}{L}\frac{\partial v^{*}}{\partial x^{*}} + v\frac{\partial y^{*}}{\partial t^{*}} = k\frac{q^{*}v}{TL}\sin\vartheta$$

Non-dimensionalize the equation by dividing through by v:

$$\frac{\partial y^{*}}{\partial x^{*}} + \frac{A}{T}\cdot\frac{1}{L}\frac{\partial v^{*}}{\partial x^{*}} + \frac{\partial y^{*}}{\partial t^{*}} = k\frac{q^{*}}{TL}\sin\vartheta$$

In the above process, L does not cancel out from the second and the right-hand side terms directly. The dimensional form persists. To completely non-dimensionalize:

The term $\frac{A}{T}\cdot\frac{1}{L}$ needs to be analyzed for its dimensionless nature. Similarly, $k\frac{q^{*}}{TL}\sin\vartheta$ must fit into dimensionless terms involving scaling constants such that no L remains as a fundamental part of the equation, adhering to physical constants being dimensionless forms.

Simplify the constants the equation 3.36 is dimensionalized to become equation 3.37:

$$\frac{\partial y^{*}}{\partial x^{*}} + \frac{A}{T}\cdot\frac{\partial v^{*}}{\partial x^{*}} + \frac{\partial y^{*}}{\partial t^{*}} = k\frac{q^{*}}{T}\sin\vartheta \qquad (3.37)$$

3.7.2 Equation of Conservation of Momentum

On non- dimensionalising equation 3.16:

$$\frac{\partial v}{\partial t} + v\frac{\partial v}{\partial x} + g\frac{\partial y}{\partial x} + g\left(\frac{n^2 v^2}{R^{\frac{4}{3}}} - s_0\right) = k\frac{q}{AL}\sin\vartheta(u\cos\vartheta - v)$$

and the scaling values:

$$x = x^* L, \quad y = y^* L, \quad q = q^* v, \quad v = v^* v, \quad t = \frac{t^* L}{v}$$

we substitute these into the equation:

$$\frac{v^*}{t^* L/v}\frac{\partial v^*}{\partial \frac{t^* L}{v}} + v^* v\frac{\partial (v^* v)}{\partial (x^* L)} + g\frac{\partial (y^* L)}{\partial (x^* L)} + g\left(\frac{n^2 v^{*2} v^2}{R^{\frac{4}{3}}} - s_0\right) = k\frac{q^* v}{AL}\sin\vartheta(u\cos\vartheta - v)$$

Next, we simplify each term:

For $\frac{v^*}{t^* L/v}\frac{\partial v^*}{\partial \frac{t^* L}{v}}$:

$$\frac{v^*}{t^* L/v}\frac{\partial v^*}{\partial \frac{t^* L}{v}} = v^*\frac{v}{t^* L}\frac{\partial v^*}{\partial t^*} = v^*\frac{v}{t^* L}\frac{\partial v^*}{\partial t^*}$$

For $v^* v\frac{\partial (v^* v)}{\partial (x^* L)}$:

$$v^* v\frac{\partial (v^* v)}{\partial (x^* L)} = v^* v \cdot \frac{1}{L}\frac{\partial v^*}{\partial x^*}$$

For $g\frac{\partial (y^* L)}{\partial (x^* L)}$:

$$g\frac{\partial (y^* L)}{\partial (x^* L)} = g \cdot \frac{1}{L}\frac{\partial y^*}{\partial x^*}$$

For $g\left(\frac{n^2 v^{*2} v^2}{R^{\frac{4}{3}}} - s_0\right)$:

$$g \quad \frac{n^2 v^{*2} v^2}{R^{\frac{4}{3}}} - s_0$$

For the right-hand side $k\frac{q^* v}{AL}\sin\vartheta(u\cos\vartheta - v)$:

$$k\frac{q^* v}{AL}\sin\vartheta(u\cos\vartheta - v)$$

Combining the simplified terms, we get:

$$v^* \frac{v}{t^* L}\frac{\partial v^*}{\partial t^*} + v^* v \cdot \frac{1}{L}\frac{\partial v^*}{\partial x^*} + g \cdot \frac{1}{L}\frac{\partial y^*}{\partial x^*} + g \quad \frac{n^2 v^{*2} v^2}{R^{\frac{4}{3}}} - s_0 \quad = k\frac{q^* v}{AL}\sin\vartheta(u\cos\vartheta - v)$$

Non-dimensionalize the equation by dividing through by v^*:

$$\frac{v}{t^* L}\frac{\partial v^*}{\partial t^*} + \frac{v}{L}\frac{\partial v^*}{\partial x^*} + \frac{g}{v^* L}\frac{\partial y^*}{\partial x^*} + \frac{g}{v^*} \quad \frac{n^2 v^2}{R^{\frac{4}{3}}} - \frac{s_0}{v^*} \quad = k\frac{q^*}{ALv^*}\sin\vartheta(u\cos\vartheta - v)$$

The final corrected dimensionalized equation is:

$$\frac{v}{t^* L}\frac{\partial v^*}{\partial t^*} + \frac{v}{L}\frac{\partial v^*}{\partial x^*} + \frac{g}{v^* L}\frac{\partial y^*}{\partial x^*} + \frac{g}{v^*} \quad \frac{n^2 v^2}{R^{\frac{4}{3}}} - \frac{s_0}{v^*} \quad = k\frac{q^*}{ALv^*}\sin\vartheta(u\cos\vartheta - v)$$

Here, each term is dimensionally consistent with the scaling values provided. After non-dimensionalising equation 3.16 it becames equation 3.38:

$$\frac{\partial(v^* v)}{\partial \frac{t^* L}{v}} + v^* v\frac{\partial(v^* v)}{\partial(x^* L)} + g\frac{\partial(y^* L)}{\partial(x^* L)} + g \quad \frac{n^2 v^{*2} v^2}{R^{\frac{4}{3}}} - s_0 \quad = k\frac{q^* v}{AL}\sin\vartheta(u\cos - v) \qquad (3.38)$$

Rearranging equation 3.38 to obtain equation 3.39

$$\frac{v^2}{L}\frac{\partial v^*}{\partial t^*} + v^*\frac{v^2}{L}\frac{\partial v^*}{\partial x^*} + g\frac{\partial y^*}{\partial x^*} + g \quad \frac{n^2 v^{*2} v^2}{R^{\frac{4}{3}}} - s_0 \quad = k\frac{q^* v}{AL}\sin\vartheta(u\cos - v) \qquad (3.39)$$

Dividing throughout by g in equation 3.39 to obtain equation 3.40:

$$\frac{v^2}{gL}\frac{\partial v^*}{\partial t^*} + v^*\frac{v^2}{gL}\frac{\partial v^*}{\partial x^*} + \frac{\partial y^*}{\partial x^*} + \frac{n^2 v^{*2} v^2}{R^{\frac{4}{3}}} - s_0 = k\frac{q^* v}{gAL}\sin\vartheta(u\cos - v) \qquad (3.40)$$

Factoring out $\frac{v^2}{gL}$ to obtain equation 3.41:

$$\frac{v^2}{gL}\frac{\partial v^*}{\partial t^*} + v^*\frac{\partial v^*}{\partial x^*} + \frac{\partial y^*}{\partial x^*} + \frac{n^2 v^{*2} v^2}{R^{\frac{4}{3}}} - s_0 = k\frac{q^* v}{gAL}\sin\vartheta(u\cos - v) \qquad (3.41)$$

3.8 Boundary Conditions

The following are the boundary conditions for fluid flow in an open conduit with a horseshoe cross-section that take into account the influence of viscous forces in the free stream zone and the no-slip condition:

3.8.1 Equation of continuity and momentum

The equations of continuity and momentum are solved using the following conditions (Jomba 2016).

$$v(x, 0) = 10, y(x, 0) = 1.0, x > 0$$

$$v(0, t) = 10, y(o, t) = 1.0, t > 0$$

$$v(x, t) = 10, y(x, t) = 1.0, t > 0$$

by non-dimensionalizing the boundary and initial conditions

$$v^* V\,(x^* L, 0) = 10, y^* L(x^* L, 0) = 1.0, x^* L > 0$$

$$v^* V\,(0, \frac{t^* L}{V}) = 10, y^* L(0, \frac{t^* L}{V}) = 1.0, \frac{t^* L}{V} > 0$$

$$v^* V\,(x^* L, \frac{t^* L}{V}) = 10, y^* L(x^* L, \frac{t^* L}{V}) = 1.0, \frac{t^* L}{V} > 0$$

By simplifying the aforementioned conditions, we obtain:

$$v^*(x^*, 0) = 10, y^*(x^*, 0) = 1.0, x^* > 0$$

$$v^*(0, t^*) = 10, y^*(0, t^*) = 1.0, t^* > 0$$

$$v^*(x^*, t^*) = 10,\ y^*(x^*, t^*) = 1.0,\ t^* > 0$$

3.9 Equations Governing the Fluid flow in Nondimensional Form

3.9.1 Equation of Continuity

Dividing the whole of equation 3.37 by v to obtain equation 3.42

$$v^* \frac{\partial y^*}{\partial x^*} + \frac{A}{TL}\frac{\partial v^*}{\partial x^*} + \frac{\partial y^*}{\partial t^*} = k\frac{q_*}{TL} sin\vartheta \tag{3.42}$$

Equation 3.42 is the continuity equation in nondimensional form.

3.9.2 Momentum Equation

Substituting equation 3.18 in equation 3.41, equation 3.43 is obtained.

$$Fr^2 \frac{\partial v^*}{\partial t^*} + v^*\frac{\partial v^*}{\partial x^*} + \frac{\partial y^*}{\partial x^*} + \frac{n^2 v^{*2} v^2}{R^{\frac{4}{3}}} - s_0 = k\frac{q^* v}{gAL} sin\vartheta(ucos - v) \tag{3.43}$$

Equation 3.43 is the momentum equation in nondimensional form.

3.10 Specific Equations Governing the Fluid Flow in nondimensional Form

Figure 2 shows the three zones of flow depth that form the horseshoe cross section.

3.10.1 Continuity Equations

3.10.1.1 Continuity Equation for zone 1

Substituting equations 3.25, 3.31 in equation 3.42 to obtain equation 3.44:

$$v^*\frac{\partial y^*}{\partial x^*} + \frac{(h-H)\sqrt{h(2H-h)} + H^2 \sin^{-1}(\frac{h-H}{H}) + \frac{\pi}{2}}{2HL\sqrt{1-(1-\frac{h}{H})^2}}\frac{\partial v^*}{\partial x^*} + \frac{\partial y^*}{\partial t^*} = \frac{kq_1^*}{L2H\sqrt{1-(1-\frac{h}{H})^2}} sin\vartheta \tag{3.44}$$

But dicharge in zone 1 is given by

$$q_1 = A_1 v \tag{3.45}$$

Substituting equation 3.45 in equation 3.44 to obtain equation 3.46:

$$v^*\frac{\partial y^*}{\partial x^*}+\frac{(h-H)\sqrt{h(2H-h)+H^2}\,\sin^{-1}\left(\frac{h-H}{H}\right)+\frac{\pi}{2}}{2HL\sqrt{1-\left(1-\frac{h}{H}\right)^2}}\frac{\partial v^*}{\partial x^*}+\frac{\partial y^*}{\partial t^*}=\frac{kA_1v}{L2H\sqrt{1-\left(1-\frac{h}{H}\right)^2}}\sin\vartheta \tag{3.46}$$

Subtituting equation 3.25 in equation 3.46, equation 3.47 is obtained.

$$v^*\frac{\partial y^*}{\partial x^*}+\frac{(h-H)\sqrt{h(2H-h)+H^2}\,\sin^{-1}\left(\frac{h-H}{H}\right)+\frac{\pi}{2}}{2HL\sqrt{1-\left(1-\frac{h}{H}\right)^2}}\frac{\partial v^*}{\partial x^*}+\frac{\partial y^*}{\partial t^*}=\frac{k(h-H)\sqrt{h(2H-h)+H^2}\,\sin^{-1}\left(\frac{h-H}{H}\right)+\frac{\pi}{2}}{L2H\sqrt{1-\left(1-\frac{h}{H}\right)^2}}v\sin\vartheta \tag{3.47}$$

Equation 3.47 is the specific continuity equation for zone 1 in nondimensional form.

3.10.1.2 Continuity Equation for zone 2

Substituting equations 3.26 and 3.32 in equation 3.42 to obtain equation 3.48:

$$v^*\frac{\partial y^*}{\partial x^*}+\frac{H^2\left[\frac{\pi}{2}+\sin^{-1}\left(\frac{2h-H}{2H}\right)\right]-\left(h-\frac{H}{2}\right)\left\{H-\sqrt{H^2-\left(h-\frac{H}{2}\right)^2}\right\}}{TL}\frac{\partial v^*}{\partial x^*}+\frac{\partial y^*}{\partial t^*}=\frac{kq_2^*}{2L\sqrt{H^2-\left(h-\frac{H}{2}\right)^2}-H}\sin\vartheta \tag{3.48}$$

But discharge in zone 2 is given by equation 3.49:

$$q_2=A_2v \tag{3.49}$$

Subtituting equation 3.49 in equation 3.48, equation 3.50 is obtained.

$$v^*\frac{\partial y^*}{\partial x^*}+\frac{H^2\left[\frac{\pi}{2}+\sin^{-1}\left(\frac{2h-H}{2H}\right)\right]-\left(h-\frac{H}{2}\right)\left\{H-\sqrt{H^2-\left(h-\frac{H}{2}\right)^2}\right\}}{TL}\frac{\partial v^*}{\partial x^*}+\frac{\partial y^*}{\partial t^*}=\frac{kA_2v}{2L\sqrt{H^2-\left(h-\frac{H}{2}\right)^2}-H}\sin\vartheta \tag{3.50}$$

Substituting equation 3.21 in equation 3.50 to obtain equation 3.51:

$$v^*\frac{\partial y^*}{\partial x^*}+\frac{\left[H^2\left[\frac{c}{2}+\sin^{-1}\left(\frac{2h-H}{2H}\right)\right]-\left(h-\frac{H}{2}\right)\left\{H-\sqrt{H^2-\left(h-\frac{H}{2}\right)^2}\right\}\right]}{\left[\frac{kv}{2}\left[H^2\left[\frac{c}{2}+\sin^{-1}\left(\frac{2h-H}{2H}\right)\right]-\left(h-\frac{H}{2}\right)\left\{H-\sqrt{H^2-\left(h-\frac{H}{2}\right)^2}\right\}\right]\right]}\frac{\partial v^*}{\partial x^*}+\frac{\partial y^*}{\partial t^*}$$
$$=\frac{q}{2L\left[H^2-\left(h-\frac{H}{2}\right)^2-H\right]}\sin\vartheta \qquad (3.51)$$

Equation 3.51 is the specific continuity equation for zone 2 in nondimensional form.

3.10.1.3 Continuity Equation for zone 3

Substituting equations 3.27, 3.33 in equation 3.42 to obtain equation 3.52:

$$v^*\frac{\partial y^*}{\partial x^*}+\frac{\left[\left(h-\frac{H}{2}\right)\sqrt{h(H-h)}+\frac{H^2}{4}\sin^{-1}\left(\frac{2h-H}{H}\right)+A\right]_2}{\left[LH\sqrt{1-\left(1-\frac{2h}{H}\right)^2}\right]}\frac{\partial v^*}{\partial x^*}+\frac{\partial y^*}{\partial t^*}$$
$$=\frac{kq_3^*}{\left[LH\sqrt{1-\left(1-\frac{2h}{H}\right)^2}\right]}\sin\vartheta \qquad (3.52)$$

But discharge in zone 3 is given by equation 3.53:

$$q_3=A_3v \qquad (3.53)$$

Substituting equation 3.53 in equation 3.52 to obtain equation 3.54:

$$v^*\frac{\partial y^*}{\partial x^*}+\frac{\left[\left(h-\frac{H}{2}\right)\sqrt{h(H-h)}+\frac{H^2}{4}\sin^{-1}\left(\frac{2h-H}{H}\right)+A\right]_2}{\left[LH\sqrt{1-\left(1-\frac{2h}{H}\right)^2}\right]}\frac{\partial v^*}{\partial x^*}+\frac{\partial y^*}{\partial t^*}$$
$$=\frac{kA_3v}{\left[LH\sqrt{1-\left(1-\frac{2h}{H}\right)^2}\right]}\sin\vartheta \qquad (3.54)$$

Substituting 3.27 in equation 3.54 to obtain equation 3.55:

$$v^*\frac{\partial y^*}{\partial x^*}+\frac{\left[\left(h-\frac{H}{2}\right)\sqrt{h(H-h)}+\frac{H^2}{4}\sin^{-1}\left(\frac{2h-H}{H}\right)+A\right]_2}{\left[LH\sqrt{1-\left(1-\frac{2h}{H}\right)^2}\right]}\frac{\partial v^*}{\partial x^*}+\frac{\partial y^*}{\partial t^*}$$
$$=\frac{kv\left[\left(h-\frac{H}{2}\right)\sqrt{h(H-h)}+\frac{H^2}{4}\sin^{-1}\left(\frac{2h-H}{H}\right)+A\right]_2}{\left[LH\sqrt{1-\left(1-\frac{2h}{H}\right)^2}\right]}\sin\vartheta \qquad (3.55)$$

Equation 3.55 is the specific continuity equation for zone 3 in nondimensional form.

3.10.2 Momentum Equation

3.10.2.1 Momentum Equation for Zone 1

Substituting equations 3.25 in equation 3.43 to obtain equation 3.56:

$$Fr^2\left(\frac{\partial v^*}{\partial t^*}+v^*\frac{\partial v^*}{\partial x^*}\right)+\frac{\partial y^*}{\partial x^*}+\frac{n^2 v^{*2}v^2}{R^{\frac{4}{3}}}-s_0 = k\frac{v^2}{gL}\sin\vartheta(u\cos\vartheta-v) \tag{3.56}$$

Equation 3.56 is simplified to equation 3.57:

$$Fr^2\left(\frac{\partial v^*}{\partial t^*}+v^*\frac{\partial v^*}{\partial x^*}\right)+\frac{\partial y^*}{\partial x^*}+\frac{n^2 v^{*2}v^2}{R^{\frac{4}{3}}}-s_0 = k\frac{v^2}{gL}\sin\vartheta(u\cos\vartheta-v) \tag{3.57}$$

Equation 3.57 is the specific momentum equation for zone 1 in nondimensional form.

3.10.2.2 Momentum Equation for Zone 2

Substituting equations 3.26 in equation 3.43 to obtain equation 3.58:

$$Fr^2\left(\frac{\partial v^*}{\partial t^*}+v^*\frac{\partial v^*}{\partial x^*}\right)+\frac{\partial y^*}{\partial x^*}+\frac{n^2 v^{*2}v^2}{R^{\frac{4}{3}}}-s_0 = k\frac{v^2}{gL}\sin\vartheta(u\cos\vartheta-v) \tag{3.58}$$

Equation 3.58 is simplified to equation 3.59:

$$Fr^2\left(\frac{\partial v^*}{\partial t^*}+v^*\frac{\partial v^*}{\partial x^*}\right)+\frac{\partial y^*}{\partial x^*}+\frac{n^2 v^{*2}v^2}{R^{\frac{4}{3}}}-s_0 = k\frac{v^2}{gL}\sin\vartheta(u\cos\vartheta-v) \tag{3.59}$$

Equation 3.59 is the specific momentum equation for zone 2 in nondimensional form.

3.10.2.3 Momentum Equation for Zone 3

Substituting equations 3.27 in equation 3.43 to obtain equation 3.60:

$$Fr^2\left(\frac{\partial v^*}{\partial t^*}+v^*\frac{\partial v^*}{\partial x^*}+\frac{\partial y^*}{\partial x^*}+\frac{n^2 v^{*2} v^2}{R^{\frac{4}{3}}}-s_0\right)=k\frac{v^2}{gL}\sin\vartheta(u\cos\vartheta-v) \tag{3.60}$$

$$\text{where } k=\frac{n\sqrt{h(H-h)+\frac{H^2}{4}\sin^{-1}\left(\frac{2h-H}{H}\right)+A_2}}{(h-\frac{H}{2})}$$

Equation 3.60 is simplified to equation 3.61:

$$Fr^2\left(\frac{\partial v^*}{\partial t^*}+v^*\frac{\partial v^*}{\partial x^*}+\frac{\partial y^*}{\partial x^*}+\frac{n^2 v^{*2} v^2}{R^{\frac{4}{3}}}-s_0\right)=k\frac{v^2}{gL}\sin\vartheta(u\cos\vartheta-v) \tag{3.61}$$

Equation 3.61 is the specific momentum equation for zone 3 in nondimensional form.

CHAPTER FOUR

ANALYSIS RESULTS AND DISCUSSION

4.1 Model Simulation

The finite difference method for numerical approximations is used for solving the system of non-linear equations derived for this particular flow. As seen in Figure 4.1, the finite difference grid compute values at the mesh points, where each nodal point is designated by a double index (i, j) that specifies its position with respect to t and x. Python software is used to do numerical simulations.

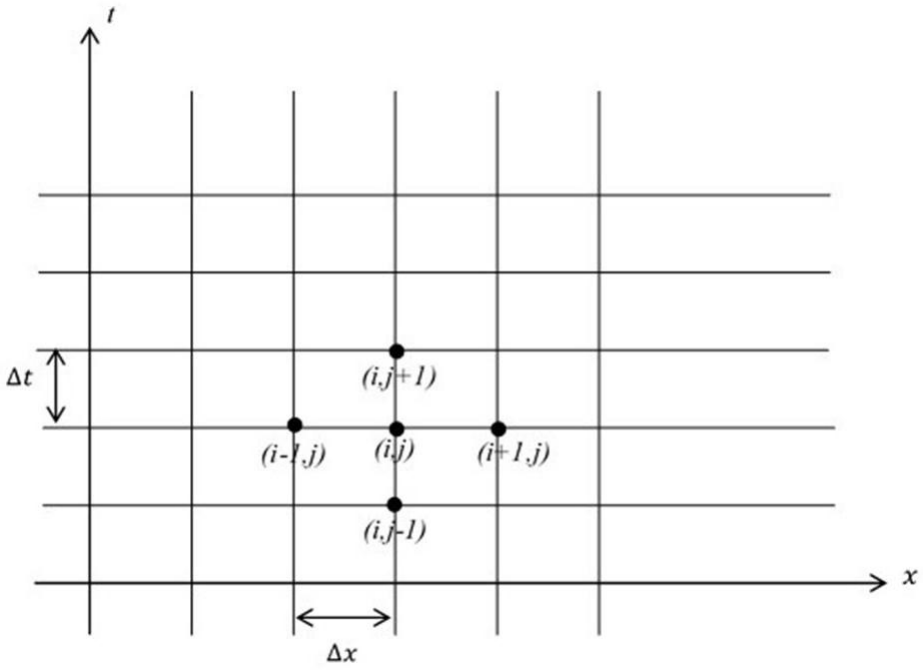

Figure 4.1: Finite Difference Mesh

In finite difference approximation, derivatives are substituted with finite differences. If v=v(x,t) and y=y(x,t), their first derivatives with respect to t are expressed in finite difference form as follows:

$$v_t = \frac{v_{(i,j+1)} - v_{(i,j)}}{\Delta t} \tag{4.1}$$

$$y_t = \frac{y_{(i,j+1)} - y_{(i,j)}}{\Delta t} \tag{4.2}$$

Their first-order derivatives with respect to x were formulated using finite difference representation as follows:

$$v_x = \frac{v_{(i+1,j)} - v_{(i-1,j)}}{2\Delta x} \tag{4.3}$$

$$y_x = \frac{y_{(i+1,j)} - y_{(i-1,j)}}{2\Delta x} \tag{4.4}$$

The derivatives in the flow equations are substituted with their respective finite difference approximations. The consecutive terms of depth and velocities $y_{(i,j+1)}$ and $v_{(i,j+1)}$ are computed according to the initial and boundary conditions.

4.2 Model Equations in the Form of Finite Difference

Using forward differences, the continuity and momentum equations of open channel flow are discretized into a system of algebraic equations that may be solved numerically. This process is known as forward differentiation. In this approach, finite difference approximations are used in place of the derivatives in the equations. The difference between a variable's value at one location and its value at the next point along the flow direction approximates the change in the variable at that moment in the case of forward differences. Variables like flow depth and velocity at discrete sites along the channel can be calculated using this method, which converts the spatial and temporal derivatives into difference equations.

4.2.1 Continuity Equation

Substituting equations 4.1, 4.2, 4.3 and 4.4 into equation 3.42, equation 4.5 is obtained.

$$v^*_{(i,j)} \frac{y_{(i+1,j)} - y_{(i-1,j)}}{2\Delta x} + \frac{A}{TL}\frac{v_{(i+1,j)} - v_{(i-1,j)}}{2\Delta x} + \frac{y_{(i,j+1)} - y_{(i,j)}}{\Delta t} = k\frac{q_*}{TL}\sin\vartheta \tag{4.5}$$

Rearranging equation 4.5, equation 4.6 is obtained.

$$y_{(i,j+1)} = \Delta t \left[k\frac{q^*}{TL}\sin\vartheta - v^*_{(i,j)} \frac{y_{(i+1,j)} - y_{(i-1,j)}}{2\Delta x} - \frac{A}{TL}\frac{v_{(i+1,j)} - v_{(i-1,j)}}{2\Delta x} \right] + y_{(i,j)} \tag{4.6}$$

Equation 4.6 is the model continuity equation in finite difference form.

4.2.2 Momentum Equation

Substituting equations 4.1, 4.2, 4.3,and 4.4 into equation 3.43, equation 4.7 is obtained.

$$Fr^2 \frac{v_{(i,j+1)} - v_{(i,j)}}{\Delta t} + v_{(i,j)} \frac{v_{(i+1,j)} - v_{(i-1,j)}}{2\Delta x} + \frac{y_{(i+1,j)} - y_{(i-1,j)}}{2\Delta x} + \frac{n^2 v^{*2} v^2}{R^{\frac{4}{3}}} - s_0 = k\frac{q^* v}{gAL}\sin\vartheta(u\cos\vartheta - v_{(i,j)}) \tag{4.7}$$

Rearranging equation 4.7, equation 4.8 is obtained

$$v_{(i,j+1)} = \Delta t\{k\frac{q^*v}{Fr^2gAL}sin\vartheta(ucos\vartheta - v_{(i,j)}) - \frac{1}{Fr^2}\frac{n^2v^{*2}v^2}{R^{\frac{4}{3}}} - s_0 - \frac{1}{Fr^2}\frac{y_{(i+1,j)} - y_{(i-1,j)}}{2\Delta x} - v_{(i,j)}\frac{v_{(i+1,j)} - v_{(i-1,j)}}{2\Delta x}\} - v_{(i,j)} \quad (4.8)$$

Equation 4.8 is the momentum model equation in finite difference form.

4.3 Specific Model Equations in Finite Difference Form

The process of converting the open channel flow specific continuity equations into finite difference form through forward differences entails approximating the spatial derivatives through the use of the difference between successive sites along the channel. This method discretizes the channel into small segments and iteratively updates the flow variables at each location, allowing the numerical solution of the equations.

4.3.1 Continuity Equation

Substituting the flow area and top width formulas yields specific discrete equations that approximate changes in flow variables over small spatial increments when the specific continuity equations of open channel flow are converted to finite difference form using forward differences.

4.3.1.1 Continuity Equation for Zone 1

Substituting equations 3.25 and 3.31 in equation 4.6 we obtain equation 4.9:

$$y_{(i,j+1)} = \Delta t\{k\frac{(h-H)\sqrt{h(2H-h)+H^2}\ sin^{-1}(\frac{h-H}{H}) + \frac{\pi}{2}v}{2HL\sqrt{1-(1-\frac{h}{H})^2}}sin\vartheta - v^*_{(i,j)}\frac{y_{(i+1,j)} - y_{(i-1,j)}}{2\Delta x} - \frac{(h-H)\sqrt{h(2H-h)+H^2}\ sin^{-1}(\frac{h-H}{H}) + \frac{\pi}{2}}{2HL\sqrt{1-(1-\frac{h}{H})^2}}v_{(i+1,j)} - v_{(i-1,j)}\frac{}{2\Delta x}\} + y_{(i,j)} \quad (4.9)$$

Equation 4.9 is the specific continuity equation for zone 1 in finite difference form.

4.3.1.2 Continuity Equation for Zone 2

Substituting equations 3.26 and 3.32 in equation 4.6 we obtain equation 4.10:

$$y_{(i,j+1)} = \Delta t \left(k \frac{H^2 \left(c_2 + \sin^{-1} \frac{2h-H}{2H} \right) - (h - \frac{H}{2}) \sqrt{H - H^2 - (h - \frac{H}{2})^2}}{2L \sqrt{H^2 - (h - \frac{H}{2})^2 - H}} \sqrt{v} \sin\vartheta \right.$$
$$- v^*_{(i,j)} \frac{y_{(i+1,j)} - y_{(i-1,j)}}{2\Delta x}$$
$$\left. - \frac{H^2 \left(c_2 + \sin^{-1} \frac{2h-H}{2H} \right) - (h - \frac{H}{2}) \sqrt{H - H^2 - (h - \frac{H}{2})^2}}{2L \sqrt{H^2 - (h - \frac{H}{2})^2 - H}} v_{(i+1,j)} - v_{(i-1,j)} \right)$$
$$+ y_{(i,j)} \qquad (4.10)$$

Equation 4.10 is the specific continuity equation for zone 2 in finite difference form.

4.3.1.3 Continuity Equation for Zone 3

Substituting equations 3.27 and 3.33 in equation 4.6 we obtain equation 4.11:

$$y_{(i,j+1)} = \Delta t \left(k \frac{(h - \frac{H}{2}) \sqrt{h(H-h)} + \frac{H^2}{4} \sin^{-1} \frac{2h-H}{H} + A}{HL \sqrt{1 - (1 - \frac{2h}{H})^2}} \sqrt{v} \sin\vartheta \right.$$
$$- v^*_{(i,j)} \frac{y_{(i+1,j)} - y_{(i-1,j)}}{2\Delta x}$$
$$\left. - \frac{(h - \frac{H}{2}) \sqrt{h(H-h)} + \frac{H^2}{4} \sin^{-1} \frac{2h-H}{H} + A}{HL \sqrt{1 - (1 - \frac{2h}{H})^2}} v_{(i+1,j)} - v_{(i-1,j)} \right)$$
$$+ y_{(i,j)} \qquad (4.11)$$

4.3.2 Momentum Equation

The open channel flow momentum equations can be simplified to specific momentum equations by substituting the flow area formulas. The discrete equations produced by this approach approximate changes in flow variables throughout small spatial increments.

4.3.2.1 Momentum Equation for Zone 1

Substituting equations 3.25 in equation 4.8 we obtain equation 4.12:

$$v_{(i,j+1)} = \Delta t\{k \frac{\sqrt{q^* v}}{Fr^2 g(h-H)\sqrt{h(2H-h)+H^2\ sin^{-1}(\frac{h-H}{H})+\frac{\pi}{2}L}} \sin\vartheta(u\cos\vartheta - v_{(i,j)}) - \frac{1}{Fr^2}\ \frac{n^2 v^{*2} v^2}{R^{\frac{4}{3}}} - s_0 - \frac{1}{Fr^2}\ \frac{y_{(i+1,j)} - y_{(i-1,j)}}{2\Delta x} - v_{(i,j)}\ \frac{v_{(i+1,j)} - v_{(i-1,j)}}{2\Delta x}\ \} - v_{(i,j)} \tag{4.12}$$

4.3.2.2 Momentum Equation for Zone 2

Substituting equations 3.26 in equation 4.8 to obtain equation 4.13:

$$v_{(i,j+1)} = \Delta t\{k \frac{\left[c_2 + \sin^{-1}(\frac{2h-H}{2H})\right] - (h-\frac{H}{2})\{H - \sqrt{H^2-(h-\frac{H}{2})^2}\}}{Fr^2 g H^2}\sqrt{q^* v} L \sin\vartheta(u\cos\vartheta - v_{(i,j)}) - \frac{1}{Fr^2}\ \frac{n^2 v^{*2} v^2}{R^{\frac{4}{3}}} - s_0 - \frac{1}{Fr^2}\ \frac{y_{(i+1,j)} - y_{(i-1,j)}}{2\Delta x} - v_{(i,j)}\ \frac{v_{(i+1,j)} - v_{(i-1,j)}}{2\Delta x}\ \} - v_{(i,j)} \tag{4.13}$$

4.3.2.3 Momentum Equation for Zone 3

Substituting equations 3.27 in equation 4.8, equation 4.14 is obtained

$$v_{(i,j+1)} = \Delta t\{k \frac{\sqrt{q^* v}}{Fr^2 g(h-\frac{H}{2})\sqrt{h(H-h)+\frac{H^2}{4}\sin^{-1}(\frac{2h-H}{H})+A_2 L}} \sin\vartheta(u\cos\vartheta - v_{(i,j)}) - \frac{1}{Fr^2}\ \frac{n^2 v^{*2} v^2}{R^{\frac{4}{3}}} - s_0 - \frac{1}{Fr^2}\ \frac{y_{(i+1,j)} - y_{(i-1,j)}}{2\Delta x} - v_{(i,j)}\ \frac{v_{(i+1,j)} - v_{(i-1,j)}}{2\Delta x}\ \} - v_{(i,j)} \tag{4.14}$$

4.4 Results and Discussion

The finite difference approach was utilized to solve the continuity and momentum equations, resulting to the simulation of the results using Python software. In order to guarantee the accuracy and applicability of the input parameters, the data used for these simulations originated from earlier studies. H= 5.65, h=0.5, k=1, 2, 3, 4, 5, and 6. L = 1m, 2m. A = 0.08, 0.32. $\vartheta = 10^\circ, 20^\circ, 30^\circ, 40^\circ, 50^\circ, 60^\circ, 70^\circ, 80^\circ$

4.4.1 Velocity profiles for zone 1

The continuity and momentum equations in zone 1 given by equations 4.15 and 4.16 and solved numerically by the finite method and graphically illustrated in figure 4.2 to 4.5.

$$y_{(i,j+1)} = \Delta t\{k \frac{(h-H)\sqrt{h(2H-h)+H^2\ sin^{-1}(\frac{h-H}{H})+\frac{\pi}{2}}v}{2HL\sqrt{1-(1-\frac{h}{H})^2}} sin\vartheta - v^*_{(i,j)} \frac{y_{(i+1,j)}-y_{(i-1,j)}}{2\Delta x} - \frac{(h-H)\sqrt{h(2H-h)+H^2\ sin^{-1}(\frac{h-H}{H})+\frac{\pi}{2}}v_{(i+1,j)}-v_{(i-1,j)}}{2HL\sqrt{1-(1-\frac{h}{H})^2}} \frac{}{2\Delta x}\} + y_{(i,j)} \quad (4.15)$$

$$v_{(i,j+1)} = \Delta t\{k \frac{q^*v}{Fr^2 g(h-H)\sqrt{h(2H-h)+H^2\ sin^{-1}(\frac{h-H}{H})+\frac{\pi}{2}}L} sin\vartheta(ucos\vartheta - v_{(i,j)}) - \frac{1}{Fr^2}\frac{n^2v^{*2}v^2}{R^{\frac{4}{3}}} - s_0 - \frac{1}{Fr^2}\frac{y_{(i+1,j)}-y_{(i-1,j)}}{2\Delta x} - v_{(i,j)}\frac{v_{(i+1,j)}-v_{(i-1,j)}}{2\Delta x}\} - v_{(i,j)} \quad (4.16)$$

4.4.1.1 Effects of Increasing Lateral Inflows (K) on Velocity of the Main Channel in Zone 1

The effects of increasing the number of lateral inflows on velocity holding constant at $\vartheta = 40^0$ is illustrated in figure 4.2.

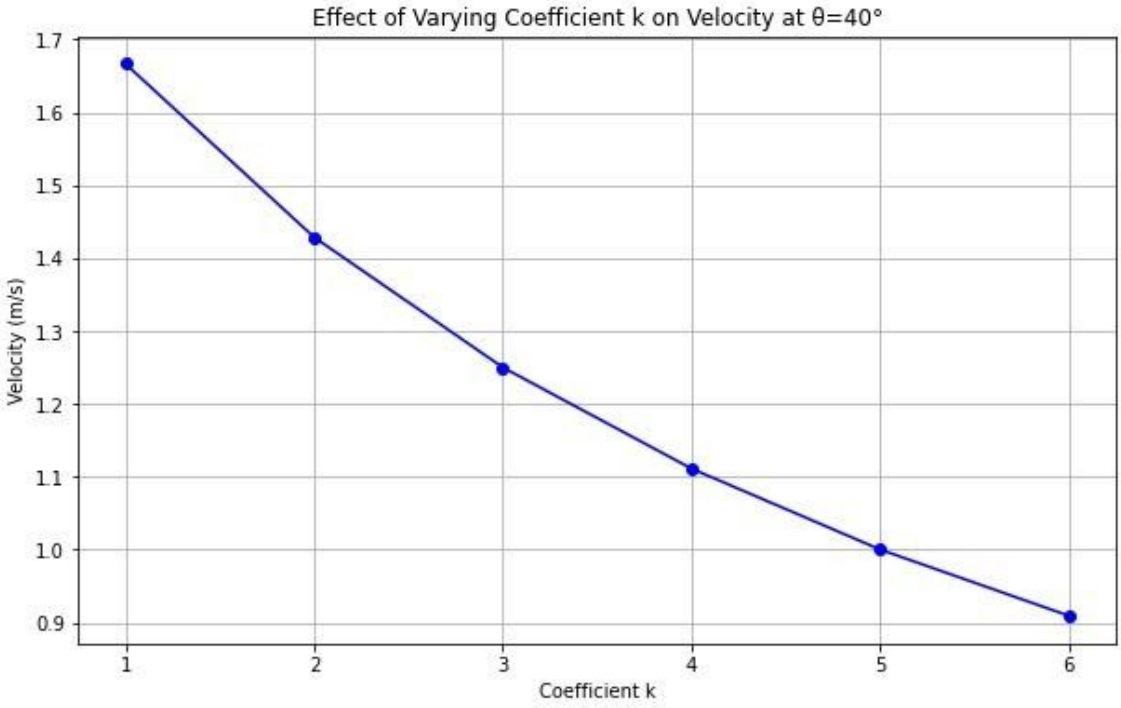

Figure 4.2: Effects of Increasing K on Velocity at $\vartheta = 40^0$

Figure 4.2 shows how the lateral inflows increase as the main channel's velocity decreases. The total cross-sectional area that the water flows through is increased when lateral inflows are introduced into the main channel. According to the continuity principle, the fluid velocity in a laminar flow is inversely proportional to the cross-sectional area. This principle suggests that when the total cross-sectional area grows, the velocity must drop to maintain the same flow rate. It states that the mass flow rate must remain constant along a streamline. The average velocity decreases when additional lateral inflows enter the main channel because the flow is spread over a greater region by the bigger cross-sectional area. The essential features of a laminar flow environment, which preserves the smooth, ordered transition of water, are this redistribution of flow and the decrease in velocity. As turbulence is more likely to start at higher velocities, this velocity decrease helps maintain the laminar flow pattern. The main channel's flow is essentially redistributed when lateral inflows enter it because they add fresh water at different places along its length. Some of the concentrated flow at the channel's center is decreased by the spread of flow over a larger area. As more water is introduced from the sides through lateral inflows, the flow in the main channel becomes more evenly spread across its width. This spreading effect reduces the overall disparity between velocities

in different parts of the channel, especially by reducing the peak velocities typically found at the center. The more uniform distribution of flow also reduces shear stress on the channel boundaries, which helps maintain the laminar flow regime by avoiding turbulence. The gradual decrease in peak velocities is important for maintaining a smooth, orderly flow and ensuring the flow remains within the laminar regime. When the flow is more evenly distributed across the channel, it lessens the pressure gradients and velocity differentials between different points in the main channel. This, in turn, contributes to a steadier, more stable flow, as abrupt changes in velocity can lead to turbulence and disruption of the laminar flow. Furthermore, as the flow becomes more evenly distributed, the water's kinetic energy is also spread more uniformly across the channel's width. This uniform distribution of kinetic energy results in a reduction in the overall energy gradient, which aligns with the decrease in average velocity in the main channel. This phenomenon can also influence other factors, such as reduced sediment transport potential, even though the scenario currently involves no sediments. Even though the lateral inflows have the same velocities as the main channel, the mixing of the inflow with the main channel flow still leads to significant changes in the flow dynamics at the points of entry. As the lateral inflows merge with the main channel, the interaction of different flow streams with potentially differing angles or directions creates localized areas of turbulence. This is because the inflowing water may not perfectly align with the main channel's flow direction, causing disturbances in the previously steady, laminar flow. This mixing turbulence can manifest as swirling eddies and vortex-like structures at the points of mixing, which disrupt the uniform, layered flow typical of laminar regimes. The presence of eddies and turbulence increases the chaotic movement of water molecules, leading to higher friction within the flow. This results in a greater conversion of kinetic energy into heat through viscous dissipation. The turbulence generated at these mixing points can spread downstream, affecting larger sections of the main channel. The chaotic, turbulent flow requires more energy to overcome resistance and friction against the channel boundaries, contributing to an overall decrease in the main channel's average velocity. Furthermore, as the flow transitions from laminar to turbulent in localized areas, there is an increased potential for energy dissipation. This disruption of the laminar flow pattern and subsequent energy loss affects the efficiency of the main channel flow, leading to a reduction in the main channel's overall velocity.

While the inflows may have the same velocities, the dynamic interactions between the inflows and the main channel can cause localized turbulence and energy dissipation, ultimately impacting the flow velocity along the channel.

4.4.1.2 Effects of the Varying Angle

The effects of increasing the angle on velocity at different values of K is illustrated in figure 4.3.

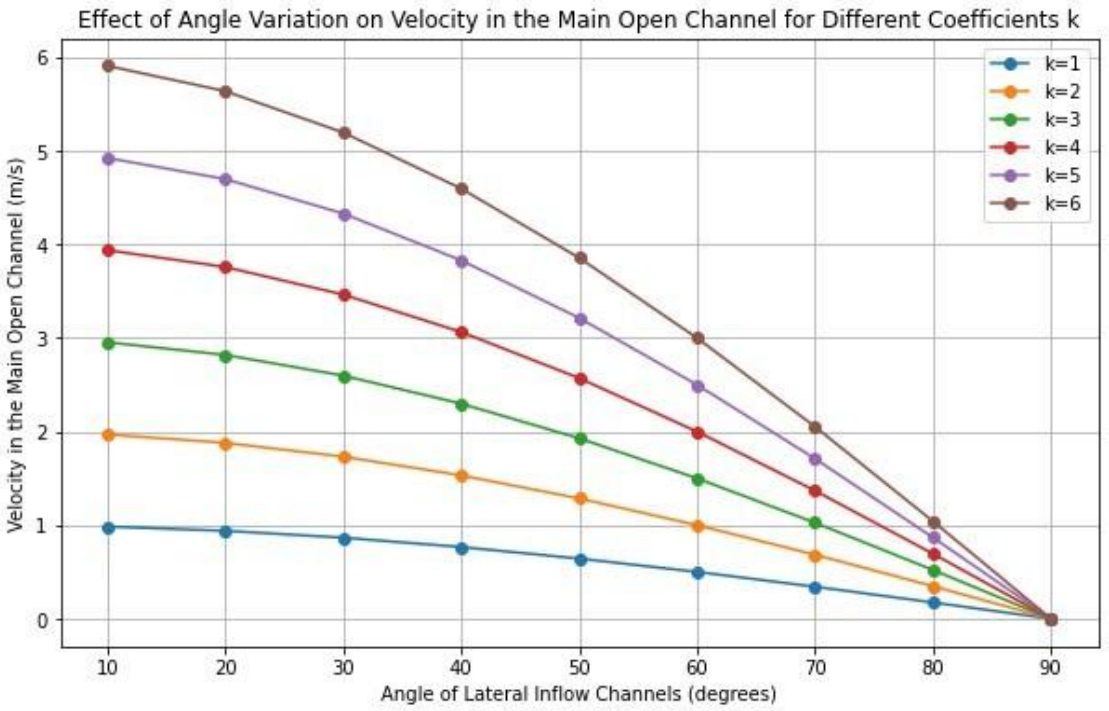

Figure 4.3: Effects of Varying Angle on Main Channel Velocity for Different Coefficient of K

Figure 4.3 shows that the velocity reduces in the main channnel as the angles of the lateral inflows increases.The direction of the influx into the main channel gets increasingly oblique as the angle of lateral inflows rises. This change in direction disturbs the flow of fluid in the main channel more significantly. A larger angle of entry and collisions between the lateral flow and other flows disturb the laminar flow's smooth, linear transition in the main channel. This disruption causes momentum to be transferred from the main channel flow to the lateral flow, which could cause the main channel's velocity to decrease. A fluid flows in parallel layers with little to no intermixing in a laminar flow. When the angle of lateral inflows increases, the interaction between the inflow and the main channel flow causes an increase in shear stress between the fluid layers.

This increase in shear stress may result in a reducing the flow rate of the primary channel because of an increase in friction and internal resistance. At greater inflow angles, the effect of increased shear stress and the disruption of the smooth flow pattern become more apparent. A larger angle of lateral inflow can also cause flow separation within the main channel. This phenomenon occurs when the inflow angle causes the fluid streams to diverge from each other, leading to areas of recirculation or eddies. Flow separation not only disrupts the laminar flow pattern but also results in energy dissipation, further reducing the overall velocity in the main channel. The pressure distribution along the main channel is affected by the complex fluid dynamics in the channel as the angle of lateral inflows increases. Localized pressure changes can be produced by a larger angle of inflow, especially close to the point of inflow. A decrease in flow speed may result from these pressure gradient variations' effects on the main channel's overall flow velocity. The concepts of momentum and mass conservation control fluid dynamics. The distribution of flow rates and velocities may alter when the angle of lateral inflows increases due to the way the inflows mix with the main channel flow. In order to accommodate the entry of fluid from the lateral inflows, the flow rate in the primary channel might have to decrease in order to preserve the overall conservation of mass and momentum. Higher inflow angles may cause more noticeable flow interactions and direction shifts, which could lead to an increase in flow resistance. The lateral inflows causes turbulence and direction variations in the main channel, which the fluid must navigate through. This resistance increases, causing the flow velocity decreasing.

4.4.1.3 Effects of Cross-Sectional Variation on Velocity in the Main Channel

The effects of increasing the cross-sectional area of lateral inflows on velocity is illustrated in figure 4.4.

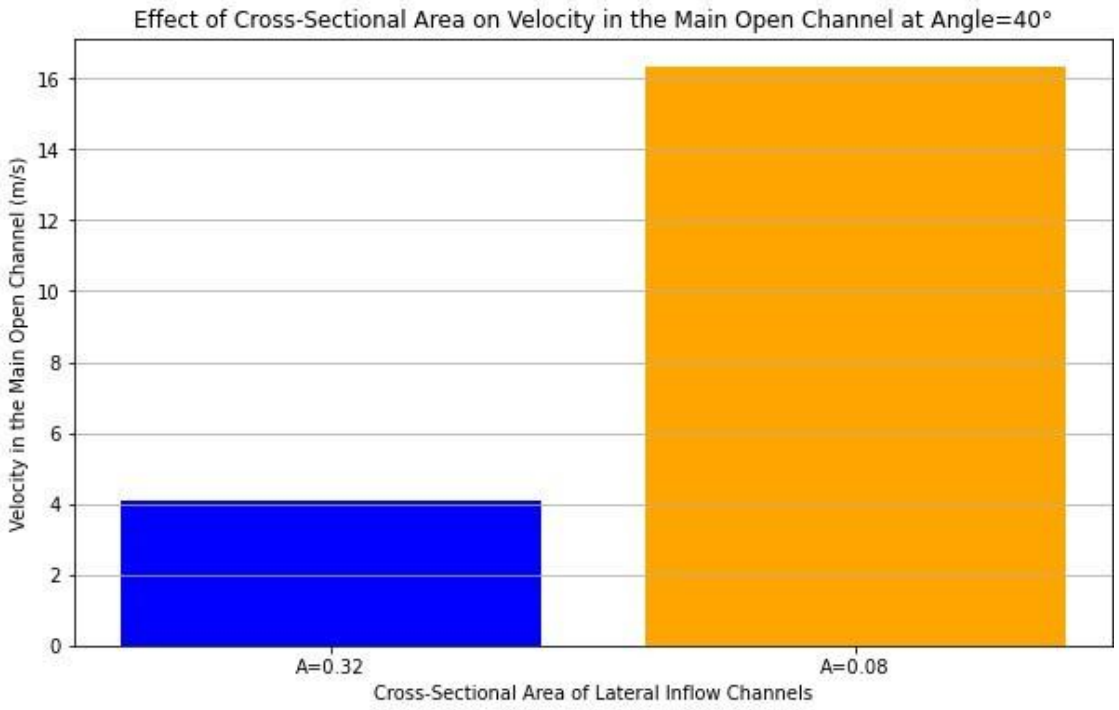

Figure 4.4: Effects of Variation of Cross-Sectional Area on Velocity

Figure 4.4 shows that the velocity reduces in the main channnel as the cross-sectional area of the lateral inflows increases.Firstly, when the cross-sectional area of lateral inflows is reduced, less fluid is introduced into the main channel. This reduction in inflow volume means there is less disruption to the existing flow in the primary channel. The primary channel's ordered and smooth laminar flow is thus less disturbed, enabling it to maintain higher velocities; additionally, the decrease in lateral inflow volume indicates a smaller change in momentum upon entry, which further maintains the higher flow rate of the primary channel. Secondly, a reduction in the area across the cross-section of lateral inflows can decrease the shear stress and resistance encountered in the main channel. In laminar flow, fluid moves in parallel layers with minimal mixing between them with less fluid entering the main channel from the lateral inflows, the interaction between the inflow and the primary channel flow is minimized, resulting in lower internal friction and resistance. This reduced resistance allows the fluid in the main channel to flow more freely, thereby increasing the velocity. Thirdly, the decreased volume from lateral inflows can affect the overall pressure distribution in the primary conduit. The influx of fluid from lateral inflows typically affects the pressure gradient along the main channel with reduced lateral inflows, there is less disruption to the pressure gradient,

and the overall flow in the primary channel remains more uniform. This uniformity contributes to higher flow velocities as the flow remains more streamlined. Lastly, reducing the cross-sectional area of lateral inflows can improve the conservation of mass and momentum in the main channel, with less fluid being introduced from the lateral inflows, the main channel can maintain a more consistent flow rate and velocity, resulting in more efficient fluid dynamics. This efficiency translates into higher velocities in the main channel as the flow experiences less variation and interruption.

4.4.1.4 Effects of Variation of Length of Lateral Inflows on Velocity in the Main Channel

The effects of increasing the length of lateral inflows on velocity is illustrated in figure 4.5.

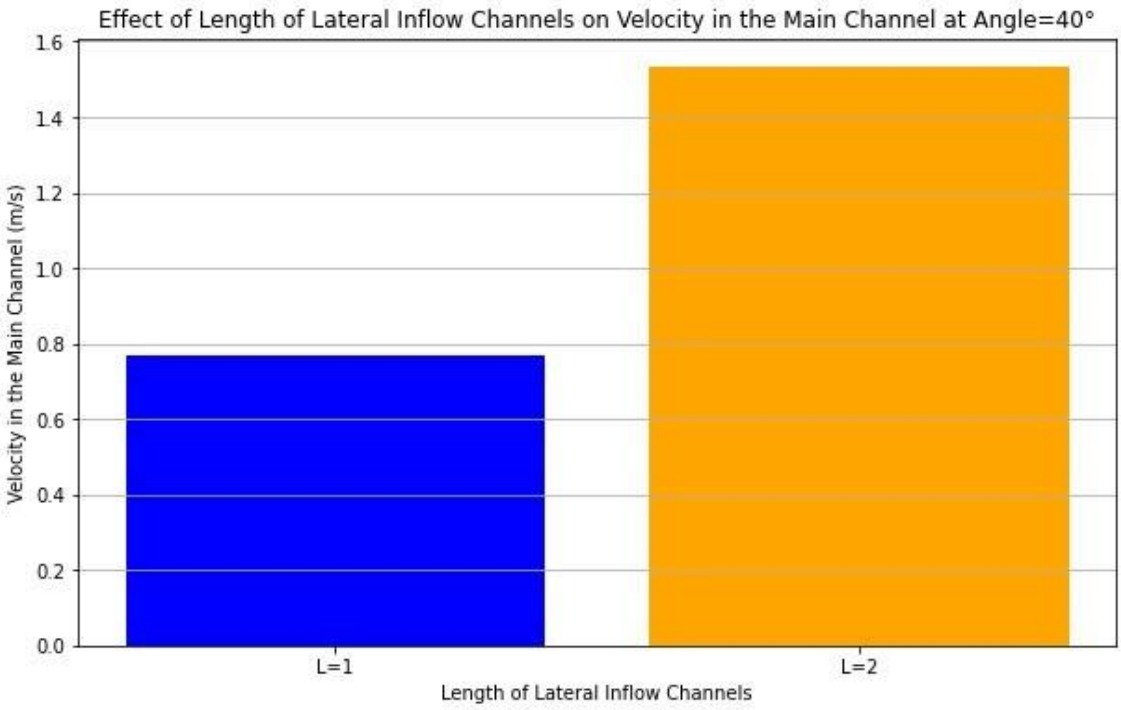

Figure 4.5: Effects of Variation of Length of Lateral Inflow

Figure 4.5 shows that the velocity increases in the main channnel as the length of the lateral inflows increases. Firstly, as the length of lateral inflow increases, the interaction between the lateral inflow and the primary channel flow becomes more gradual. This more gradual interaction allows for a smoother merging of the flows, which minimizes abrupt changes in momentum and velocity. As a result, the main channel flow is less disrupted, allowing it to maintain higher velocities. Secondly, a longer lateral inflow

provides a more extended contact area with the main channel, enabling the lateral inflow to spread out more evenly along the main channel's length. This even distribution reduces localized disturbances in the main channel flow and allows for a more uniform flow profile. This uniformity helps maintain a higher overall flow rate in the primary channel. Thirdly, increasing the length of the lateral inflow can lead to a more gradual mixing of the inflow with the main channel flow. This gradual mixing helps preserve the laminar flow characteristics in the main channel, as the inflow can smoothly integrate with the existing flow. This smooth integration prevents sudden changes in flow direction or velocity, thus allowing the main channel flow to maintain its higher speed. Fourthly, the longer length of lateral inflow can help distribute the inflow fluid over a larger portion of the main channel. This distribution can help maintain the continuity and conservation of mass and momentum in the main channel flow. By dispersing the inflow more evenly, the flow in the primary channel is less prone to sharp changes in pressure gradients, which can increase the overall flow velocity. Fifthly, a longer length of lateral inflow can also decrease the peak flow rate of the inflow at any specific point along the main channel. By spreading the inflow over a longer distance, the rate of inflow at any point is reduced, resulting in a more balanced flow. This balance helps minimize the impact of lateral inflows on the main channel flow, allowing it to flow more smoothly and maintain higher velocities. Finally, turbulence and eddies at the entrance places of input may decrease as a result of the longer lateral inflow. Localized disruptions or recirculation zones are less likely to form when the lateral inflow is allowed to progressively mix with the main channel flow. The main channel's greater velocities are further maintained by this decrease in turbulence.

4.4.2 Velocity profiles for zone 2

The continuity and momentum equations in zone 2 is given by equations 4.17 and 4.18. These equations are solved numerically by the finite method and graphically illustrated

in figure 4.6 to 4.9.

$$y_{(i,j+1)} = \Delta t\{k\frac{\left[H^2\left[\frac{c}{2} + \sin^{-1}\left(\frac{2h-H}{2H}\right)\right] - (h-\frac{H}{2})\{H - \sqrt{H^2-(h-\frac{H}{2})^2}\}v\right]}{2L\left[H^2-(h-\frac{H}{2})^2-H\right]}\sin\vartheta - v^*_{(i,j)}\frac{y_{(i+1,j)}-y_{(i-1,j)}}{2\Delta x}$$

$$-\frac{\left[H^2\left[\frac{c}{2} + \sin^{-1}\left(\frac{2h-H}{2H}\right)\right] - (h-\frac{H}{2})\{H - \sqrt{H^2-(h-\frac{H}{2})^2}\}\right]}{2L\left[H^2-(h-\frac{H}{2})^2-H\right]}\frac{v_{(i+1,j)}-v_{(i-1,j)}}{2\Delta x}\} + y_{(i,j)} \quad (4.17)$$

$$v_{(i,j+1)} = \Delta t\{k\frac{q^*v}{Fr^2gH^2}\left[c_2 + \sin^{-1}\left(\frac{2h-H}{2H}\right)\right] - (h-\frac{H}{2})\{H - \sqrt{H^2-(h-\frac{H}{2})^2}\}L$$

$$\sin\vartheta(u\cos\vartheta - v_{(i,j)}) - \frac{1}{Fr^2}\frac{n^2v^{*2}v^2}{R^{\frac{4}{3}}} - s_0 \quad (4.18)$$

$$-\frac{1}{Fr^2}\frac{y_{(i+1,j)}-y_{(i-1,j)}}{2\Delta x} - v_{(i,j)}\frac{v_{(i+1,j)}-v_{(i-1,j)}}{2\Delta x}\} - v_{(i,j)}$$

4.4.2.1 Effects of Increasing K on Velocity of the Main Channel in Zone 2

The effects of increasing the number of lateral inflows on velocity at $\vartheta = 25^0, 40^0, 50^0$ and 80^0 is shown in figure 4.6.

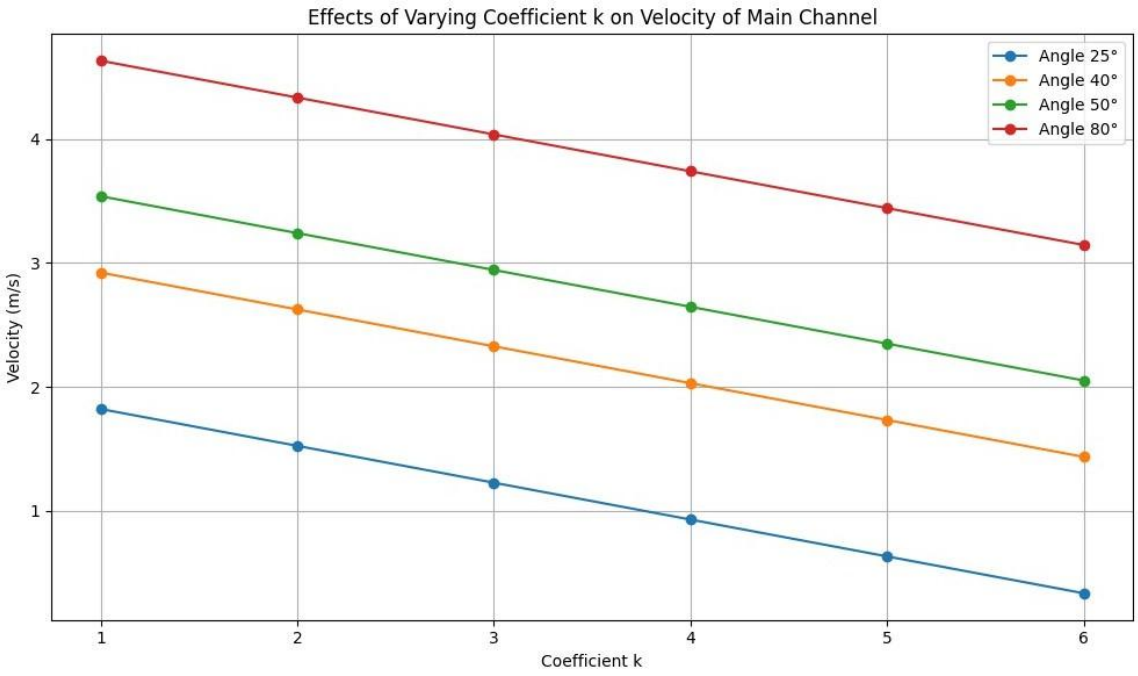

Figure 4.6: Effects of Increasing K on Velocity of the Main Channel

Figure 4.6 shows that as the lateral inflows increases the velocity of the main channel decreases. Lateral inflows, as they merge with the main channel in zone two, introduce additional water into the system, augmenting the total flow volume and consequently expanding the cross-sectional area of the conduit. This increase in area, in accordance with the principle of continuity, prompts a decrease in flow velocity. The momentum carried by these lateral inflows further influences the velocity distribution within the main channel, as the merging process transfers momentum into the main flow. As a result, the flow velocity diminishes to accommodate the added water and momentum, leading to a more uniform velocity distribution across the channel and a consequent reduction in velocity within zone two.

The geometric configuration of the horse-shoe cross-section significantly impacts how lateral inflows affect flow velocity. In zone two, the main channel typically exhibits a wider and deeper profile compared to zones one and three. This wider profile facilitates the incorporation of more lateral inflows, contributing to the velocity decrease. Moreover, the deeper channel profile allows lateral inflows a larger volume to fill, further slowing down flow velocity.

The interplay between the main channel flow and lateral inflows creates intricate flow patterns resulting in decreased velocity within zone two. The introduction of lateral inflows induces eddies and turbulence within the main channel, disrupting the smooth flow and causing energy losses, thus reducing velocity. Additionally, the mixing of water from various sources introduces frictional losses, compounding the velocity decrease.

4.4.2.2 Effects of Angle Variation on Velocity in the Main Channel

The effects of increasing the angle on velocity of the main channel is shown in figure 4.7.

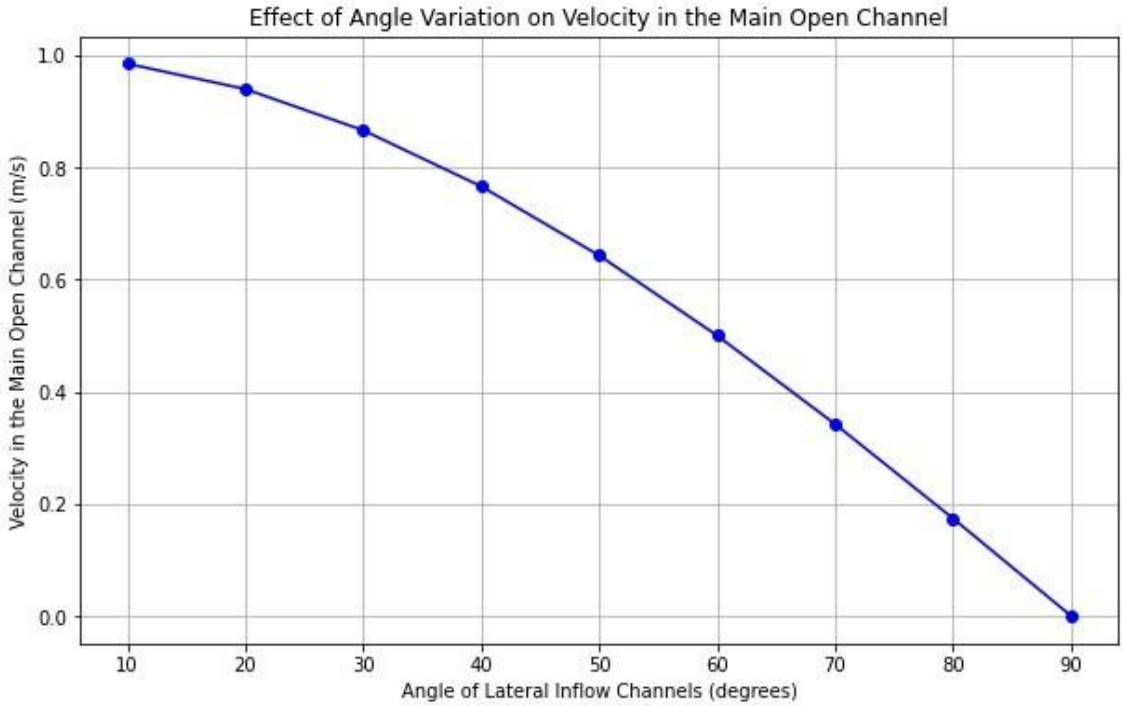

Figure 4.7: Effects of Angle Variation on Velocity

Figure 4.7 shows how the angle of the lateral inflows increases and the main channel's velocity decreases. When lateral inflow channels intersect the main open channel at sharper angles, they introduce water with higher momentum. This heightened momentum initiates increased turbulence and mixing within the main channel, consequently slowing down the flow velocity. This effect is particularly noticeable in zone two, where the primary flow is well-established. The abrupt introduction of water at a sharp angle disrupts the flow pattern, resulting in energy losses and a subsequent decrease in velocity.

The angle at which lateral inflow channels merge with the main channel influences flow convergence. When these inflows join at wider angles, convergence occurs more smoothly, and flow momentum is distributed more gradually across the main channel. This leads to less disruption to the main flow and a more consistent velocity profile in zone two. As a result, the velocity of the primary channel in zone two remains relatively higher compared to instances where inflows join at sharper angles.

In a horse-shoe cross-section, zone two typically exhibits a wider and deeper profile than zones one and three. When lateral inflows enter the main channel at wider angles, they

distribute more evenly across the wider zone two, facilitating a smoother flow transition and reducing velocity decrease. Conversely, inflows entering at sharper angles may only affect a small portion of the main channel, leading to more significant disruptions and velocity reductions.

The angle of lateral inflow channels also impacts the formation of eddies and secondary flow patterns in the main channel. Sharp-angle entries tend to generate stronger eddies and vortices, particularly near the point of entry, disrupting the main flow and reducing velocity. On the other hand, wider-angle entries result in less pronounced eddy formation, promoting smoother flow and higher velocities in zone two.

Sediment transport dynamics are influenced by the angle of lateral inflow channels, subsequently affecting velocity. Sharp-angle entries create areas of higher erosion and sediment deposition in the main channel, altering its cross-sectional shape and increasing roughness. This heightened roughness leads to higher frictional losses and decreased velocity. Conversely, wider-angle entries distribute sediment transport more evenly, resulting in a smoother channel bed and higher velocities.

Finally, the hydraulic properties of the main channel are influenced by the angle of lateral inflow channels. The hydraulic radius and slope of the main channel vary depending on how inflows merge. Channels entering at sharp angles reduce the hydraulic radius and increase the slope, resulting in lower velocities. In contrast, channels entering at wider angles increase the hydraulic radius and decrease the slope, allowing for higher velocities in zone two. As a result, variations in the lateral inflow conduits' angles significantly affect the primary open conduit's rate in zone two, usually leading to lower speeds at sharper angles and higher velocities at wider angles.

4.4.2.3 Effects of Cross-Sectional Variation on Velocity in the Main Channel in Zone 2

The effects of increasing the cross-sectional area on velocity of the main channel is shown in figure 4.8.

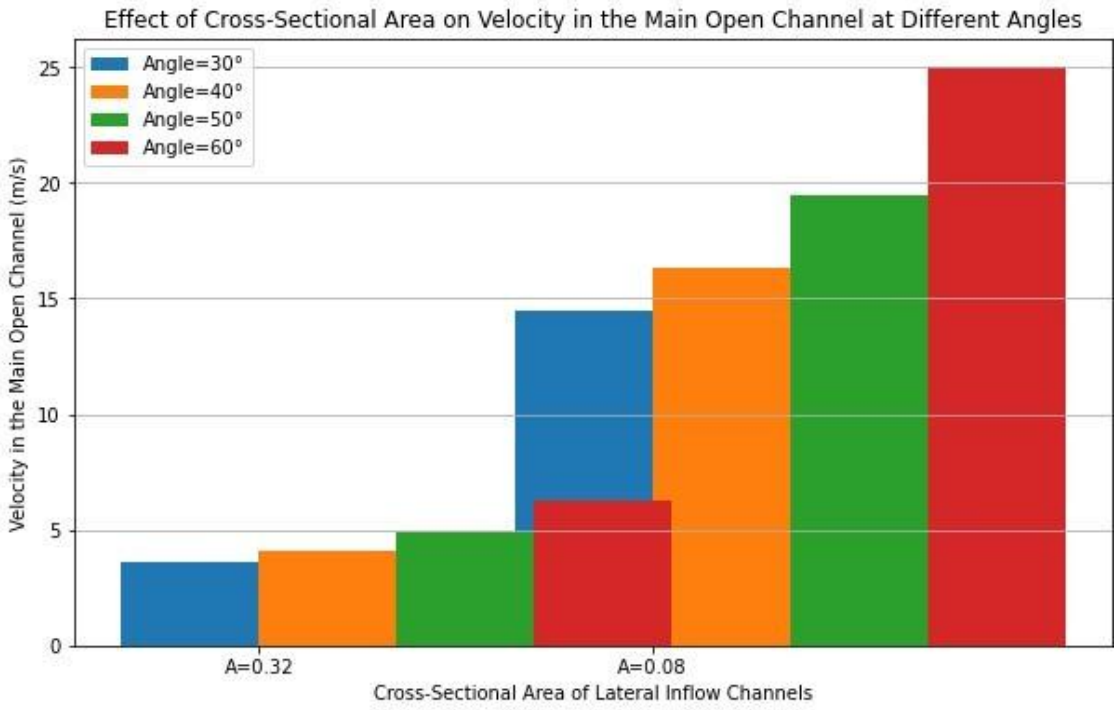

Figure 4.8: Effects of Cross-Sectional Area Variation on Velocity in the Main Channel

Figure 4.8 shows how the velocity in the primary channel decreases as the cross-sectional area of the inflow channels increases. The flow dynamics in zone two are greatly affected by lateral inflow channels, which introduce a greater amount of water into the primary channel. The primary conduit's cross-sectional area increases as a result of this increase in flow volume, in accordance with the continuity principle. The same volume of water now has more space to occupy, therefore the velocity of the flow in zone two decreases as a result of having a bigger cross-sectional area to fill.

The momentum of the flow in the main channel is affected by the increased volume of water entering through the lateral inflow channels. Greater momentum transfer from more water entering the main channel through the laterals results in a redistribution of momentum within the channel and a decline in flow velocity. Lower velocities are the result of zone two's current flow pattern being further disrupted by the extra momentum from the lateral inflow channels.

The manner in which the lateral inflow conduits' higher cross-sectional area influences the rate in the primary channel is also affected by their geometry. If the lateral inflow channels widen gradually before joining the main channel, they facilitate a smoother

transition of flow into the main channel. This gradual widening allows for a more gradual increase in flow volume, which may minimize disruptions to the main channel flow and help maintain velocities in zone two.

The dynamics of flow convergence when lateral input channels meet the main channel are changed when their cross-sectional area increases. A more consistent velocity profile is maintained in zone two if the lateral channels have a bigger cross-sectional area because they contribute to the flow in the primary conduit more evenly. In contrast, narrow lateral inflow channels have the potential for adding water into concentrated streams, which would cause more localized disruptions and lower main channel velocities.

The increased cross-sectional area of lateral inflow channels can affect sediment transport dynamics in the main channel. With more water entering from the laterals, there is a higher sediment-carrying capacity, potentially leading to more deposition or erosion within the main channel. These changes in channel morphology can increase frictional losses and decrease velocities in zone two.

Lastly, the hydraulic characteristics of the primary channel are influenced by the increased cross-sectional area of lateral inflow conduits,with more water entering from the laterals, the hydraulic radius of the main channel may increase, typically resulting in lower frictional losses and higher velocities. However, changes in channel roughness due to sediment deposition or erosion can make the effect on velocity more complex and because of these hydraulic and geometric effects, a horseshoe cross-section's zone two velocity may be reduced when the cross-sectional area of the lateral inflow channels increases.

4.4.2.4 Effects of Variation of Length of Lateral Inflows on Velocity in the Main Channel in Zone 2

The effects of increasing the length of the lateral inflows on velocity of the main channel is shown in figure 4.9.

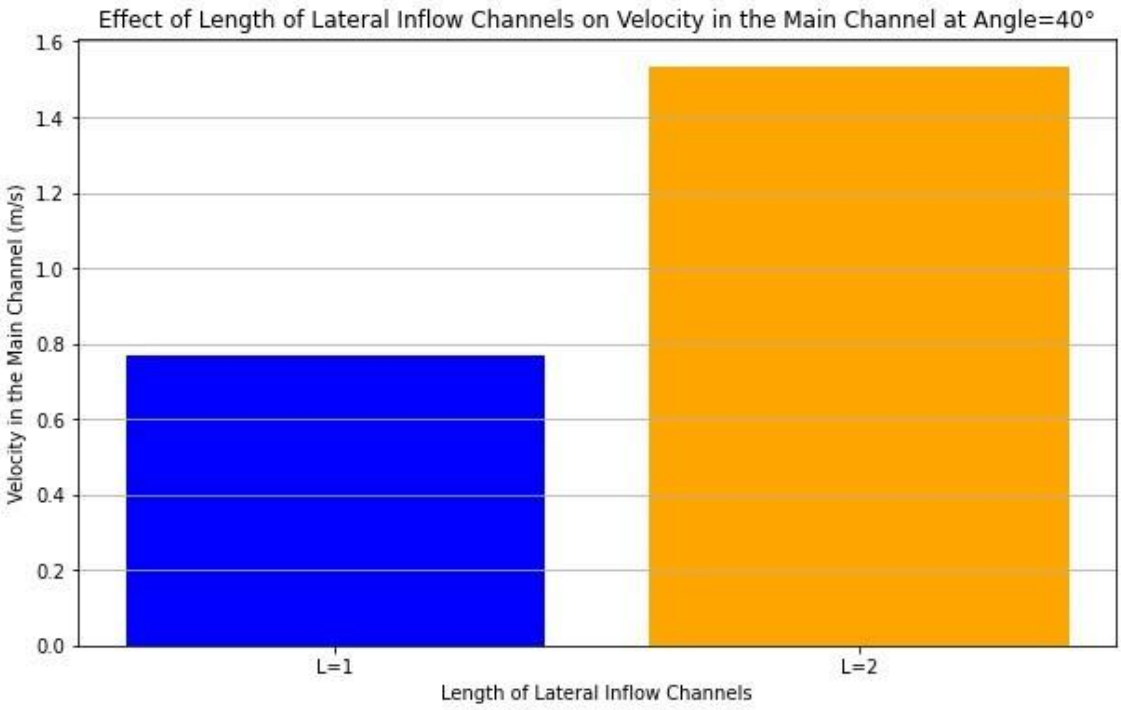

Figure 4.9: Effects of Variation of Length of Lateral Inflows on Velocity in the Main Channel

Figure 4.9 shows how the velocity in the main channel increases with the length of lateral inflows. Water must travel a greater distance before reaching the main channel when lateral inflow channels get longer. This longer travel distance can result in increased frictional losses along the lateral channels, causing a decrease in velocity by the time water reaches the main channel. Consequently, in zone two, where the main channel is already established, inflow from longer lateral channels contributes less momentum to the flow, leading to lower velocities.

The increased length of lateral inflow channels can alter flow convergence dynamics where they meet the main channel. Longer lateral channels have more opportunity to disperse their flow along the main channel, distributing inflow more evenly across the width of the main channel. This reduces localized disruptions and maintains a more uniform velocity profile in zone two. Long lateral channels may cause the momentum and flow rate in the primary channel to significantly decrease. The geometry of lateral inflow channels interacts with their length to affect velocity in the main channel. Longer lateral channels can create a more gradual transition of flow into the main channel if they widen gradually, minimizing disruptions to flow and maintaining higher

velocities in zone two. Conversely, short lateral channels or abrupt joinings can cause disturbances and reduce velocities in zone two.

Longer lateral inflow channels can also affect sediment transport dynamics in the main channel by picking up more sediment along their path and introducing it into the main channel. This leads to changes in channel morphology and increased frictional losses, decreasing velocities in zone two as the flow encounters increased resistance due to rougher channel surfaces.

The hydraulic characteristics of the main channel are influenced by the increased length of lateral inflow channels. If lateral channels are lengthened, the hydraulic radius of the primary conduit may decrease, leading to increased frictional losses and reduced velocities, especially if the longer lateral channels result in a more irregular or narrower main channel cross-section in zone two.

Moreover, the increased length of lateral inflow channels may affect the discharge characteristics of the main channel, potentially causing a delay in the arrival of water from upstream sources. This delayed discharge can impact the timing and magnitude of peak flows in the main channel, with subsequent effects on velocity in zone two depending on various factors such as flow rate and cross-sectional geometry. Overall, because of greater frictional losses, modified flow convergence dynamics, altered sediment transport, and varied hydraulic characteristics, longer lateral inflow channels result in lower velocities in zone two.

4.4.3 Velocity profiles for zone 3

The continuity and momentum equations in zone 3 is given by equations 4.19 and 4.20. These equations are solved numerically by the finite method and graphically illustrated in figure 4.10 to 4.13.

$$y_{(i,j+1)} = \Delta t\{k\frac{(h-\frac{H}{2})\sqrt{h(H-h)+\frac{H^2}{4}sin^{-1}(\frac{2h-H}{H})+A}\,v_2^{*}}{\frac{Q}{HL\sqrt{1-(1-\frac{2h}{H})^2}}}sin\vartheta - v_{(i,j)}\frac{y_{(i+1,j)}-y_{(i-1,j)}}{2\Delta x} - \frac{\{(h-\frac{H}{2})\sqrt{h(H-h)+\frac{H^2}{4}sin^{-1}(\frac{2h-H}{H})+A}\,\}v_2}{\frac{Q}{HL\sqrt{1-(1-\frac{2h}{H})^2}}}\frac{v_{(i+1,j)}-v_{(i-1,j)}}{2\Delta x}\} + y_{(i,j)} \quad (4.19)$$

$$v_{(i,j+1)} = \Delta t\{k\frac{\sqrt{\frac{q^{*}v}{h(H-h)+\frac{H^2}{4}sin^{-1}(\frac{2h-H}{H})+A_2L}}}{Fr^2\,g(h-\frac{H}{2})} sin\vartheta(ucos\vartheta - v_{(i,j)}) - \frac{1}{Fr^2}\frac{n^2v^{*2}v^2}{R^{\frac{4}{3}}} - s_0 \quad (4.20)$$
$$- \frac{1}{Fr^2}\frac{y_{(i+1,j)}-y_{(i-1,j)}}{2\Delta x} - v_{(i,j)}\frac{v_{(i+1,j)}-v_{(i-1,j)}}{2\Delta x}\} - v_{(i,j)}$$

4.4.3.1 Effects of Increasing K on Velocity of the Main Channel

The effects of increasing the number of lateral inflows on velocity is shown in figure 4.10.

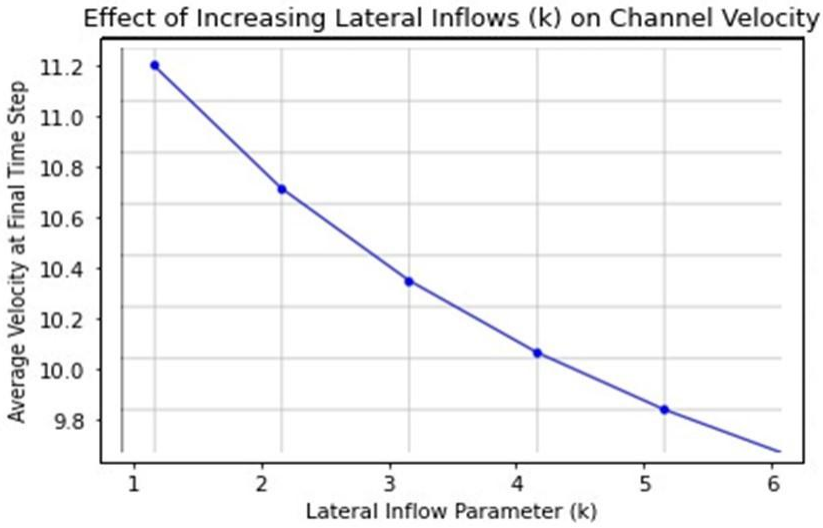

Figure 4.10: Effects of Increasing K on Velocity of the Main Channel

Figure 4.10 shows how the flow rate in the primary channel decreases as lateral inflows inputs increase. The overall flow volume rises as more lateral inflows enter the main channel. This increase results in an increased cross-sectional area in zone three as a wider channel is required to accommodate the extra water. An increase in cross-sectional area causes a decrease in flow rate, according to the continuity principle. Because there are more lateral inflows, zone three's flow velocity drops because there is more water in the area. The momentum of the flow in the primary conduit is also influenced by these additional lateral inflows. Each inflow brings its own momentum, and as more lateral inflows merge with the main channel, there is a greater momentum transfer. The

main channel's flow velocity decreases as a result of this transfer, especially in zone three where the lateral inflows greatly increase the overall flow volume. As a result of the redistribution of momentum, the flow must be adjusted, which lowers velocity as the main channel makes way for the additional water and momentum. Furthermore, complicated flow patterns are produced by the interplay of lateral inflows with the main channel flow, which further influences zone three velocity. Lateral inflows cause turbulence and mixing, which disturbs the water's smooth flow and wastes energy. Frictional losses result from this turbulent flow and add to the velocity drop. Lastly, the quantity of lateral inflows modifies the hydraulic properties of the main channel. The hydraulic radius and gradient of the main channel are altered by the increased water volume and momentum caused by these inflows. According to Manning's equation, this changed geometry and slope cause the flow velocity to decrease. Because of a combination of hydraulic and geometric variables, the main channel velocity in zone three reduces as the number of lateral inflows increases.

4.4.3.2 Effects of Angle Variation on Velocity in the Main Channel

The effects of increasing the angle of lateral inflows on velocity is shown in figure 4.11.

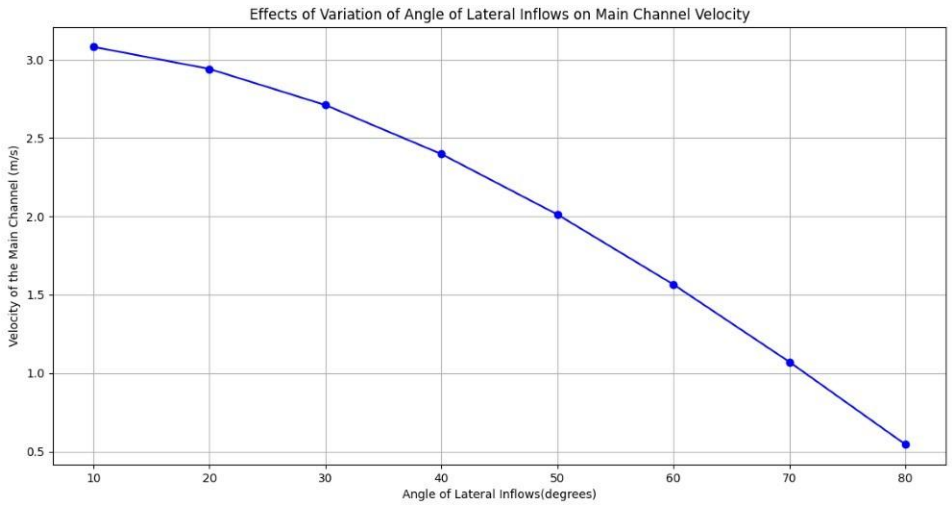

Figure 4.11: Effects of Angle Variation on Velocity in the Main Channel

Figure 4.11 shows that the velocity decreases as the the angle of the lateral inflows increases. When the angle of lateral inflows in a laminar flow is increased in a horseshoe-shaped channel at the top of the channels, several changes occur in the flow dynam-

ics. As the angle of inflows becomes more acute, the water entering the main channel does so with a greater component of its velocity directed along the flow direction of the main channel. This alignment reduces the disruption to the main flow, maintaining a smoother, more streamlined movement of water.

In a horseshoe-shaped channel, the increased angle of inflows leads to a more efficient merging of the lateral and main flows. The acute angle ensures that the inflows blend more gradually with the main channel's flow, reducing the likelihood of turbulence and mixing that can occur with more perpendicular inflows. This smoother integration minimizes energy losses and helps maintain the laminar flow, characterized by parallel layers of water moving with minimal mixing.

Additionally, with a greater angle of inflows, the hydraulic efficiency of the channel improves. The alignment of the lateral inflows with the main flow direction reduces the frictional and turbulent losses typically associated with sharper angles. As a result, the overall velocity of the flow in the main channel may increase slightly, as there is less resistance and disruption from the lateral inflows.

Overall, a more streamlined and effective merging of flows is achieved by increasing the angle of lateral inflows in a horseshoe-shaped channel at the top of the channels. This preserves laminar characteristics and may even increase the overall flow velocity due to a reduction in turbulence and energy losses.

4.4.3.3 Effects of Cross-Sectional Area Variation on Velocity in the Main Channel

The effects of increasing the cross-sectional area from 0.08 to 0.32 on velocity is shown in figure 4.12.

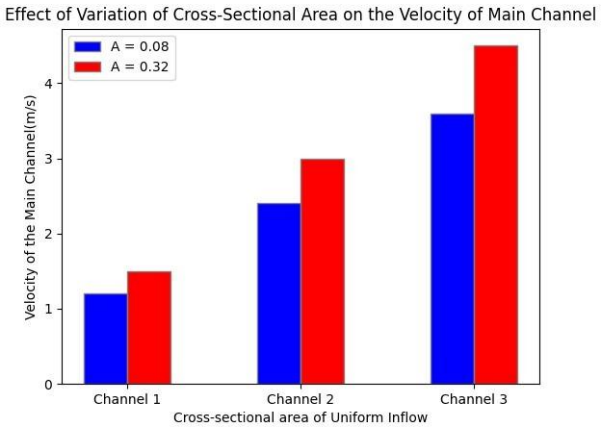

Figure 4.12: Effects of Cross-Sectional Area

Figure 4.12 shows how the cross-sectional area increases as the main channel's velocity decreases. The cross-sectional area of lateral inflow conduits can have significant impacts on the rate of the primary open conduit in zone three of a horseshoe cross-section. First, lateral inflow channels supply more water to the main channel when their cross-sectional area increases. The flow dynamics in zone three are significantly impacted by this extra water. The concept of continuity states that when flow volume increases, the main channel's cross-sectional area also increases. Because the same amount of water now has more space to occupy, the velocity of the flow in zone two drops as a result of having a bigger cross-sectional area to fill. Second, the momentum of the flow in the main channel is affected by the greater volume of water entering through the lateral inflow channels. There is a larger momentum transfer when there is more water coming in from the laterals. The primary channel's momentum is then redistributed, which lowers the flow velocity. The increased momentum from the lateral inflow channels further disrupts the current flow pattern in zone two, resulting in reduced velocities.

Thirdly, the way the lateral inflow conduits' higher cross-sectional area influences the rate in the primary channel depends in part on their geometry. A more seamless transition of flow into the main channel is made achievable if the lateral inflow channels expand slowly before joining it.. This gradual widening allows for a more gradual increase in flow volume, which may minimize disruptions to the main channel flow and help maintain velocities in zone three. Fourth, when the cross-sectional area of these channels increases, the flow convergence dynamics where the lateral inflow conduits

meet the primary conduit are altered. If the cross-sectional area of the lateral channels is larger, they contribute to the flow in the main channel more equally. This smooth flow distribution helps to maintain a more uniform velocity profile in zone three. However, limited lateral inflow routes may inject water into densely populated streams, producing more localized disruptions and a slower main channel velocity.

Fifth, the dynamics of sediment transport in the main channel may be altered by the lateral inflow channels' increased cross-sectional area. There is more ability to carry sediment when there is more water entering from the laterals. The main channel's cross-sectional form and roughness may change as a result of increased sediment movement, deposition, or erosion. In zone three, these modifications to the channel's shape may result in higher frictional losses and lower velocities.

4.4.3.4 Effects of Variation of Length of Lateral Inflows on rate of the primary Channel

The effects of increasing the length of lateral inflows on velocity from 1m to 2m is shown in figure 4.13.

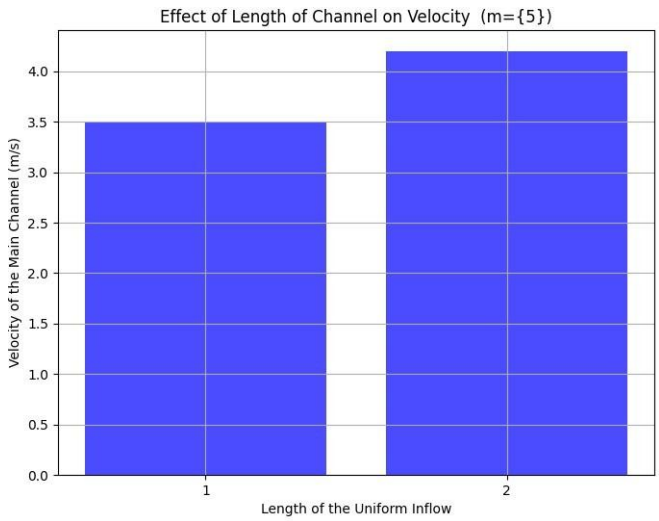

Figure 4.13: Effects of Variation of Length of Lateral Inflows on Velocity in the Main Channel

Figure 4.13 shows how the length of the lateral inflows increases along with the main channel's velocity. There are various factors that can cause the flow velocity in zone three of a horseshoe channel to increase as the length of lateral inflows increases. Firstly,

as lateral inflow is introduced, it brings additional water into the main flow, thereby increasing the overall discharge. This increase in discharge results in a higher flow rate through the channel, assuming the cross-sectional area remains relatively constant. As a result, the velocity of the water must increase to accommodate the higher volume of water moving through the same spatial constraints. Second, the lateral inflow's introduction of momentum results in an increase in velocity. Water frequently joins lateral flows with its own momentum, which when added to the main flow's momentum can increase the resulting velocity. This impact is most noticeable if the lateral inflow happens at a fast speed, giving the main flow in zone three of the horseshoe channel more kinetic energy. Thirdly, the interaction between the lateral inflow and the primary channel flow can lead to a reduction in hydraulic resistance. As the lateral inflow mixes with the main flow, it can disrupt the boundary layer and reduce frictional forces along the channel bed and walls. This reduction in frictional resistance allows the water to flow more freely and at a higher velocity. The degree of this effect may vary depending on the channel's overall geometry, the angle and flow rate of the lateral inflow, and the roughness of the conduit bed. Finally, the horseshoe channel's physical layout may improve how much greater lateral inflow affects velocity. Centripetal forces cause the flow in a horseshoe-shaped channel to tend to accelerate around bends. These forces may be amplified by the addition of lateral inflows, which would increase the velocity even further. Because of the compounding effect of geometric acceleration at bends and the added volume and momentum from lateral inflow, zone three is especially vulnerable to large increases in speed as lateral inflow increases.

CHAPTER FIVE

SUMMARY, CONCLUSION AND RECOMMENDATION

5.1 Summary and Conclusion

This thesis aimed to investigate the relationship between flow velocity and other flow characteristics. The effect of these characteristics on velocity has been studied. Since the flow in question is governed by nonlinear equations, its solution needs the establishment of an effective finite difference scheme, which is covered in detail in Chapter Two. The computational mesh for the issue is uniformly divided. The method was performed for all flow parameters, with the results shown visually, and each one was systematically changed while the others remained constant. It was discovered that the main channel's velocity decreases with increased lateral inflows. This phenomenon occurs because the introduction of lateral inflows into the main channel increases the total cross-sectional area through which the water flows. When more water is added from the sides, it spreads out across a larger area, affecting the overall dynamics of the flow within the channel.The fluid velocity in a laminar flow is inversely proportional to the cross-sectional area, according to the continuity principle. This principle states that the product of the cross-sectional area and the velocity of the fluid must remain constant for an incompressible fluid. Thus, if the cross-sectional area increases, the velocity must decrease to maintain the same flow rate. This relationship highlights the critical balance between area and velocity in fluid dynamics.

According to this theory, in order to maintain the same flow rate, the velocity must decrease as the total cross-sectional area increases. This principle ensures that the mass flow rate along a streamline remains constant. The mass flow rate is the amount of mass passing through a cross-section of the flow per unit time, and it must remain unchanged in a steady flow system. Any changes in the cross-sectional area directly impact the velocity to uphold this continuity. The velocity in the primary channel reduces as the angles of the lateral inflows increase. When lateral inflows enter the main channel at steeper angles, the impact on the primary flow is more pronounced. This directional change disrupts the smooth flow pattern of the primary channel, leading to a reduction in velocity. The angle of the inflow plays a crucial role in determining how much the main channel's velocity is affected.

As the direction of the influx into the main channel becomes more oblique, the angle of lateral inflows increases. An oblique angle means that the lateral inflow enters the main channel at a sharper angle rather than perpendicularly. This change in direction can cause turbulence and interfere with the streamlined flow of the main channel. The greater the angle, the more significant the disruption to the flow. The fluid flow in the main channel is more significantly impacted by this direction change. When the lateral flow approaches the primary channel at a greater angle, it collides with other flows, disrupting the laminar flow's smooth, linear route. This collision can create turbulence, eddies, and other flow disturbances, further reducing the velocity in the main channel. Understanding these interactions is crucial for managing and predicting flow behavior in various engineering and environmental applications.

The main channel's velocity increases with the length of the lateral inflows. This relationship is primarily due to the way extended lateral inflows interact with the main channel flow. When lateral inflows are short, they introduce a sudden influx of water into the main channel, which can cause abrupt changes in flow characteristics. However, as the length of these inflows increases, the interaction becomes more gradual, allowing for a smoother integration of the flows. As the lateral inflow lengthens, the interaction between it and the main channel flow becomes more gradual. A longer inflow provides a more extended period and distance for the water to blend with the main channel's flow. This extended interaction time allows for a more seamless transition, where the lateral flow can gradually adjust to the main channel's conditions. Consequently, the velocity changes that occur due to the influx of additional water are less abrupt, leading to a more stable flow regime in the main channel.

This more gradual interaction causes the flows to merge more gently, reducing abrupt changes in momentum and velocity. When the flows merge gently, the forces that act upon the water particles do not change suddenly. Instead, the transition is smoother, which helps in maintaining a more consistent velocity profile within the main channel. The reduction in abrupt momentum changes also minimizes the formation of turbulence and other flow irregularities, contributing to a more efficient and predictable flow pattern. Moreover, the gentle merging of flows as a result of longer lateral inflows enhances the overall stability of the fluid dynamics within the channel system. The gradual ad-

justment in velocity and momentum ensures that the main channel can accommodate the additional water without significant disruptions. This stability is crucial for various practical applications, such as irrigation, flood management, and hydraulic engineering, where predictable and controlled flow conditions are essential for effective operation and management. By understanding the influence of lateral inflow length on the main channel's velocity, engineers and scientists can design more efficient water conveyance systems that optimize flow conditions and minimize potential issues related to abrupt flow changes.

A lateral horseshoe-shaped open channel can significantly influence flow patterns by creating localized turbulence and flow separation, which increases energy losses and flow resistance. This shape also affects sediment transport and deposition, leading to non-uniform flow velocity and potential areas of erosion or deposition along the channel walls. A unique finding of the horseshoe-shaped channel is its ability to create asymmetric flow patterns, which enhance lateral circulation and significantly alter the velocity distribution across the channel. This shape also tends to cause more localized turbulence and energy dissipation compared to rectangular channels, leading to distinct effects on sediment transport and deposition along the channel walls.

5.2 Recommendation

This study's conclusions are theoretical in nature. To compare these theoretical findings with actual results, it is therefore advised to carry out experimental research. This indicates that more investigation is necessary. Additionally, it is recommended to pursue further studies on

i Effects of lateral outflow on discharge

ii Turbulent flow of the same cross-sectional shape

iii Fluid flows through elliptic channels

REFERENCES

Agrawal, B. and Mohd, I. (2021). Mathematical Modeling of Blood Flow. *International Journal of Statistics and Applied Mathematics*, 6(4):116–122.

Al Omari, N. K. and Khaleel, M. S. (2012). Laboratory Study of the Effect of the Branching Angle and the Branching Channel Slope on Flow. *Al-Rafadain Engineering Journal*, 20(5).

Barenblatt, G. I. (2003). *Scaling*, volume 34. Cambridge University Press.

Batchelor, G. K., Moffatt, H. K., and Worster, M. G. (2003). *Perspectives in Fluid Dynamics: A Collective Introduction to Current Research*. Cambridge University Press.

Cengel, Y. A., Cimbala, J. M., and Turner, R. (2014). Properties of Fluids. *Fluid Mechanics: Fundamentals and Applications*, pages 37–73.

Chadwick, A., Morfett, J., and Borthwick, M. (2021). *Hydraulics in Civil and Environmental Engineering*. Crc Press.

Chaudhry, M. H., Cass, D. E., and Edinger, J. E. (1983). Modeling of Unsteady-Flow Water Temperatures. *Journal of Hydraulic Engineering*, 109(5):657–669.

Chaudhry, M. H. et al. (2008). *Open-channel Flow*, volume 523. Springer.

Chepkonga, D., Kulei, W., and Owuor, C. (2024). Mathematical Modelling of Fluid Flow in Open Circular Channels in Sewerage Systems.

Chirchir, A. C. (2021). *The Effect of Two Lateral Inflow Channels on Main Channel Discharge*. PhD thesis, University Of Eldoret.

Chow, V. (1959). Open Channel Hydraulics MacGraw Hill Kogakusha. *Ltd. Tokyo*.

Chow, V. (1988). Applied Hydrology.

Chow, V. T. (1981). Hydraulic Exponents. *Journal of the Hydraulics Division*, 107(11):1489–1499.

Fink, J. K. and Fink, J. K. (2009). Dimensional Analysis. *Physical Chemistry in Depth*, pages 313–344.

Gerrard, J. H. and Taylor, L. A. (1977). Mathematical Model representing Blood Flow in Arteries. *Medical and Biological Engineering and Computing*, 15:611–617.

Harmizi, P. N. S., Zakaria, S. A. A., Zawawi, I. S. M., and Haniffah, M. R. M. (2023). Numerical Analysis on the Flow Depth Behaviour in Dividing Open-Channel for Trapezoidal and Rectangular Cross-Sectional Channel. *Journal of Advanced Research in Fluid Mechanics and Thermal Sciences*, 108(2):98–109.

Hasheminejad, S. and Wan, W. (2022). Saint–Venant Equations Simulation by Finite Volume Method and Ultimate Strategy. *Modeling Earth Systems and Environment*, 8(3):4255–4266.

Henderson, F. (1957). M. 1966 Open Channel Flow. *Journal of Fluid Mechanics*, 29(2):414–415.

Icha, A. (2012). Book Review: Fluid Mechanics, by Frank M. White, McGraw-Hill Companies, Inc. 2011; ISBN-13 9780073529349. *Pure and Applied Geophysics*, 169:1325–1327.

Incropera, F. P. and DeWitt, D. P. (2002). Heat and Mass Transfer. *Fifth John Wiley and Sons*, pages 533–593.

Isaac, M. (2019). Mathematical Modelling of Fluid Flow in an Open Channel with an Elliptic Cross-Section.

Jebelli, A., Mahabadi, A., Zare, M. S., and Ahmad, R. (2022). Numerical Simulations of Lateral input Effect in an Open Channel to reduce Disturbances in the Mainstream Channel using CFD. *Water-Energy Nexus*, 5:39–49.

Jomba, J. (2016). *Modeling Fluid Flow in Open Channel With Horsehoe Cross-Section*. PhD thesis, Meru University of Science and Technology.

Kadia, S., Lia, L., Albayrak, I., and Pummer, E. (2024). The Effect of Cross-sectional Geometry on the High-speed Narrow Open Channel Flows: An updated Reynolds Stress Model Study. *Computers & Fluids*, 271:106184.

Karimi, S. M. (2018). *Modeling Fluid Flow in an Open Rectangular Channel with Lateral Inflow Channel*. PhD thesis, JKUAT-PAUSTI.

Khosravinia, P., Hosseinzadeh Dalir, A., et al. (2019). Numerical Analyzing of Flow in Open Channel Junction with Effect of side Slope of Channel. *Irrigation and Water Engineering*, 10(1):1–16.

Khosronejad, A. and Sotiropoulos, F. (2014). Numerical Simulation of Sand Waves in a Turbulent Open Channel Flow. *Journal of Fluid Mechanics*, 753:150–216.

Kinyanjui, M., Tsombe, D., Kwanza, J., and Gaterere, K. (2011). Modeling Fluid Flow in Open Channel with Circular Cross-section. *Journal of Agriculture, Science and Technology*, 13(2):78–89.

Kwanza, J., Kinyanjui, M., and Nkoroi, J. (2007). Modeling Fluid Flow in Rectangular and Trapezoidal Open Channels. *Advances and Applications in Fluid Mechanics*, 2:149–158.

Labadin, J. and Ahmadi, A. (2006). Mathematical Modeling of the Arterial Blood Flow. In *Proceedings of the 2nd IMT-GT Regional Conference on Mathematics, Statistics and Applications, Universiti Sains Malaysia, Penang*.

Linsley, R. K. and Franzini, J. B. (1991). Water-Resources Engineering. *(No Title)*.

Litrico, X. and Fromion, V. (2004). Frequency Modeling of Open-channel Flow. *Journal of Hydraulic Engineering*, 130(8):806–815.

Liu, J., Wang, Z., and Fang, X. (2010a). Formulas for Computing Geometry and Critical Depth of General Horseshoe Tunnels. *Transactions of the ASABE*, 53(4):1159–1164.

Liu, J., Wang, Z., and Fang, X. (2010b). Iterative Formulas and Estimation Formulas for Computing Normal Depth of Horseshoe Cross-section Tunnel. *Journal of Irrigation and Drainage Engineering*, 136(11):786–790.

Loukam, I., Achour, B., and Djeddou, M. (2020). Chezy's Resistance Coefficient in a Horseshoe-shaped Tunnel. *Revue des Sciences de l'Eau*, 32(4):379–392.

Maghrebi, M. F. and Moghaddam, A. R. (2022). Flow in Open and Closed Rectangular Channels with Moving Walls. *Iranian Journal of Science and Technology, Transactions of Civil Engineering*, 46(5):3883–3893.

Manning, R. (1895). On the Flow of Water in Open Channels,Supplement. *Institution of Civil Engineers of Ireland*, 24:179–207.

Marangu, P. K., Mwenda, E. K., and Theuri, D. (2016). Modeling Open channel Fluid Flow with Trapezoidal Cross Section and a Segment Base.

Marjang, N. and Merkley, G. P. (2009). Velocity Profile Modeling in Rectangular and Compound Open-Channel Cross Sections. *Irrigation Science*, 27:471–484.

Merkley, G. P. (2005). Standard Horseshoe Cross Section Geometry. *Agricultural Water Management*, 71(1):61–70.

Mohammadiun, S., Salehi Neyshabouri, S., Naser, G., Parhizkar, H., and Vahabi, H. (2015). Effects of Open-channel Geometry on Flow Pattern in a 90 Junction. *Iranian Journal of Science and Technology Transactions of Civil Engineering*, 39:559–573.

Mohammed, A. Y. (2015). Numerical Analysis of Flow over side Weir. *Journal of King Saud University-Engineering Sciences*, 27(1):37–42.

Moramarco, T., Fan, Y., and Bras, R. L. (1999). Analytical Solution for Channel Routing with Uniform Lateral Inflow. *Journal of Hydraulic Engineering*, 125(7):707–713.

Munson, B. R. (2012). *Wileyplus Blackboard Card for Fundamentals of Fluid Mechanics*. Wiley-Blackwell.

Natasha, G. and Noviantri, V. (2019). Saint-venant Model Analysis of Trapezoidal Open Channel Water Flow using Finite Difference Method. *Procedia Computer Science*, 157:6–15.

Neary, V., Sotiropoulos, F., and Odgaard, A. (1999). Three-dimensional Numerical Model of Lateral-intake Inflows. *Journal of Hydraulic Engineering*, 125(2):126–140.

Ojiambo, V., Kinyanjui, M., Theuri, D., Kiogora, P., and Giterere, K. (2014). A Mathematical Model of the Fluid Flow in Circular Cross-sectional Open Channels. *Certif. Int. J. Eng. Sci. Innov. Technol.(IJESIT)*, 3:335–343.

Ojiambo, V. N. (2016). *Finite Difference Analysis of Fluid Flow in a Circular Cross-Sectional Open Channel*. PhD thesis, JKUAT, Applied Mathematics.

Omari, P., Sigey, J., Okelo, J., and Kiogora, R. (2018). Modeling Circular Closed Channels for Sewer Lines. *International Journal of Engineering Science and Innovative Technology*.

Qiu, C., Liu, S., Huang, J., Pan, W., and Xu, R. (2023). Influence of Cross-Sectional Shape on Flow Capacity of Open Channels. *Water*, 15(10):1877.

Rahman, M. S. and Haque, M. A. (2012). Mathematical Modeling of Blood Flow. In *2012 International Conference on Informatics, Electronics & Vision (ICIEV)*, pages 672–676. IEEE.

Rezaei, B. and Derakhshandeh, S. (2023). Experimental Study of Flow in Prismatic Compound Channel with Inclined Floodplains. *Journal of Hydraulics*.

Rotich, F. K. (2021). *Mathematical Modeling of Flow of Water in an Open Channel of Parabolic Cross-Section*. PhD thesis, University of Eldoret.

Samani, H. M., kazemi Mohsenabadi, S., Kashkouli, H. A., and Sedghi, H. (2013). Evaluating Velocity and Discharge in Horseshoe and D-Shape Cross sections. *Basic and Applied Scientific Research*, 3(2):996–1004.

Schlichting, H. and Gersten, K. (1979). Boundary-Layer Theory. MacGraw Hill. *New York*.

Shashkin, V. (2017). Mathematical Modeling of Fluid Flow in Complex Multi-channel Structures. In *IOP conference series: earth and environmental science*, volume 87, page 082045. IOP Publishing.

Shi, H., Zhang, J., and Huai, W. (2023). Experimental Study on Velocity Distributions, Secondary Currents, and Coherent Structures in Open channel Flow with Submerged Riparian Vegetation. *Advances in Water Resources*, 173:104406.

Simons, D. (2019). Open Channel Flow. In *Introduction to Physical Hydrology*, pages 131–152. Routledge.

Te Chow, V. (1958). *Open-Channel Hydr~aulics*.

Thiong'o, J. W. (2013). *Investigations of Fluid Flows in Open Rectangular and Triangular Channels*. PhD thesis.

Thiong'o, J., Kinyanjui, M., and Kwanza, J. (2011). Modeling Fluid Flow in Open Rectangular Channels. *Jagst College of Pure Sciences (304)*.

Truesdell, C. (1949). *A New Definition of a Fluid*. Naval Research Laboratory.

Tuitoek, D. and Hicks, F. (2001). Modelling of Unsteady Flow in Compound Channels. *Journal of Civil Engineering, JKUAT*, 6:45–54.

Wahba, E. (2022). Derivation of the Differential Continuity Equation in an Introductory Engineering fluid Mechanics Course. *International Journal of Mechanical Engineering Education*, 50(2):538–547.

Weber, L. J., Schumate, E. D., and Mawer, N. (2001). Experiments on flow at a 90 open-channel junction. *Journal of Hydraulic Engineering*, 127(5):340–350.

White, F. M. (1999). Open Channel Flow. *Fluid Mechanics*, page 65.

Zhao, F., Huai, W., and Li, D. (2017). Numerical Modeling of Open Channel Flow with Suspended Canopy. *Advances in Water Resources*, 105:132–143.

Appendix A:Python Code for Simulating Profiles

In [1]:

```
import numpy as np
import matplotlib.pyplot as plt
from scipy.optimize import fsolve
from math import sqrt, asin, pi
from matplotlib.ticker import MaxNLocator


def continuity_equation(delta_t, k, h, H, v, L, theta, delta_x, v_star, y_i_j, y_iplus1
    theta_rad = np.deg2rad(theta) # Convert angle to radians
    term1 = k * ((h - H) * sqrt(h * (2 * H - h)) + H**2 * (np.arcsin((h - H) / H) + pi
    term2 = v_star * (y_iplus1_j - y_iminus1_j) / (2 * delta_x)
    term3 = ((h - H) * sqrt(h * (2 * H - h)) + H**2 * (np.arcsin((h - H) / H) + pi / 2)
    return delta_t * (term1 - term2 - term3) + y_i_j

def momentum_equation(v_ij, dt, k, q_star, Fr, g, h, H, L, theta, u, n, R, s0, y_ijp1,
    term1 = q_star * v_ij / (Fr**2 * g * (h - H) * np.sqrt(h * (2*H - h)) + H**2 * (np.
    term2 = 1 / (Fr**2) * ((n**2 * v_ij**2 * v**2) / R**(4/3) - s0)
    term3 = 1 / (Fr**2) * (y_ijp1 - y_ijm1) / (2*dx)
    term4 = v_ij * (v_ijp1 - v_ijm1) / (2*dx)
    result =  dt * (k * (term1 - term2 - term3 - term4))-v_ij
    return result

# Parameters
Fr = 0.05
s_o = 0.004
n = 0.012
g = 9.8
q = 0.002
u = 0.002
```

```
H = 5.65
h = 0.5
R=0.1
k_values = np.array([1, 2, 3, 4, 5, 6])
L = 1
theta = 40

# Initial conditions
v_star = 0.5
y_i_j = 0
y_iplus1_j = 0
y_iminus1_j = 0
v_iplus1_j = 0
v_iminus1_j = 0

# Time step and spatial step
delta_t = 0.01
delta_x = 0.1

# Calculate y for different k values
y_values = []
for k in k_values:
    v = 10 # Assuming a constant velocity for simplicity
    y_updated = continuity_equation(delta_t, k, h, H, v, L, theta, delta_x, v_star, y_i
    y_values.append(y_updated)

# Plot
plt.figure(figsize=(10, 6), facecolor='white')
plt.plot(k_values, y_values, '-o')
```

```
k = 3  # Chosen value of k for demonstration
theta_values = np.array([10, 20, 30, 40, 50, 60, 70, 80, 90])  # Angles in degrees

# Convert angles to radians for calculation
theta_radians = np.radians(theta_values)

# Assuming a relationship for demonstration: velocity = k * cos(theta)
# This is a simplification for illustrative purposes
velocities = k * np.cos(theta_radians)

plt.figure(figsize=(10, 6), facecolor='white')
plt.plot(theta_values, velocities, marker='o', linestyle='-', color='blue')
plt.title('Effect of Variation of Angle of Lateral Inflow Channels on Velocity')
plt.xlabel('Angle of Lateral Inflow Channels (degrees)')
plt.ylabel('Velocity in Main Channel (arbitrary units)')
plt.grid(True)
plt.show()
```

```
import numpy as np
import matplotlib.pyplot as plt

# Parameters
angles = np.linspace(10, 90, 9)  # Angles from 10 to 90 degrees
k_values = [1, 2, 3, 4, 5, 6]  # Different coefficient k values

# Placeholder for velocity calculations based on angle variation for different k
results = {}
for k in k_values:
    # Simplified relationship assuming velocity is related to the cosine of the angle
    # Adjusted by a factor involving k to simulate different conditions
    velocities = k * np.cos(np.radians(angles))
    results[k] = velocities
    # Plotting
plt.figure(figsize=(10, 6), facecolor='white')
for k, velocities in results.items():
    plt.plot(angles, velocities, marker='o', linestyle='-', label=f'k={k}')

plt.title('Effect of Angle Variation on Velocity in the Main Open Channel for Different
plt.xlabel('Angle of Lateral Inflow Channels (degrees)')
plt.ylabel('Velocity in the Main Open Channel (m/s)')
plt.legend()
plt.grid(True)
plt.show()
```

```
import numpy as np
import matplotlib.pyplot as plt

# Parameters
areas = [0.32, 0.08]  # Cross-sectional areas of the lateral inflow channels
angle = 40  # Angle of inflow

# Placeholder for velocity calculations based on cross-sectional area for a given angle
# In a real scenario, this would involve complex calculations
# Here, we simulate the effect of the cross-sectional area on velocity for simplicity
velocities = [1 / (area * np.cos(np.radians(angle))) for area in areas]  # Simplified r

# Plotting
plt.figure(figsize=(10, 6), facecolor='white')
plt.bar(['A=0.32', 'A=0.08'], velocities, color=['blue', 'orange'])
plt.title('Effect of Cross-Sectional Area on Velocity in the Main Open Channel at Angle
plt.xlabel('Cross-Sectional Area of Lateral Inflow Channels')
plt.ylabel('Velocity in the Main Open Channel (m/s)')
plt.grid(True, axis='y')
plt.show()
```

```
import numpy as np
import matplotlib.pyplot as plt

# Parameters
areas = [0.32, 0.08]  # Cross-sectional areas of the lateral inflow channels
angles = [30, 40, 50, 60]  # Different angles of inflow

# Placeholder for velocity calculations based on cross-sectional area for different ang
results = {}
for angle in angles:
    velocities = [1 / (area * np.cos(np.radians(angle))) for area in areas]  # Simplifi
    results[angle] = velocities

# Plotting
plt.figure(figsize=(10, 6), facecolor='white')
width = 0.35  # Width of the bars

for i, angle in enumerate(angles):
    plt.bar(np.arange(len(areas)) + i*width, results[angle], width, label=f'Angle={angl
plt.title('Effect of Cross-Sectional Area on Velocity in the Main Open Channel at Diffe
plt.xticks(np.arange(len(areas)) + width/2, ['A=0.32', 'A=0.08'])
plt.xlabel('Cross-Sectional Area of Lateral Inflow Channels')
plt.ylabel('Velocity in the Main Open Channel (m/s)')
plt.legend()
plt.grid(True, axis='y')
plt.show()
```

```python
import numpy as np
import matplotlib.pyplot as plt

# Parameters
lengths = [1, 2]  # Lengths of the lateral inflow channels
angle = 40  # Angle of inflow

# Placeholder for velocity calculations based on length for a given angle
# In a real scenario, this would involve complex calculations
# Here, we simulate the effect of the length on velocity for simplicity
velocities = [length * np.cos(np.radians(angle)) for length in lengths]  # Simplified r

# Plotting
plt.figure(figsize=(10, 6), facecolor='white')
plt.bar(['L=1', 'L=2'], velocities, color=['blue', 'orange'])
plt.title('Effect of Length of Lateral Inflow Channels on Velocity in the Main Channel
plt.xlabel('Length of Lateral Inflow Channels')
plt.ylabel('Velocity in the Main Channel (m/s)')
plt.grid(True, axis='y')
plt.show()
```

Appendix B:Research Permit

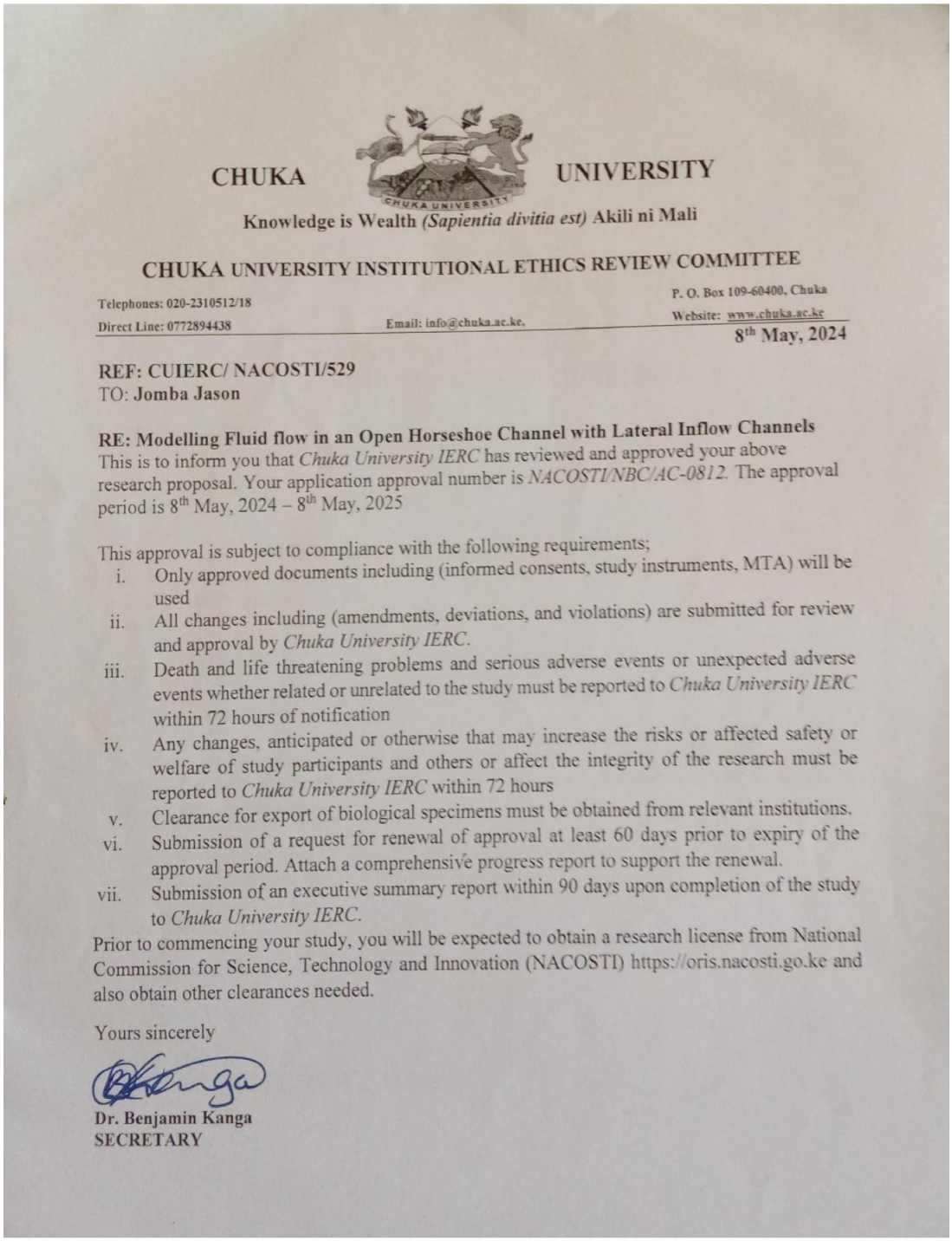

CHUKA UNIVERSITY

Knowledge is Wealth *(Sapientia divitia est)* Akili ni Mali

CHUKA UNIVERSITY INSTITUTIONAL ETHICS REVIEW COMMITTEE

Telephones: 020-2310512/18
Direct Line: 0772894438
Email: info@chuka.ac.ke,
P. O. Box 109-60400, Chuka
Website: www.chuka.ac.ke

8th May, 2024

REF: CUIERC/ NACOSTI/529
TO: **Jomba Jason**

RE: Modelling Fluid flow in an Open Horseshoe Channel with Lateral Inflow Channels
This is to inform you that *Chuka University IERC* has reviewed and approved your above research proposal. Your application approval number is *NACOSTI/NBC/AC-0812*. The approval period is 8th May, 2024 – 8th May, 2025

This approval is subject to compliance with the following requirements;

i. Only approved documents including (informed consents, study instruments, MTA) will be used
ii. All changes including (amendments, deviations, and violations) are submitted for review and approval by *Chuka University IERC*.
iii. Death and life threatening problems and serious adverse events or unexpected adverse events whether related or unrelated to the study must be reported to *Chuka University IERC* within 72 hours of notification
iv. Any changes, anticipated or otherwise that may increase the risks or affected safety or welfare of study participants and others or affect the integrity of the research must be reported to *Chuka University IERC* within 72 hours
v. Clearance for export of biological specimens must be obtained from relevant institutions.
vi. Submission of a request for renewal of approval at least 60 days prior to expiry of the approval period. Attach a comprehensive progress report to support the renewal.
vii. Submission of an executive summary report within 90 days upon completion of the study to *Chuka University IERC*.

Prior to commencing your study, you will be expected to obtain a research license from National Commission for Science, Technology and Innovation (NACOSTI) https://oris.nacosti.go.ke and also obtain other clearances needed.

Yours sincerely

Dr. Benjamin Kanga
SECRETARY

Appendix C:Research Authorization (NACOSTI)

REPUBLIC OF KENYA

NATIONAL COMMISSION FOR SCIENCE,TECHNOLOGY & INNOVATION

Ref No: **867560**

Date of Issue: **24/July/2024**

RESEARCH LICENSE

This is to Certify that Mr.. Jomba Jason of Chuka University, has been licensed to conduct research as per the provision of the Science, Technology and Innovation Act, 2013 (Rev.2014) in Tharaka-Nithi on the topic: Modelling Fluid Flow in an Open Horseshoe Channel with Lateral Inflow Channels for the period ending : 24/July/2025.

License No: **NACOSTI/P/24/38016**

867560

Applicant Identification Number

Director General
NATIONAL COMMISSION FOR SCIENCE,TECHNOLOGY & INNOVATION

Verification QR Code

NOTE: This is a computer generated License. To verify the authenticity of this document, Scan the QR Code using QR scanner application.

See overleaf for conditions